RESERVOIR CHARACTERIZATION AND MODELING OF THE PERMIAN WOLFCAMP AND BONE SPRING FORMATIONS IN WOLFBONE FIELD, SOUTHEAST DELAWARE BASIN, WEST TEXAS, USA

A Thesis

by

ABDULLAH ABDULRAHMAN M. ALKHALDI

Submitted to the Office of Graduate and Professional Studies of
Texas A&M University
in partial fulfillment of the requirements for the degree of

MASTER OF SCIENCE

Chair of Committee,	Juan Carlos Laya
Committee Members,	Lin Ying Hu
	Ruud Weijermars
Head of Department,	Julie Newman

May 2020

Major Subject: Geology

ABSTRACT

The west of Texas and New Mexico Permian Basin is defined as a complex sedimentary system which is placed in the Marathon-Ouachita Orogenic Belt's Foreland. It extends across 52 counties with an area of 75,000 square miles with a width of approximately 250 miles and a length of 300 miles composed of more than 7,000 fields. Furthermore, the hydrocarbon generation started about 100 years ago in the Permian Basin. The U.S. Energy Information Administration stated that the Basin's contribution to the entire U.S. hydrocarbon production was around 18% in 2013 and approximately 20% in 2017 including almost 9% of the entire U.S. dry gas production. Though, the study area is located southeast of Delaware Basin within the Giant Permian Basin, at Pecos County, Texas, USA. The subsurface data were taken from seven vertical wells that cover an area of almost 40 square miles targeting Bone Spring and Wolfcamp Formations.

The intention of this research is to focus on the Delaware Basin, one of the Permian Basin's sub basins, by delivering a 3D geological model that illustrates an implementation of a field development strategy on both Unconventional Wolfcamp and Bone Spring Formations. The steps include interpreting the subsurface petrophysical and geomechanical data to identify sweet spots for the landing of horizontal wells as well as estimating the hydrocarbon's volumetric in our area of interest. Nevertheless, total organic carbon content 'TOC' is the most important parameter in terms of determining the hydrocarbon storage in unconventional resources. Since geochemistry data analysis

is not available and mineralogy and elemental analysis are also absent, the hydrocarbon in place was estimated based on water saturation and porosity.

Our result shows that the Bone Spring and Wolfcamp formation have an estimated ultimate recovery ‘EUR’ of 1.5 billion barrel of oil ‘BBO’ and 500 million barrel of oil ‘MMBO’ respectively as a total resource assessment. However, cut off values have been assigned to find the best tier in the field for original oil in place ‘OOIP’ calculation. The net/gross is determined by applying suitable reservoir parameters cut offs so that uneconomic or unproductive zones are not included. These cut offs are applied to porosity above or equal to 5%, water saturation equal or less than 40 % and brittleness index greater or equal to 30%. Thus, the EUR of the best areas in the field for Bone Spring and Wolfcamp formations are calculated to be around 786 million barrel of oil ‘MMBO’ and 276 million barrel of oil ‘MMBO’, respectively. Moreover, the best landing zones of both formations were mainly associated with organic rich mudstone that shows an average porosity of greater than 10% and water saturation less than 20%.

DEDICATION

I am dedicating this thesis to my best friend Abdulmajeed Alzahrani who has been diagnosed with Leukemia, may god bless him, comfort him in his pain, remove every cancer cell and award his family strength and patience. I also want to dedicate this project to my beloved father Abdulrahman Alkhaldi and dearly loved mother Haya Alkhaldi for their continuous support and pray to make this thesis successful. Finally, I dedicate this effective work and give special thanks to my wife Norah Alkhaldi, my daughter Haya Alkhaldi and my son Abdulrahman Alkhaldi for their patience, encouragement and being around me throughout the entire master's degree program.

ACKNOWLEDGEMENTS

First, I thank god for allowing me to live and for providing me a good health to see this thesis completed and successful. I would like to begin thanking my advisors Dr. Mamdouh Shebl, Dr. Lin Ying Hu and Prof. William David Kennedy for their support by exchanging the knowledge and experience to develop the right skills I need in both Petrophysics and Modeling.

I would also like to thank Dr. Juan Carlos Laya and Dr. Ruud Weijermars for their help and guidance. Moreover, a special thanks to Dr. Mukul Bhatia for providing me the data set of this project and being supportive. Without his help and inspiration, the accomplishment of this project would not be achievable. I would also thank Mr. John Tackett and University Lands for granting me an access to utilize their data in one of their potential project areas.

Finally, I would like to thank my technical advisor at Saudi Aramco Mr. Mohammed Ojeh who assisted me in this project. His enthusiasm and eagerness to offer feedbacks made the success of this thesis a pleasant experience.

CONTRIBUTORS AND FUNDING SOURCES

Contributors

This thesis was supported by a thesis committee comprising of Prof. Juan Carlos Laya (Chair), Prof. Lin Ying Hu (Advisor) and Prof. Ruud Weijermars (Department of Petroleum Engineering). The work in this thesis was accomplished by the student, under the supervision of Prof. Mamdouh Shebl and Prof. Lin Ying Hu from Department of Geology and Geophysics.

Funding Sources

Graduate study was advocated by a scholarship from Saudi Arabian American Company of Oil (Saudi Aramco). Its contents are solely the responsibility of the author and do not necessarily correspond to the official views of the Saudi Aramco.

TABLE OF CONTENTS

Page

LIST OF FIGURES

LIST OF TABLES

CHAPTER I

INTRODUCTION

The west of Texas and New Mexico Permian Basin was the target for scientists to investigate and understand the geology of the region since the inception of G. G. Shumard in the 1850's when he was interpreting the fossils, Permian age, that were collected from the lower bed of El Capitan Formation. The Permian Basin interest resumed not only to get a full geological understanding of the basin; indeed, the interest was also to determine hydrocarbon producing provinces in North America and started in 1920's when oil was discovered (Keller, Hills & Djeddi, 1980). Regardless of the vast attempts that have been prepared to reveal the history of the basin geology, there are still various aspects where further studies are needed (Crosby, 2015).

The hydrocarbon generation started about 100 years ago in the Permian Basin. Recently, the Texas and New Mexico Permian Basin became the top oil producing province in the United States overreaching Gulf of Mexico federal offshore section. The U.S. Energy Information Administration stated that the Basin's contribution to the entire U.S. hydrocarbon production was around 18% in 2013 (EIA, 2014) and approximately 20% in 2017 including 9% of the entire U.S. dry gas production (EIA, 2018). Between 2007 and 2013, an increase in oil production was recorded in the Permian Basin from 850,000 barrels per day to 1,350,000 barrels per day '60% production increase'. This growth in production was mainly from six formations including Wolfcamp and Bone Springs. As of September 2018, the Basin's production exceeded 33.4 billion barrels of oil and approximately 118 trillion cubic feet of natural gas (EIA, 2018). However, the

residual proven reserves were estimated in the Permian Basin in 2016 by EIA to be more than 5 billion barrels of oil and around 19.1 trillion cubic feet ‘TCF’.

The purpose of this project is to characterize reservoir parameters and incorporate them in a 3D geological model to enhance productivity by landing the horizontal wells in the zones of interest ‘Sweet Spots’ in Wolfbone Field at Pecos County, Texas. This may support any development programs in the oil industry to optimize the placement of their production wells on Delaware Basin, hence it should reduce the uncertainty. This reservoir modeling should integrate populated isochore, porosity, permeability, hydrocarbon saturation and brittleness of both Bone Spring and Wolfcamp Formations. These properties will be analyzed and calculated using methods of well logging ‘Petrophysics’ on the provided subsurface data.

CHAPTER II

WELL AND FIELD DATA

Studied Area

The west of Texas and New Mexico Permian Basin is defined as a complex sedimentary system which is placed in the Marathon-Ouachita Orogenic Belt's Foreland. It extends across 52 counties with an area of 75,000 square miles (EIA, 2018). It has a width of approximately 250 miles and a length of 300 miles composed of more than 7,000 fields (RRC, 2019). Figure 1 illustrates the location of the study area, marked by a rectangle on the left image, southeast of Delaware Basin within the Giant Permian Basin, at Pecos County, Texas, USA. The subsurface data were taken from seven vertical wells in block 21, 23 and 24 in section 2, 6, 7, 13, 18, 30 and 34 leased by University Lands. The drilled wells in our study area cover an area of almost 66 square miles targeting Bone Spring and part of Wolfcamp Formations.

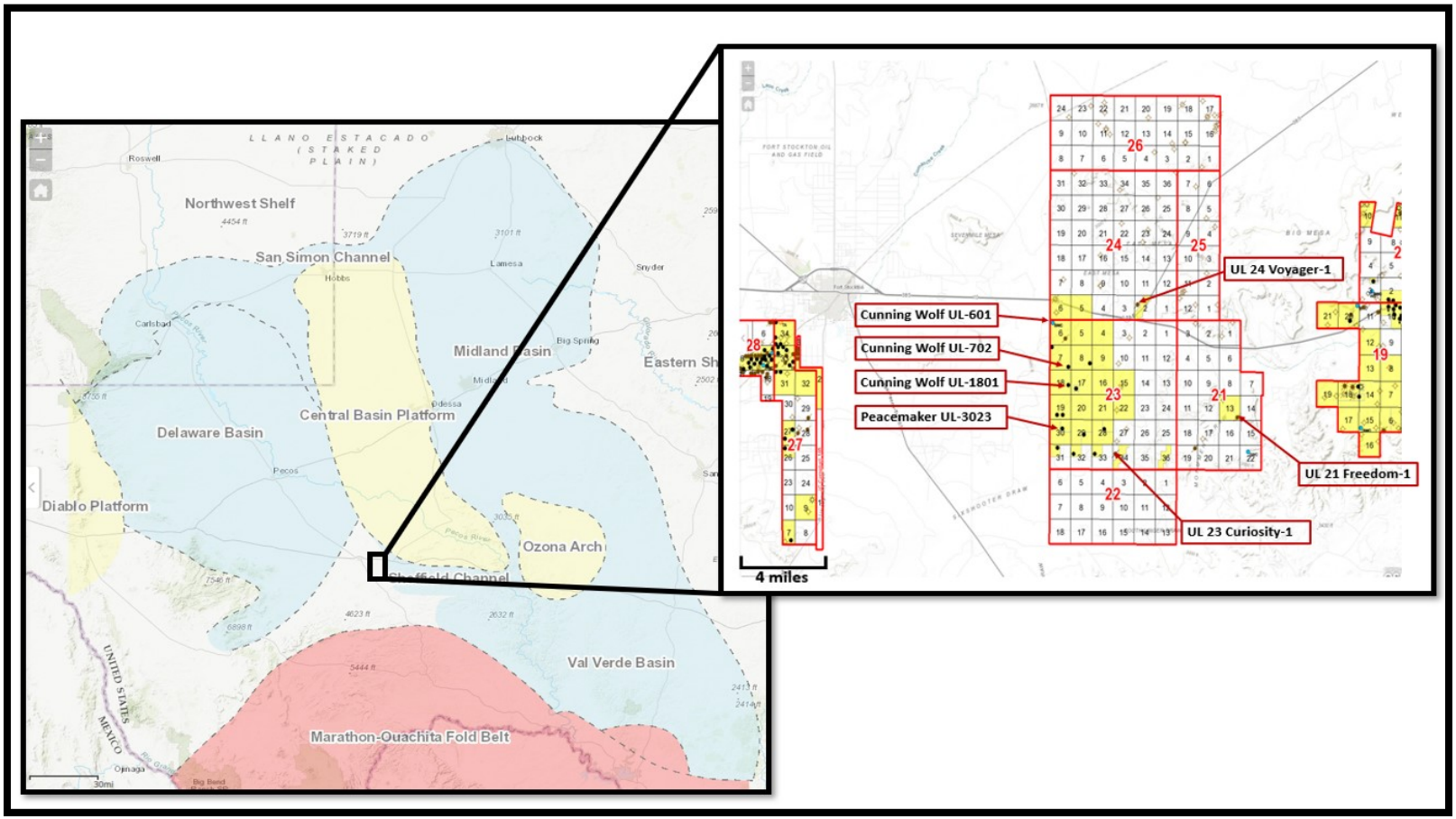

Figure 1. Location maps represent Permian sub-basins and study location reprinted from (University Lands, 2019).

Well Data

Wolfbone Field Subsurface Data is provided by University Lands 'for public domain' as well logs and sidewall core analysis of one well 'Reference Well' along with both Wolfcamp and Bone Spring Formations tops of each well. There are petrophysical logs of seven vertical wells granted in this project as follow:

A) UL 21 Freedom-1 'Reference Well', available logs are Gamma Ray 'GR', Shallow 'LLS' and Deep Resistivities 'LLD', Photoelectric Effect 'Pe', Density 'RHOB', Neutron 'NPHI' and Compressional Sonic 'DTc' with Mud log. The Wolfcamp top is expected to be at 6879 ft True Vertical Depth 'TVD' and Bone Spring top is estimated to be at 4782 ft TVD.

B) Cunning Wolf UL 601, available logs are Gamma Ray 'GR', Shallow 'LLS' and Deep Resistivities 'LLD', Photoelectric Effect 'Pe', Density 'RHOB', Neutron 'NPHI' and Compressional 'DTc' with Shear Sonic 'DTs'. The Wolfcamp top is expected to be at 8020 ft TVD and Bone Spring top is estimated to be at 5767 ft TVD.

C) Cunning Wolf UL 702, available logs are Gamma Ray 'GR', Neutron 'NPHI', Compressional 'DTc' with Shear Sonic 'DTs'. The Wolfcamp top is expected to be at 7805 ft TVD and Bone Spring top is estimated to be at 5934 ft TVD.

D) Cunning Wolf UL 1801, available logs are Gamma Ray 'GR', Compressional Sonic 'DTc'. The Wolfcamp top is expected to be at 7636 ft TVD and Bone Spring top is estimated to be at 5959 ft TVD.

E) Peacemaker UL 3023, available logs are Gamma Ray ‘GR’ and Neutron ‘NPHI’. The Wolfcamp top is expected to be at 7401 ft TVD and Bone Spring top is estimated to be at 5473 ft TVD.

F) UL 23 Curiosity-1, available logs are Gamma Ray ‘GR’, Shallow ‘LLS’ and Deep Resistivities ‘LLD’, Photoelectric Effect ‘Pe’, Density ‘RHOB’, Neutron ‘NPHI’ and Compressional Sonic ‘DTc’. The Wolfcamp top is expected to be at 7799 ft TVD and Bone Spring top is estimated to be at 5612 ft TVD.

G) UL 24 Voyager-1, available logs are Gamma Ray ‘GR’, Shallow ‘LLS’ and Deep Resistivities ‘LLD’, Photoelectric Effect ‘Pe’, Density ‘RHOB’, Neutron ‘NPHI’ and Compressional Sonic ‘DTc’. The Wolfcamp top is expected to be at 7520 ft TVD and Bone Spring top is estimated to be at 5317 ft TVD.

Sidewall Core ‘SWC’ Analysis of UL 21 Freedom-1 well, conducted by Forge Energy, LLC, is also provided by University Lands which contains about 60 samples ‘Plugs not Crushed’ examined under reservoir condition. These samples were measured under standard prodcedure to extract air and klinkenberg permeability, total porosity, grain density and water saturation. In this project, the total depth of each well is inconsistent in Wolfcamp formation with a minimum penetrated interval of 400 ft and a maximum interval of 2000 ft. This variation will make uncertain thickness map of Wolfcamp hence uncertain 3D geological model.

Geological Setting and Tectonic Evolution

The west of Texas and New Mexico Permian Basin is placed in the Marathone-Ouachita Orogenic Belt's Foreland. This foreland is complex and comprises of several sub-basins that are segregated by intra-foreland uplifts. Thus, the present-day structure map is characterized by three main sub-basins. These are Delaware Basin, Central Basin Platform and Midland Basin as shown in firgure 2 (EIA, 2018). The Delaware Basin is restricted in the west by Diablo Platform, Northern and Northwestern Shelf to the north and in the south by Marathon Orogenic Belt. This Delaware Basin is detached from Midland Basin by the North-South trending Central Basin Platform. While the Midland Basin is restricted to east by a composite sequence of North-South trending segments of fault known as Fort Chadbourne Fault Zone. This fault zone accords with the transition from facies of marine platform on the Eastern Shelf to the basinal facies towards Midland Basin. Whereas to the south, Midland Basin Stratigraphy thins onto the Ozona Arch, which is defined as an extension of the Southern Central Basin Platform towards the East that divides the Midland and Val Verde Basins (Yang & Dorobek, 1995).

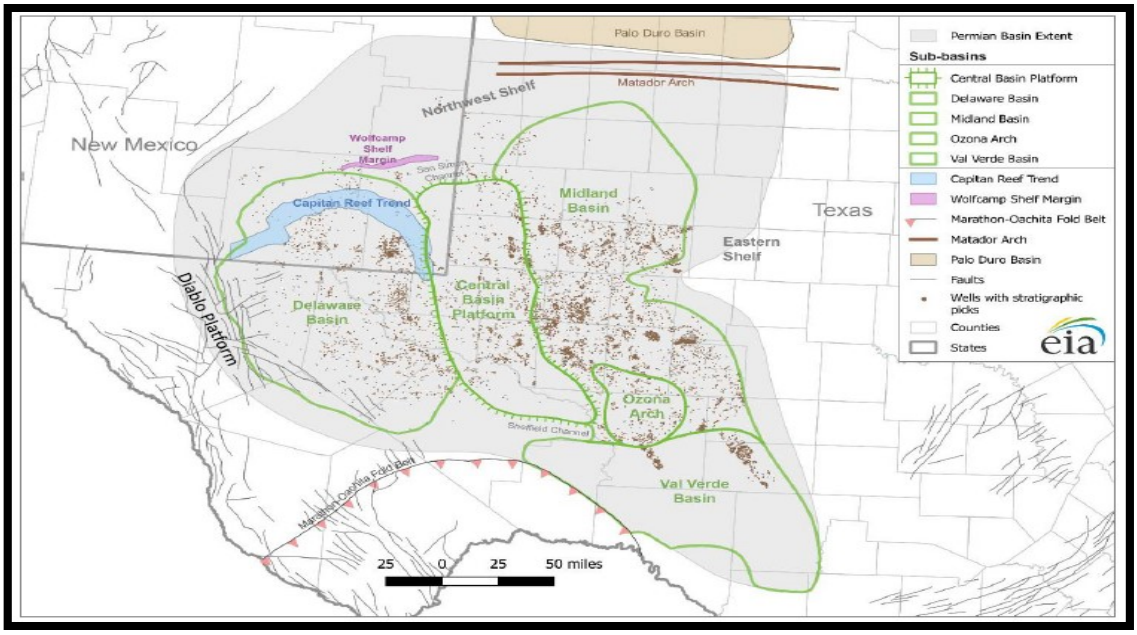

Figure 2. Present-day structure map of the Permian Band and its sub-basins reprinted from (EIA, 2018).

The Permian Basin tectonic history has a direct involvement on the accumulation and preservation of the massive hydrocarbon reserves. The Permian Basin has formed, as low region on the North American Craton southwestern edge, in the late Proterozoic time 'Tobosa Basin' (Galley, 1958). During this time, part of the province may have been influenced by crustal rifting south of the present basin. This rifting is believed to extend northward to New Mexico and was conducted by right horizontal faulting (Keller, Hills & Djeddi, 1980). Moreover, a long period of uplift then erosion occurred throughout the latest Pre-Cambrian and Early Cambrian time followed by thin deposits of Upper Cambrian and Early Ordovician clastics in the Tobosa Basin. During Early and Middle Paleozoic period, the basin was covered by shallow water deposits mainly

limestones and shales. These deposits were affected by a series of interruptions of subaerial erosions during the same time of deposition (Keller, Hills & Djeddi, 1980).

Minor tectonic activities began during Mississippian period along with vertical movements in the weakness zones that was formed by the Late Pre-Cambrian lateral faulting. These movements had exaggerated and deformed the Central portion of Tobosa Basin into small faulted and folded high regions during Middle Pennsylvanian period. This resulted in dividing the basin into two main sub-basins, the Delaware and Midland Basins (Cys & Gibson, 1988). As these basins were developing, wide shelves of limestone produced around them while fine sand and shales were delivered into the basin by stream channels cutting the limestone shelves (Hills, 1963). During Early Permian period 'Wolfcamp', these limestones covered the eroded portions of highlands as well as the shelves hence creating the Central Basin Platform. Furthermore, clastic sedimentation resumed in the basins on both sides of the platform (Keller, Hills & Djeddi, 1980).

Moreover, vertical movement along the previous weakness zones of the faulted Pre-Cambrian resumed to cause the eastern side deepening of Delaware Basin (Soreghan & Soreghan, 2013). Though, comparable deepening happened on the western side of the Midland Basin, but in lesser scale (Keller, Hills & Djeddi, 1980). Throughout the Middle Permian period, back-reef evaporites were formed due to the development of shelf-edge carbonates besides a minor low of eustatic 'sea level' (Keller, Hills & Djeddi, 1980). During the Late Permian time, deposition of carbonates was restricted around the Delaware Basin because of the high Capitan reef complex barrier while the central part

of the basin resumed to obtain a small amount of fine clastic sediment deposits in a reducing environment. By the end of the Permian period and as a result of sea retreat, continental red beds and evaporates covered over the whole basin. The tectonic activities, were minimal throughout the Middle and Late Permian, is causing slight tilting and gradual deepening of the Delaware Basin toward the east (Keller, Hills & Djeddi, 1980).

During Late Triassic, continental deposition continued at the similar location as in the Permian followed by a hiatus which represents Jurassic period. In Cretaceous time, deposition of shallow marine sandstones and limestones took place on a different pattern 'from southeast' (Keller, Hills & Djeddi, 1980). However, Uplifting of Permian shelf-edge carbonates and nearby basinal rocks were strongly affected by the Laramide Orogeny. Nevertheless, early and late vertical movements 'downfaulting' is believed to form the Salt Basin Graben which was a geological reason for another tilting of the Delaware Basin toward the east and development of Guadalupe sediments and Delaware Mountains. This late tilting reactivated joints and fractures around the weakness zone beside the eastern edge of the Delaware Basin. These fractures have a systematic change in orientation at Delaware Basin from North East-South West in the northern portion to East-West in the central part and North West-South East in the southern part of the basin (Schwartz, 2018). Finally, during Late Cenozoic period thin sediments were deposited across the basin except on Salt Basin Graben and Eastern edge of Delaware Basin where thick sediments accumulated (Keller, Hills & Djeddi, 1980).

Stratigraphy

The heterogeneity of Permian rocks is demonstrated by many scientists and they are grading upward from a sequence of clastic carbonate to a sequence of evaporite. The Upper Pennsylvanian and Wolfcampian Stratigraphy expand over the Permian Basin and the thickest portion are in the southern and central portions of the Delaware Basin as seen in figure 3 (EIA, 2014).

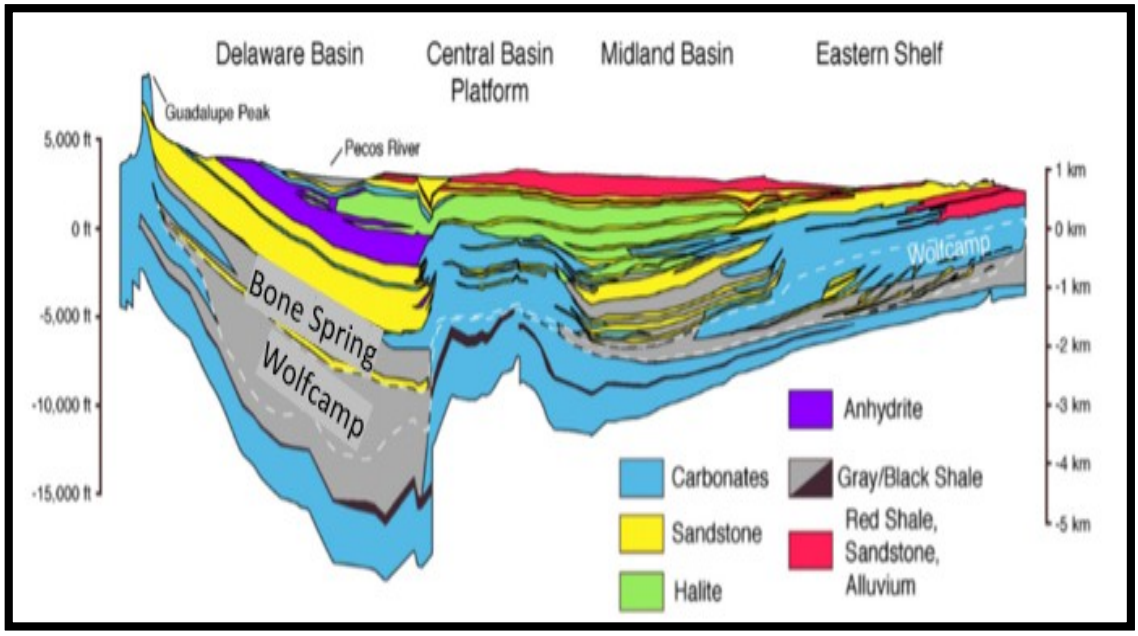

Figure 3. East-West cross section across the Permian basin basins with the focus of the thickest portion of Bone Spring and Wolfcamp reprinted and modified from (Engle, 2016).

Wolfcamp Formation

The Wolfcamp Shale is an organic rich shale that spreads in all three sub-basins of the Permian Basin in the subsurface and it is the most productive tight shale oil and gas formation. It is defined as an unconventional play that consists of a mixture of fine sandstone and siltstone beds interbedded with layers of shale and carbonate deposited in a marine environment (Lohoefer, et al., 2014). It is divided into four members recognized as Wolfcamp A, B, C and D, figure 4. The Upper Pennsylvanian Wolfcamp D is characterized as the Cline Shale while the top three members were deposited in the Wolfcampian stage. However, the furthermost drilled target zones up to date are Wolfcamp A and B members (EIA, 2018). There are 9 facies described in Wolfcamp formation, but the major facies are Argillaceous Siliceous Mudstone, Calcareous Siliceous Mudstone and Skeletal Mudstone Dominated Wackestone/Packstone, as they show vertical and lateral heterogeneity (Bievenour & Sonnenberg, 2019). The four members exhibit different properties in terms of lithology, porosity and total organic content (Gaswirth et al., 2018). The Wolfcamp formation shows low quality of reservoir properties of porosity and permeability ranges between 5 – 8% and 0.001 – 0.1 mD respectively (Fairhurst & Hanson, 2012) and an average water saturation of 48% (Sieler, 2018).

Bone Spring Formation

The Bone Spring Formation is another unconventional play in the Delaware Basin that lies comformably above Wolfcamp Formation. It is described as interbedded sandstone, carbonates and shale sequence that deepens and thickens towards south and east and thins into the Central Basin Platform until it disappears (Kelly, et al., 2012). The Bone Spring Formation is divided into third, second and first Bone Spring sandstone and carbonate overlain by the Avalon Shale as displayed in figure 4 (Schwartz, 2018). This formation has deposited under sea level fluctuations to form a system of mixed carbonate siliciclastic throughout the Leonardian stage where carbonates were deposited during sea level rise and sandstones deposited during sea level drop. Layers of carbonates within the Bone Spring Formation are illustrated by the occurrence of interbedded carbonaceous shaly strata and muddy lithology from mudstone and wackestone. Whereas, the strata of sandstone within the Bone Spring represent the submarine fan deposits and consist mostly of carbon rich, calcareous shale and siltstone (Montgomery, 1997). Moreover, fine grained sandstone with dolomite and cement of authigenic clay in siliciclastic turbidites are abundant within the three units of Bone Spring Sandstone (Gawloski, 1986). There are 9 facies described in Bone Spring formation, but the major facies are Argillaceous Siliceous Mudstone, Argillaceous Siliceous Siltstone and Dolomite Skeletal Packstone, as they show vertical and lateral heterogeneity (Bievenour & Sonnenberg, 2019). The Bone Spring formation shows a range of porosity between 8 -20% and an average of few millimeter Darcy in

permeability (Jackson, Palisch & Lehman, 2014) while the average water saturation is 60% (Sieler, 2018).

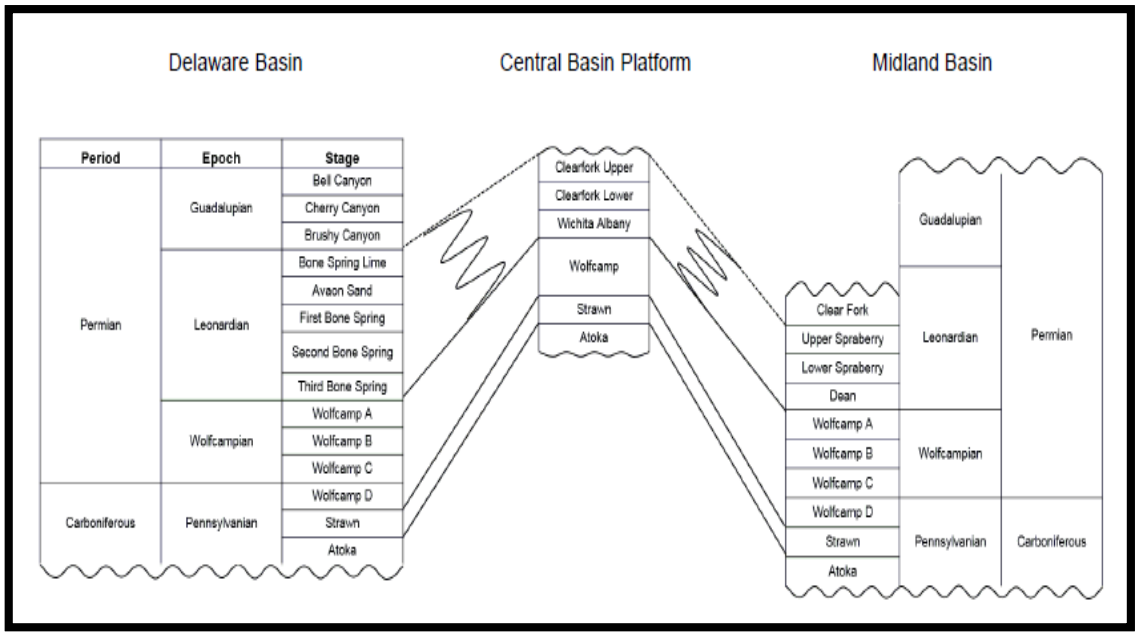

Figure 4. Stratigraphic column of the Upper Carboniferous and Permian intervals of the Permian Basin reprinted from (EIA, 2018).

CHAPTER III

RESERVOIR CHARACTERIZATION

Data Editing

Editing well log curves is an essential phase prior to analyzing and interpreting these log data. Data is received by University Lands as they are ready to use and environmentally corrected; but found, in our seven well logs, minor gaps that need to be filled and unrealistic data 'Shifted' that need to be corrected with slight noises which affect the data 'Cycle Skipping Effect' that should be corrected too especially in compressional and shear sonic logs, figure 5 and 6. Cycle Skipping Effect means high measurements in transit time represented by spikes on the log that is caused by fractures, gas in the pores, and unconsolidated formations. In filling and substituting small gaps, good interpretation and judgment from above and below log data intervals are needed besides a logical practice or trends of other log curves in the same well. In this project, Interactive Petrophysics Software 'IP' is utilized for petrophysical and geomechanical analysis.

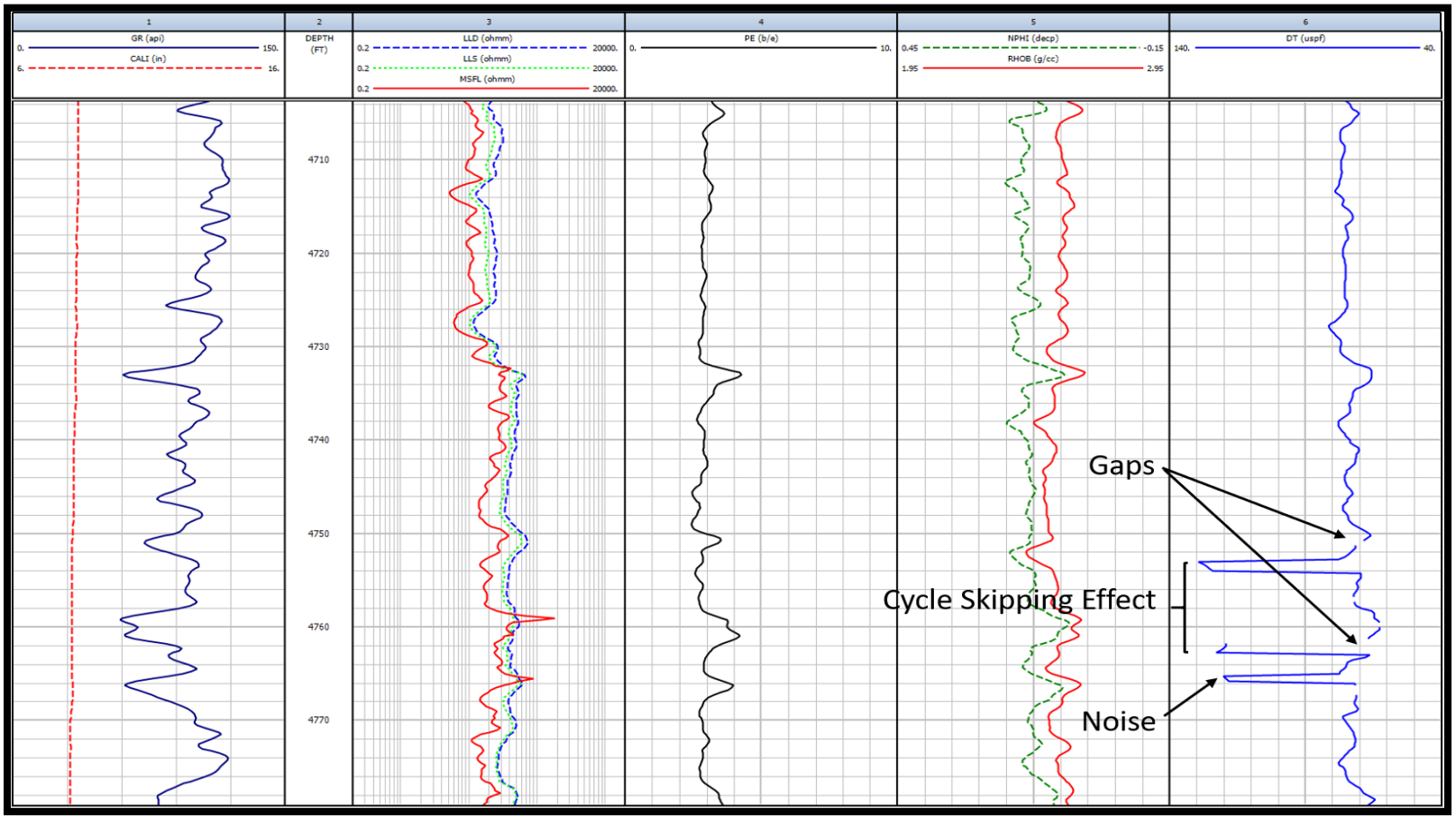

Figure 5. Data editing of UL 21 Freedom-1 well where gaps, cycle skipping effect and Noise are marked.

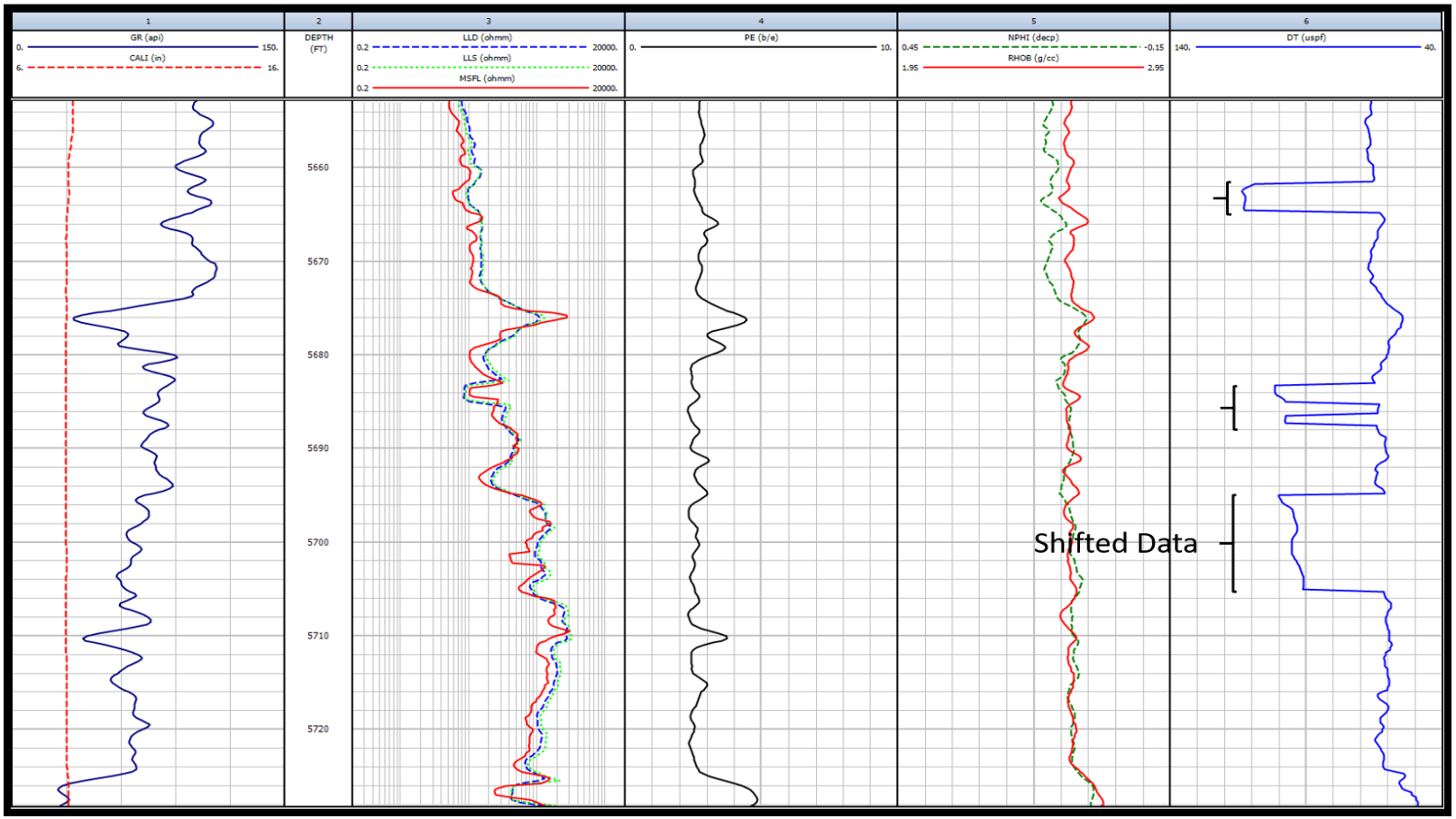

Figure 6. Data editing of UL 21 Freedom-1 well where shifted data are marked.

Generating Synthetic Curves

Wireline well logs display a comprehensive curve of formation parameters contrasted with depth. However, in many cases petroleum companies often acquire few curves of the targeted formations due to either drilling complications or the cost. Thus, synthetic curves may assist in analyzing formation properties in zones where the essential set of curves 'logs' are absent. In this project, as marked in the data section, three out of seven wells have two to three curves but not full suite of curves 'logs' as our reference well 'UL 21 Freedom-1' does.

Multi-linear regression analysis is used to generate synthetic curves and predict the missing curves on the three wells stated above. This analysis is statistical processes that determine the relationship between a dependent variable and more independent variables using Gaussian distribution. Though, these synthetic curves are not reflecting the formations signatures but are sort of imaginary data created to fill in the missing curves. Once synthetic curves are generated, they have to be normalized based on the concept where rescaling a synthetic log should matches its neighbour logs scale.

The multi-linear regression analysis is applied on the reference well UL 21 Freedom-1 since it has full suite of curves needed for our petrophysical analysis to predict the missing curves on Cunning Wolf UL 1801, Cunning Wolf UL 701 and Peacemaker UL 3023 wells. The figures 7, 8, 9 and 10, illustrate the raw data in black curves and the normalized synthetic data in red curves.

For Cunning Wolf UL 1801 well, the missing curves are Shallow 'LLS' and Deep Resistivities 'LLD', Density 'RHOB', Neutron 'NPHI' and Photoelectric Effect 'Pe', figure 7, which can be calculated as follow:

$$LLS = 10^{(19.8+0.03*\log(GR)-10.06*\log(DTc))} \quad (1)$$

$$LLD = 10^{(17.1-0.44*\log(GR)-7.96*\log(DTc))} \quad (2)$$

$$RHOB = 10^{(0.5+2.04*10^{-4}*GR-0.002*DTc)} \quad (3)$$

$$NPHI = -0.3 - 1.8 * 10^{-5} * GR + 0.006 * DTc \quad (4)$$

$$Pe = 7.14 + 0.003 * GR - 0.06 * DTc \quad (5)$$

For Cunning Wolf UL 702 well, the missing curves are Shallow 'LLS' and Deep Resistivities 'LLD', RHOB and Pe, figure 8, which can be calculated as follow:

$$LLS = 10^{(11.4+0.3*\log(GR)-0.7*\log(NPHI)-6.1*\log(DTc))} \quad (6)$$

$$LLD = 10^{(9.3+0.2*\log(GR)-0.7*\log(NPHI)-4.3*\log(DTc))} \quad (7)$$

$$RHOB = 10^{(0.45+2.02*10^{-4}*GR-0.13*NPHI-6.4*10^{-4}*DTc)} \quad (8)$$

$$Pe = 6.3 + 0.003 * GR - 2.54 * NPHI - 0.05 * DTc \quad (9)$$

For Peacemaker UL 3023 well, the missing curves are Shallow 'LLS' and Deep Resistivities 'LLD', RHOB, DTC and Pe, figure 9, which can be calculated as follow:

$$LLS = 10^{(-0.11+0.1*\log(GR)-1.45*\log(NPHI))} \quad (10)$$

$$LLD = 10^{(1.3-0.33*\log(GR)-1.2*\log(NPHI))} \quad (11)$$

$$RHOB = 10^{(0.42+1.7*10^{-4}*GR-0.21*NPHI)} \quad (12)$$

$$DTc = 49.7 + 0.05 * GR + 112.5 * NPHI \quad (13)$$

$$Pe = 10^{(0.08+0.1*\log(GR)-0.2*\log(NPHI))} \quad (14)$$

Moreover, the linear regression analysis is applied on Cunning Wolf UL 601 since it has needed curves of both Compressional and Shear Sonic for our geomechanical analysis to predict the missing curve of the Shear Sonic on all wells as shown in figure 10 except Cunning Wolf UL 701 since it has its own Shear sonic curve which can be calculated as follow:

$$DTs = 10^{(0.12+1.06*\log(DTc))} \quad (15)$$

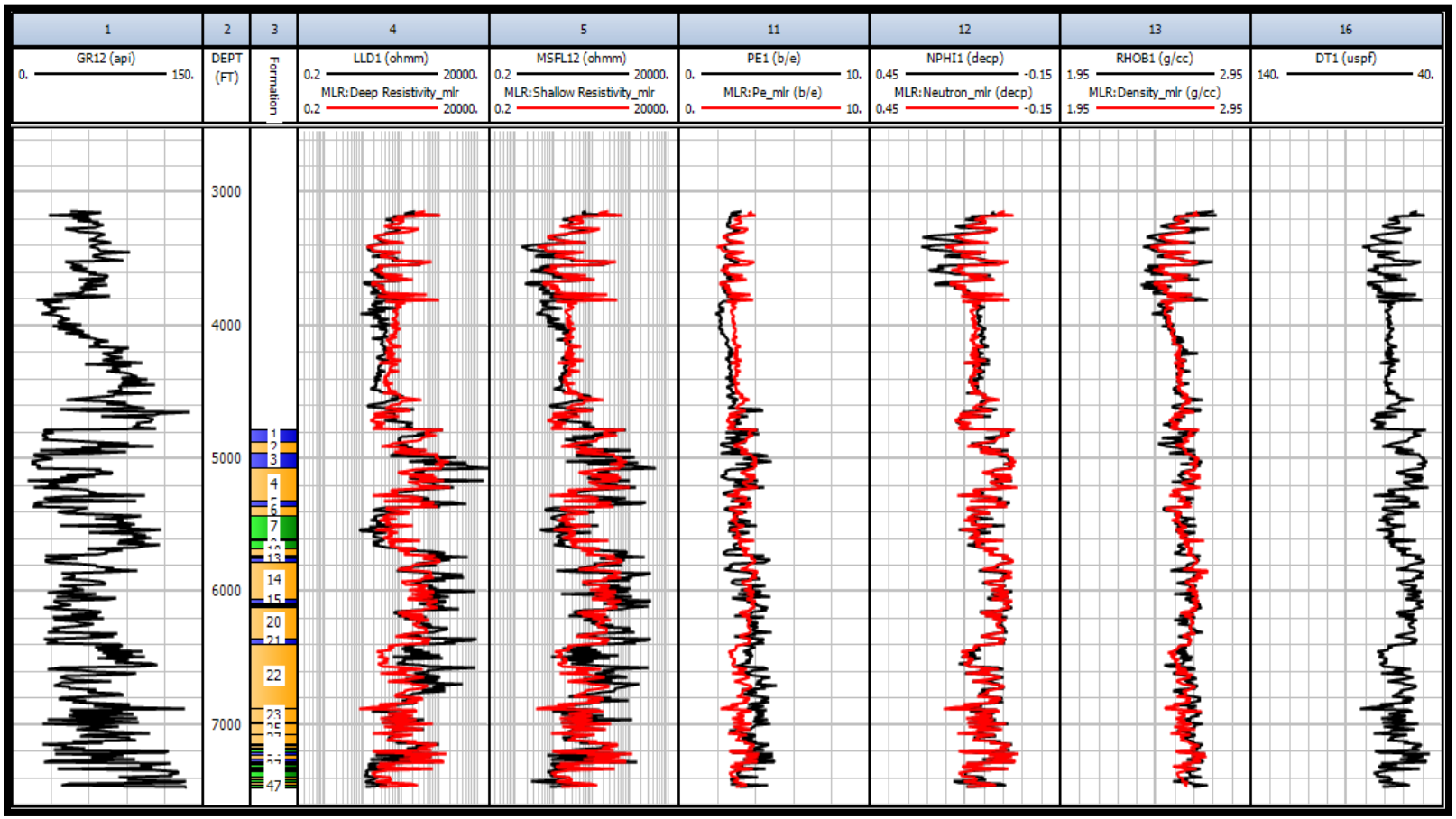

Figure 7. Synthetic curves from GR and DTc of UL 21 Freedom-1 well to be used for Cunning Wolf UL 1801.

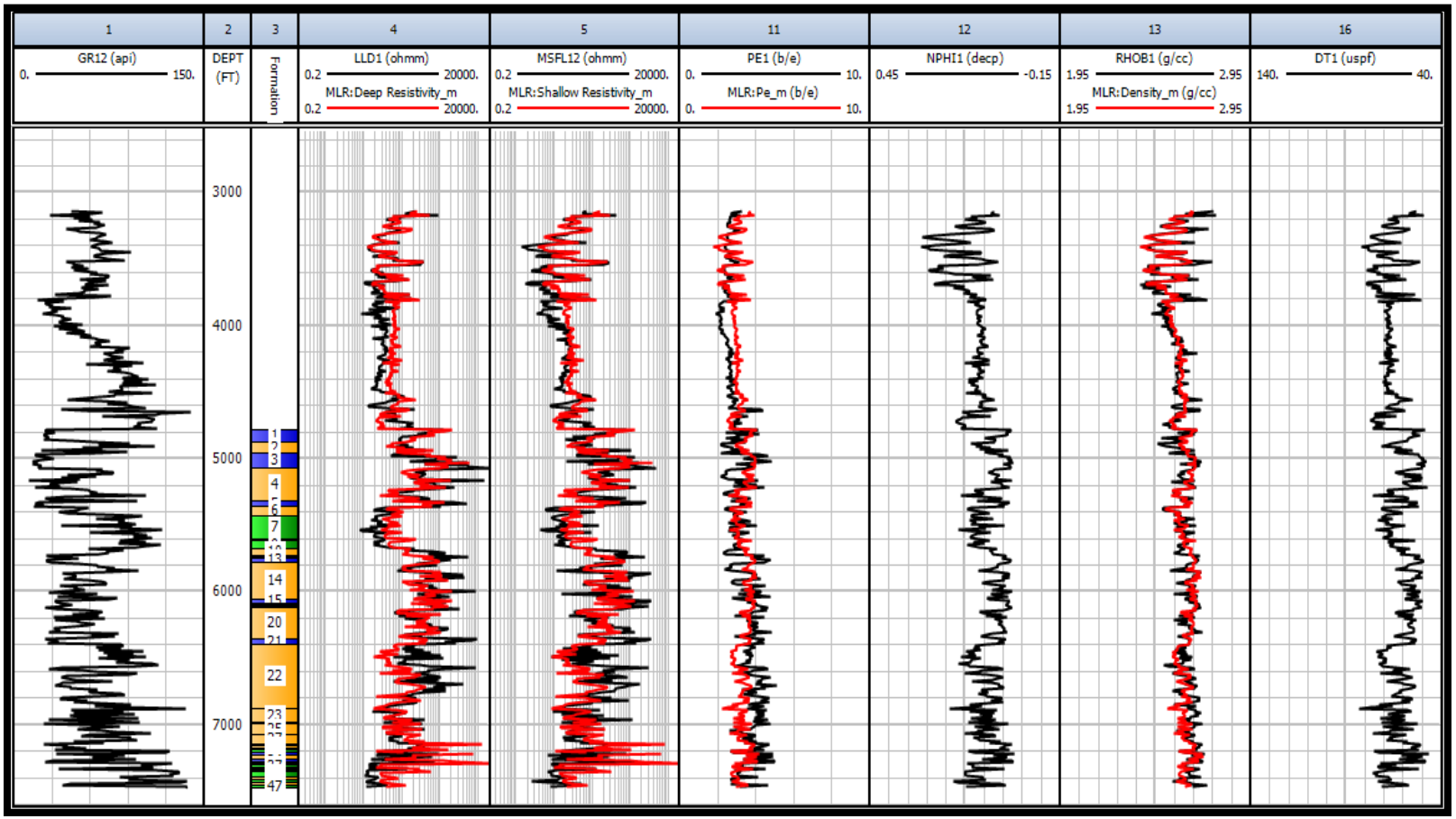

Figure 8. Synthetic curves from GR, NPHI and DTc of UL 21 Freedom-1 well to be used for Cunning Wolf UL 702.

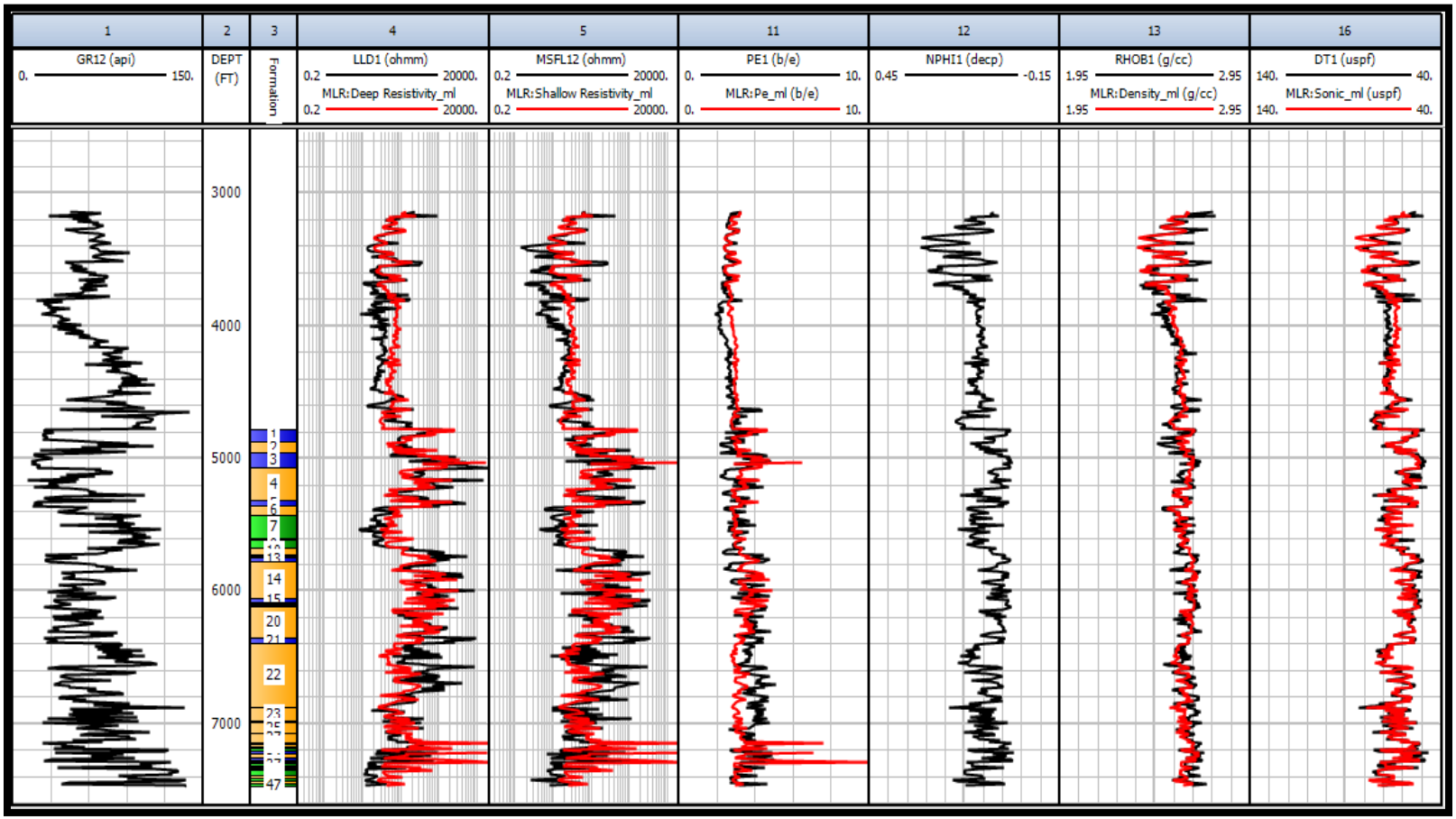

Figure 9. Synthetic curves from GR and NPHI of UL 21 Freedom-1 well to be used for Peacemaker UL 3023.

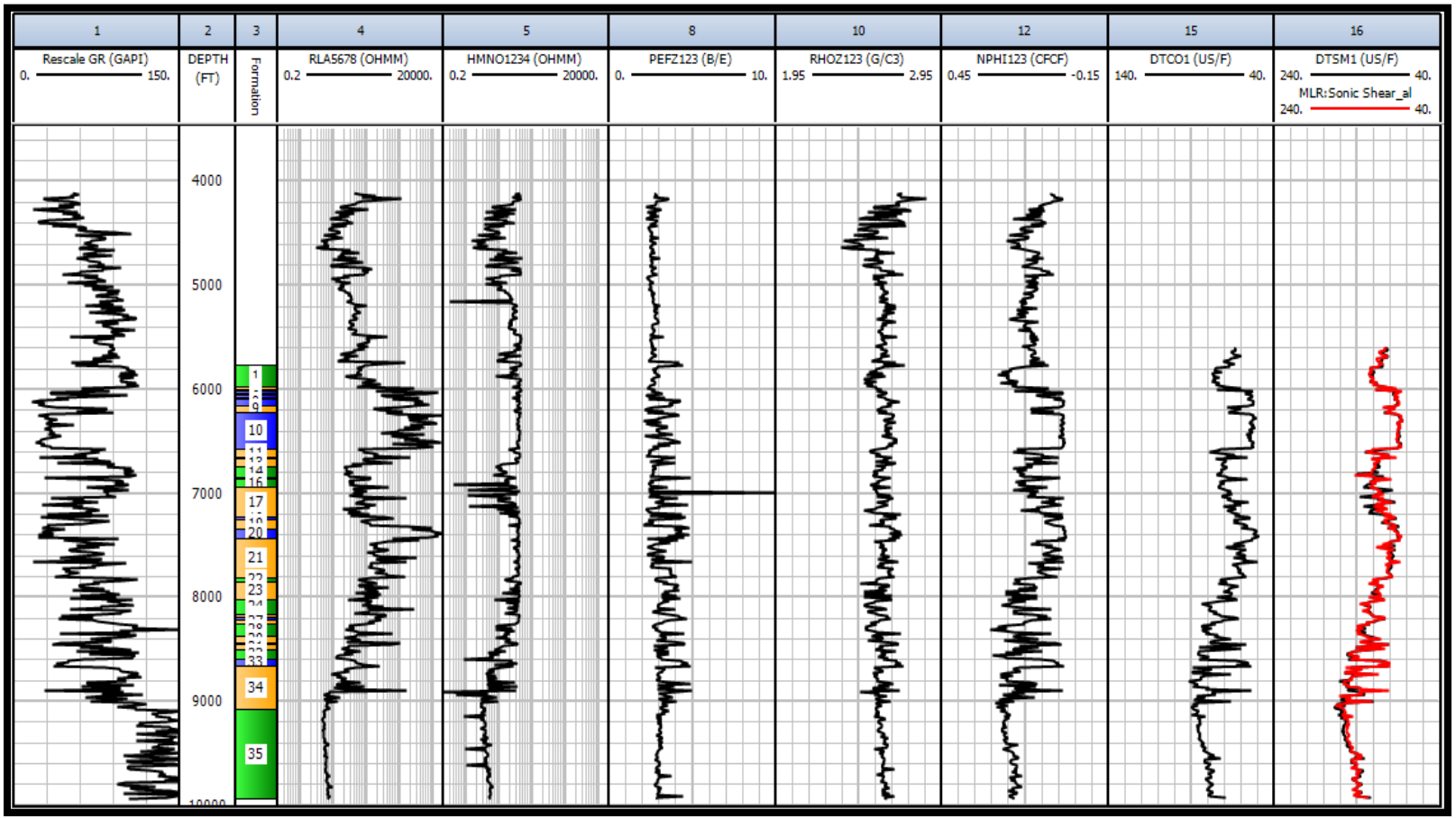

Figure 10. Synthetic curves from DTc of Cunning Wolf UL 601 well to be used for other wells that do not have DTs.

Petrophysical Analysis

Porosity Estimations

Porosity is defined as the fraction of the voids volume over the total volume of a rock and can be measured by wireline logging tools from neutron, density and sonic. For many years, unconventional porosity systems have been poorly understood within the oil industry and within literature. Most of the geologic models used the concept of clay compaction and diagenesis process to propose a complete porosity destruction. Thus, petrologic imaging such as advanced Focused Ion Beam 'FIB' and advanced Scanning Electron Microscope 'SEM' technology provide an image of these nanoscale porosities in unconventional shale plays (Ahmed & Meehan, 2016). Besides, the multiscale reservoir characterization utilizing the above technologies requires integration of well core description and analysis. However, in this project neither SEM nor FIB are available to characterize the nanoscale porosity system as well as missing core description and analysis. In this project, three facies were defined using only petrophysical logs 'limestone compatible scale' with the absence of core description. Those are, cherty limestone 'blue', organic rich mudstone interbedded with shale 'Orange' and shale 'Green', figure 17. Cherty limestone is distinguished by the low GR values and slight separation of neutron and density, density shifted towards low value due to silica presence, while the organic rich mudstone is characterized by the high GR value, due to uranium concertation, and an overly of the density and neutron curves. Shale has high GR values and separation of neutron and density 'Shale Effect', neutron shifted towards high value due to the existence of Clay bound water. Nevertheless, in the

petrophysical and geomechanical analysis UL 21 Freedom well, the reference well, was picked to do detailed analysis in this report and this analysis was repeated on the other six wells of this project.

Porosity from Neutron Tool (NPHI)

When a neutron is emitted from the tool, it propagates into the formation and loses its energy by inelastic scattering interactions. Hydrogen in the pore system controlled the neutron's slowing down, whereas neutron's count rates at the detectors resulted in computing porosity. Thus, the first porosity value 'Φ_N' or 'NPHI' is estimated from neutron log (Ellis & Singer, 2007).

Porosity from Density Tool (DPHI)

Density log determines the density of the formation 'Bulk Density (ρ_b)' by measuring the Gamma Ray attenuation due to Compton scattering between a source and a detector. The porosity is produced from density log as follows:

$$DPHI = \frac{\rho ma - \rho b}{\rho ma - \rho fl} \quad (16)$$

Where ρ_{ma} is the matrix density and ρ_{fl} is the fluid density.

In order to calculate the porosity, density of matrix and fluid density must be known. The matrix type can be defined by the cutting description on the mudlog as well as the photoelectric effect curve. Both Wolfcamp and Bone Spring Formations cuttings description in clean and shaly-clean lithology provide that we are dealing with cherty limestone and organic mudstone respectively. Likewise, the photoelectric effect curve shows a value of almost 5 in a clean interval which represents a limestone matrix. Thus,

the matrix density and drilling fluid 'Brine' density used to calculate density porosity 'DPHI' are 2.71 g/cm^3 and 1.1 g/cm^3, respectively.

Porosity from Acoustic Sonic (SPHI)

Sonic log is also recognized as slowness log or sonic travel time which propagates sound from the source of the tool passing the formation to receivers that relies on the properties of Snell's Law. The porosity is calculated from compressional sonic travel time Wyllie's method which is reliable in consolidated sediments (Ellis & Singer, 2007).

$$SPHI = \frac{\Delta tlog - \Delta tma}{\Delta tfl - \Delta tma} \quad (17)$$

Where Δt_{log} is the transit time from log, Δt_{ma} is the transit time from matrix and Δt_{fl} is the fluid transit time.

As stated above in porosity from density section, the matrix is limestone and the fluid type is brine. Thus, the slowness of limestone used in equation 17 is 47.6 microsec/ft and fluid slowness of brine is 189 microsec/ft.

Porosity from Density and Neutron (NDPHI)

The combination of neutron and density logs in complex lithologies delivers a good porosity estimation. Thus, better porosity estimates are conceivable with the combination rather than using each log separately. Therefore, the density-neutron porosity is calculated from either the cross plot of density and neutron, figures 11-16, or from equation 18 (Ellis & Singer, 2007).

$$NDPHI = \sqrt[2]{\frac{NPHI^2 + DPHI^2}{2}} \quad (18)$$

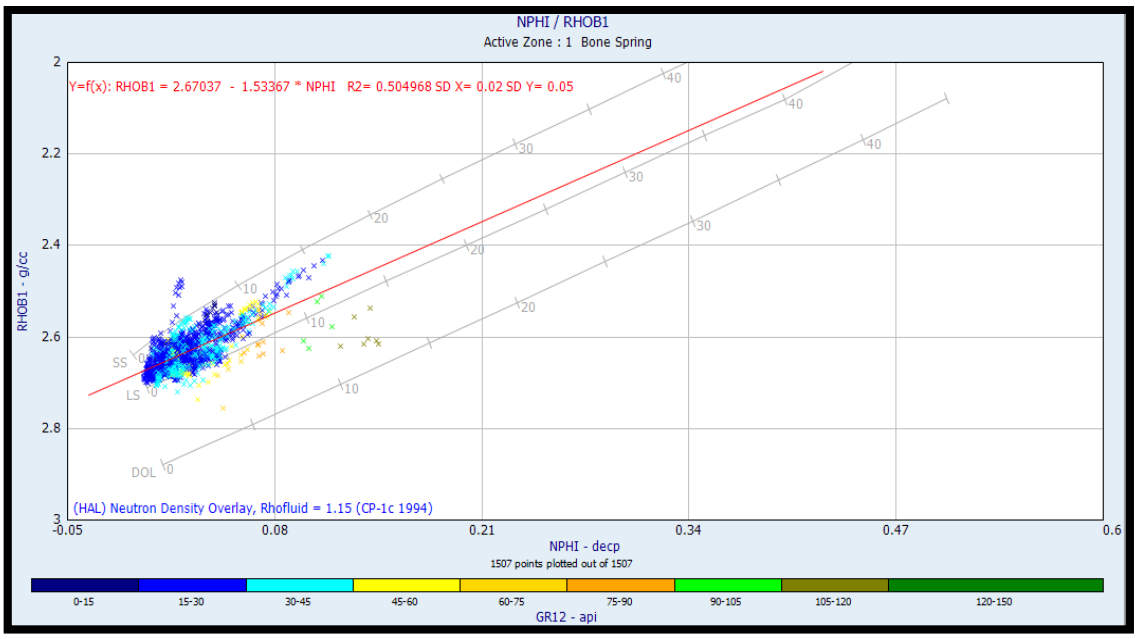

Figure 11. Density-Neutron cross-plot of UL 21 Freedome-1 well of cherty limestone in Bone Spring Formation shows porosity values from 0 to 14 %.

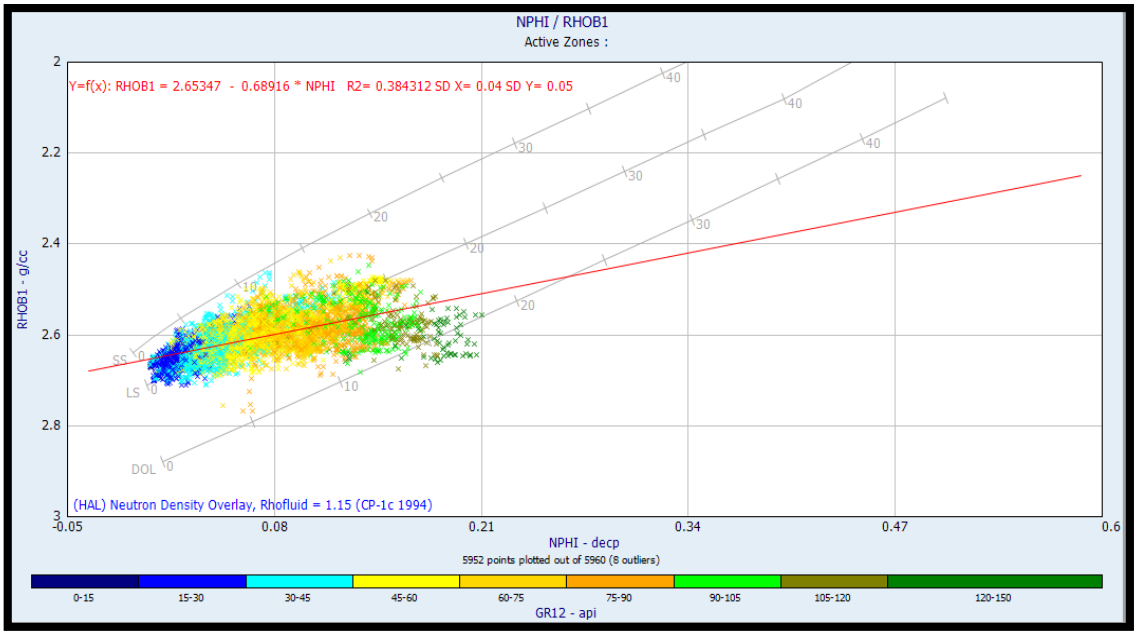

Figure 12. Density-Neutron cross-plot of UL 21 Freedome-1 well of organic rich mudstone in Bone Spring Formation shows porosity values from 0 to 18 %.

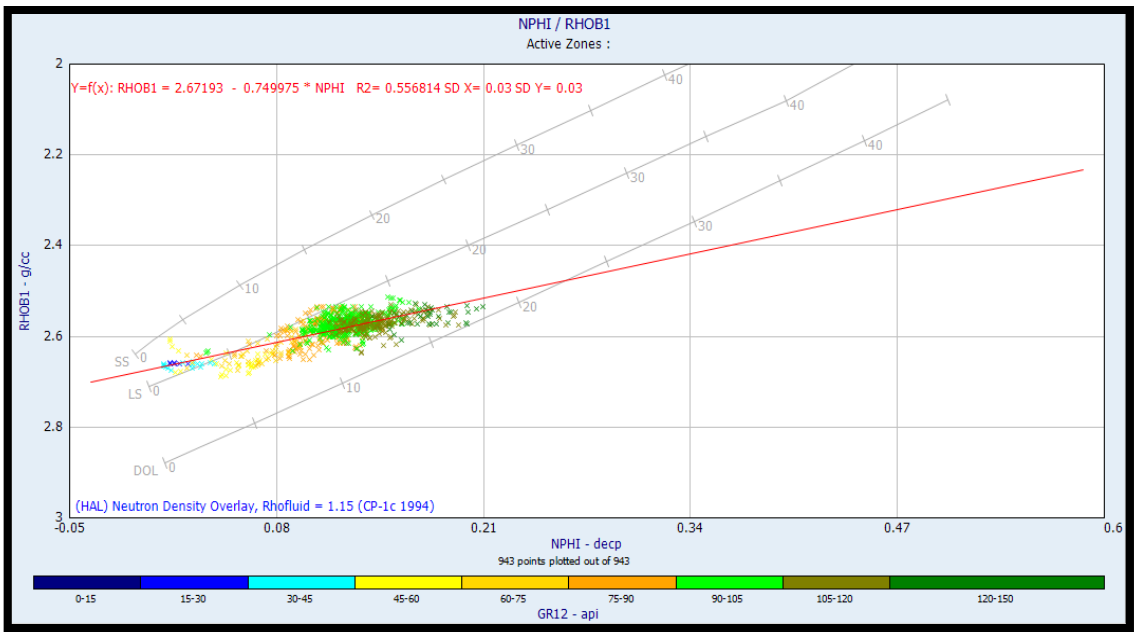

Figure 13. Density-Neutron cross-plot of UL 21 Freedome-1 well of the shale in Bone Spring Formation shows porosity values from 2 to 18 %.

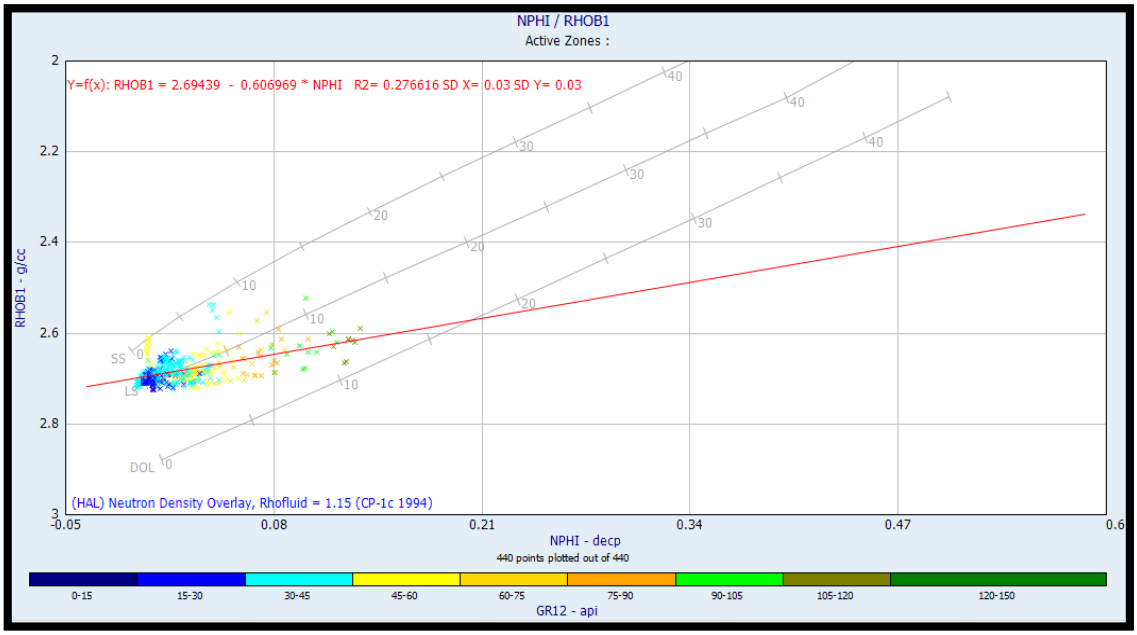

Figure 14. Density-Neutron cross-plot of UL 21 Freedome-1 well of the cherty limestone in Wolfcamp Formation shows porosity values from 0 to 12 %.

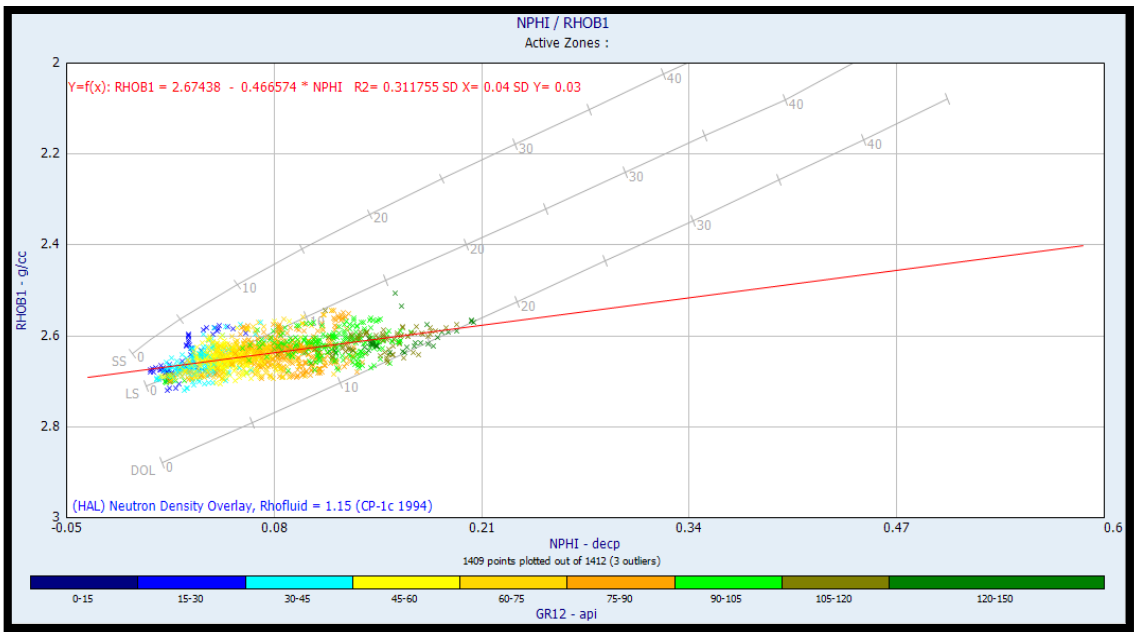

Figure 15. Density-Neutron cross-plot of UL 21 Freedome-1 well of the organic rich mudstone in Wolfcamp Formation shows porosity values from 0 to 17 %.

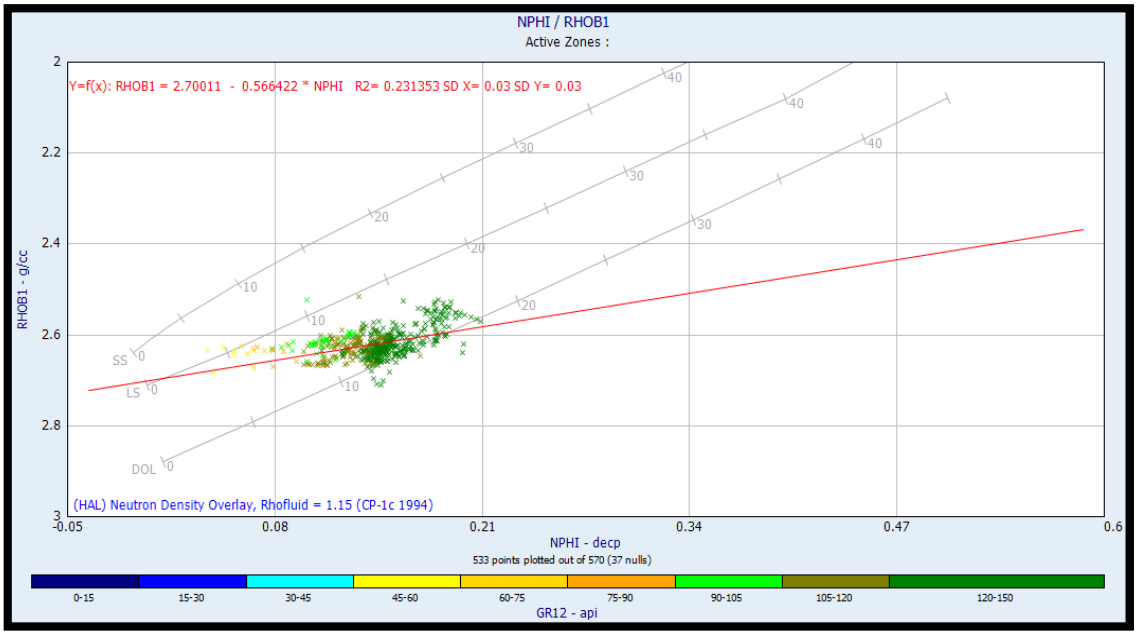

Figure 16. Density-Neutron cross-plot of UL 21 Freedome-1 well of the shale in Wolfcamp Formation shows porosity values from 3 to 17 %.

Porosity from Neutron, Density and Sonic (AVGPHI)

Taking the average of the three calculated porosities is another method in reducing the high neutron porosity value, especially in shale due to clay bond water and provide a legitimate porosity prediction.

$$AVGPHI = \frac{NPHI+DPHI+SPHI}{3} \quad (19)$$

Porosity from density seems to be the best porosity estimation that fit the data interpretation and porosity from core measurements and will be evaluated during the prediction of the two exponents, cementation 'm' and saturation 'n' utilizing Pickett plot in the water saturation calculation section. Moreover, in Bone Spring and Wolfcamp formations the cherty limestone facies have lower porosity estimation than the organic rich mudstone does, figure 17.

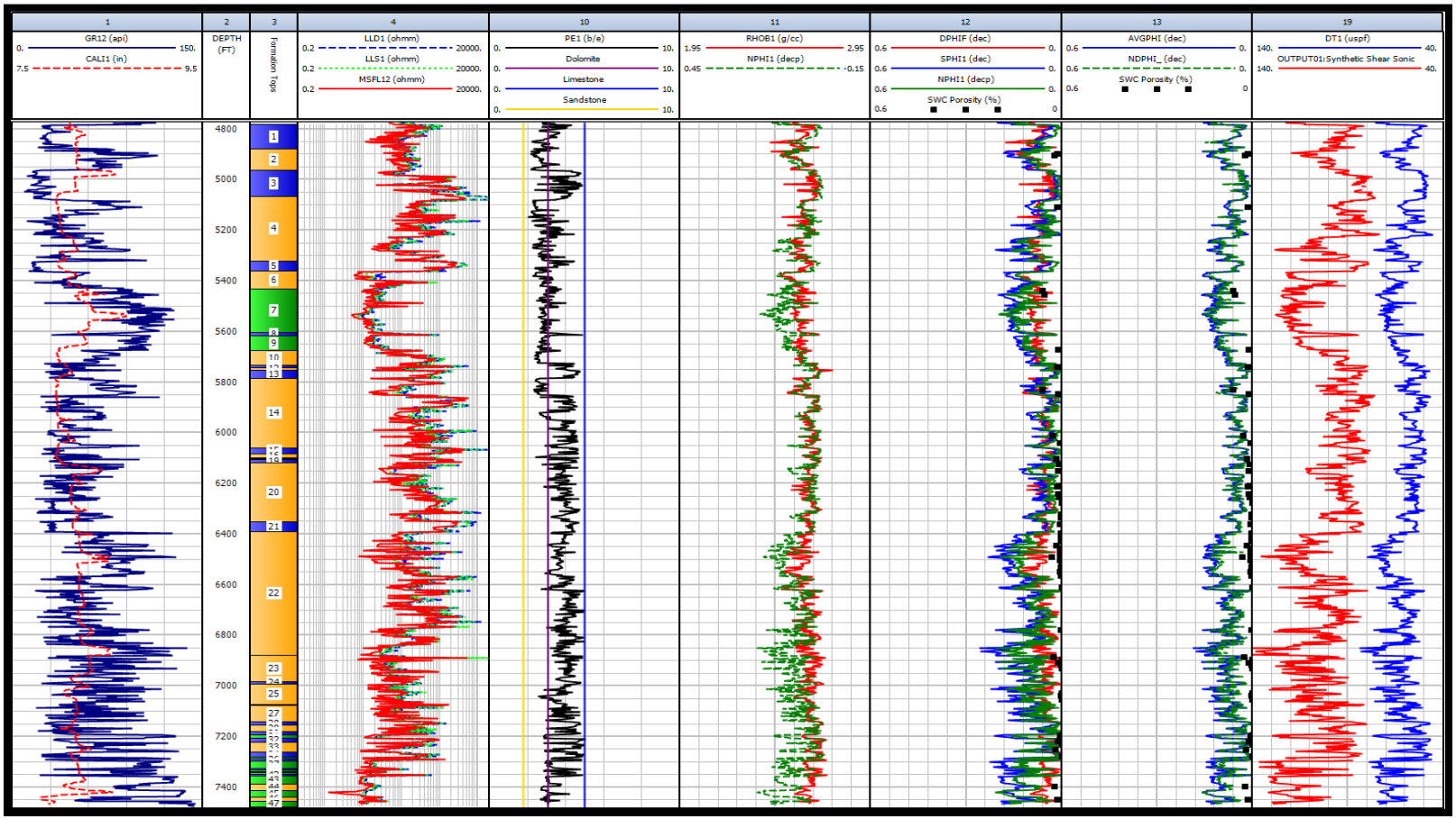

Figure 17. Porosity estimations of UL 21 Freedom-1 well from density, neutron, sonic in track 12, neutron-density and average of the three tools in track 13.

Permeability Estimation

Generally, permeability has a weak correlation with porosity in carbonate reservoirs due to the diagenesis effect; while in sandstone reservoirs it shows better correlation. In this project, we are dealing with tight cherty limestone and organic mudstone interbedded with shale and should expect a weaker correlation between the measured porosity and measured permeability 'nano-darcy' than in sandstone reservoirs. In Sidewall Core Measurement, measured porosity is given as a total porosity and measured permeability is given as air and klinkenberg permeabilities. Air permeability always shows higher values than klinkenberg due to the slippage 'grain surface' that results in a greater flow rate at a given pressure differential for the gas. In order to determine permeability from porosity, a cross plot of the measured porosity and measured permeability from SWC is required to calculate permeability from wireline log porosity (Amirov, 2016). In conventional reservoirs, the cross plot of porosity 'PHI' and permeability 'K' shows segregation 'groups of facies' in scattered data where we can classify the porosity type of each facies and predict the permeability. While in unconventional reservoirs such as Wolfcamp and Bone Spring Formations, the data are distributed all over the cross plot and groups of facies are difficult to categorize thus equation 20 is not adopted in this project, figure 18. Therefore, the missing mineral 'XRD' and elemental 'XRF' composition analysis are required along with core description to identify the facies and get better permeability correlation.

$$K = 0.0046 * PHI + 0.0362 \quad (20)$$

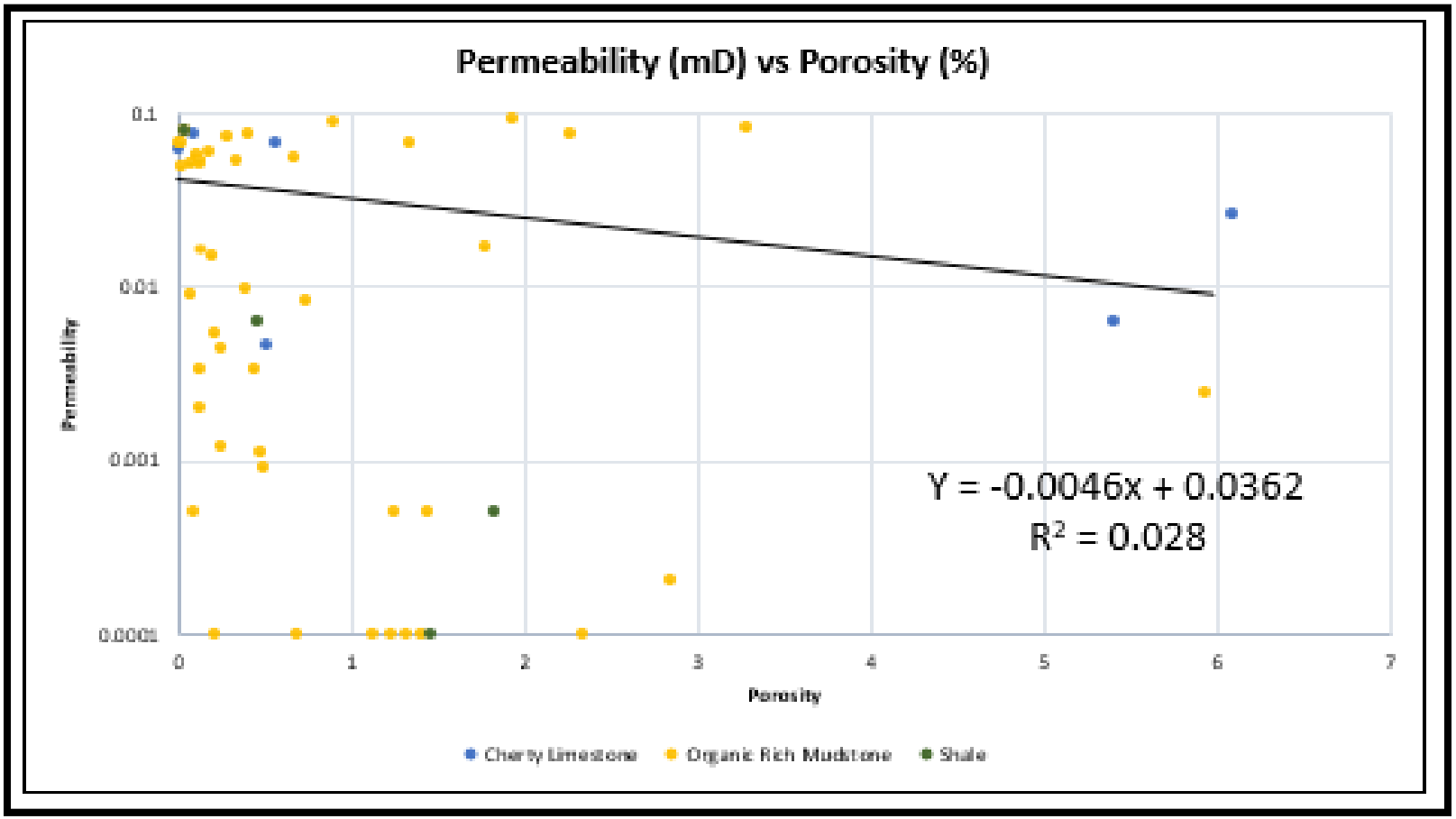

Figure 18. Cross-plot of UL 21 Freedom well Sidewall Core porosity and permeability.

Water Saturation Estimation

Water saturation estimation of porous rocks from petrophysical logs has been a useful tool of formation evaluation since Archie in 1942. He revealed a relationship between resistivity, porosity and water saturation 'Sw' for unconsolidated sandstone. This sandstone is moderately homogeneous, fully water saturated and consists of almost equidimensional grains. The discovered relationship is represented as follow:

$$Sw = \sqrt[n]{\frac{Rw}{Rt * PHI^{(m)}}} \tag{21}$$

Where Rw is the water 'brine' resistivity, Rt is the true resistivity or resistivity of a rock that is partially saturated with water, PHI is the porosity, m is the cementation factor and n is the saturation factor. Archie showed that the ratio of fully water saturated rock resistivity 'Ro' to the brine resistivity 'Rw' was a constant for any rock sample and provided a constant name of resistivity formation factor 'F' in uninvaded zone (Archie, 1942).

$$F = \frac{Ro}{Rw} \tag{22}$$

He also displayed a strong linear relationship between the resistivity formation factor in logarithmic scale 'F' and porosity 'PHI' and defined the slope of the line as the cementation factor 'm' with a value of 2.

$$F = \frac{1}{PHI^{(m)}} \tag{23}$$

In the same paper, he figured out that the ratio of partially water saturated rock resistivity 'Rt' to the fully saturated water resistivity 'Ro' has a relationship to the

fractional water saturation and stated the slope as a saturation factor ‘n’ with a value of 2 (Archie, 1942).

$$\frac{Rt}{Ro} = \frac{1}{\sqrt[n]{Sw}} \quad (24)$$

Grouping equations 22, 23 and 24 delivers Archie’s equation as stated in equation 21. However, in order to predict water saturation value using Archie’s equation Rw, m and n must be solved. Formation water resistivity ‘Rw’ can be calculated from Spontaneous Potential logs ‘SP’ which are not available in all the wells but the only way to calculate ‘Rw’ in this project is by the Resistivity Ratio method. In a water bearing zone that is invaded by drilling fluid, water saturation ‘Sw’ should be equal to 1 which is equal to the Resistivity of the invaded zone ‘Sxo’. By eliminating saturations and porosity we will be left out with equation 25, (Ellis & Singer, 2007 & Amirov, 2016).

$$\frac{Ro}{Rw} = \frac{Rxo}{Rmf} \quad (25)$$

In UL 21 Freedom-1 well, resistivity of mud filtrate ‘Rmf’ at surface temperature is provided but has to be converted to the bottom hole temperature, shallow resistivity ‘Rxo’ and deep resistivity ‘Ro’ are known variables in the wireline logs. Thus, Rw was calculated in 5 different invaded zones in both formations and came up with a result of 0.049 ohmm which is close to University Lands Rw of 0.05 ohmm.

Moreover, Archie’s equation does not provide a correct saturation determination when used in heterogeneous lithology unless both cementation factor ‘m’ and saturation factor ‘n’ are verified and calibrated with laboratory data (Harrick & Kennedy, 2009). In this project, those factors were not measured in the laboratory, but it can be estimated by the Pickett plot ‘a log-log illustration of porosity and resistivity’. In this plot, water

saturation is illustrated by a series of lines with a slope equal to m and separation of these lines equal to n. The cementation factor ‘m’ and saturation factor ‘n’ were estimated in the three defined facies of Bone Spring and Wolfcamp formations using Pickett plot.

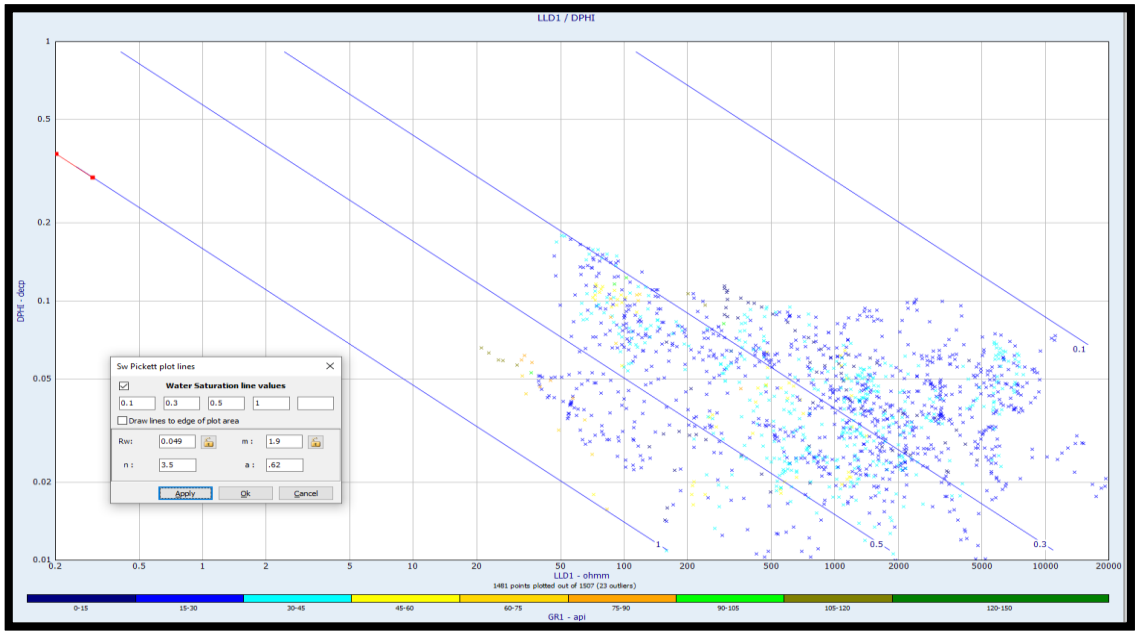

Figure 19. Pickett plot of cherty limestone in Bone Spring formation of UL 21 Freedom-1 well, cementation factor ‘m’ is 1.9 and saturation factor is 3.5.

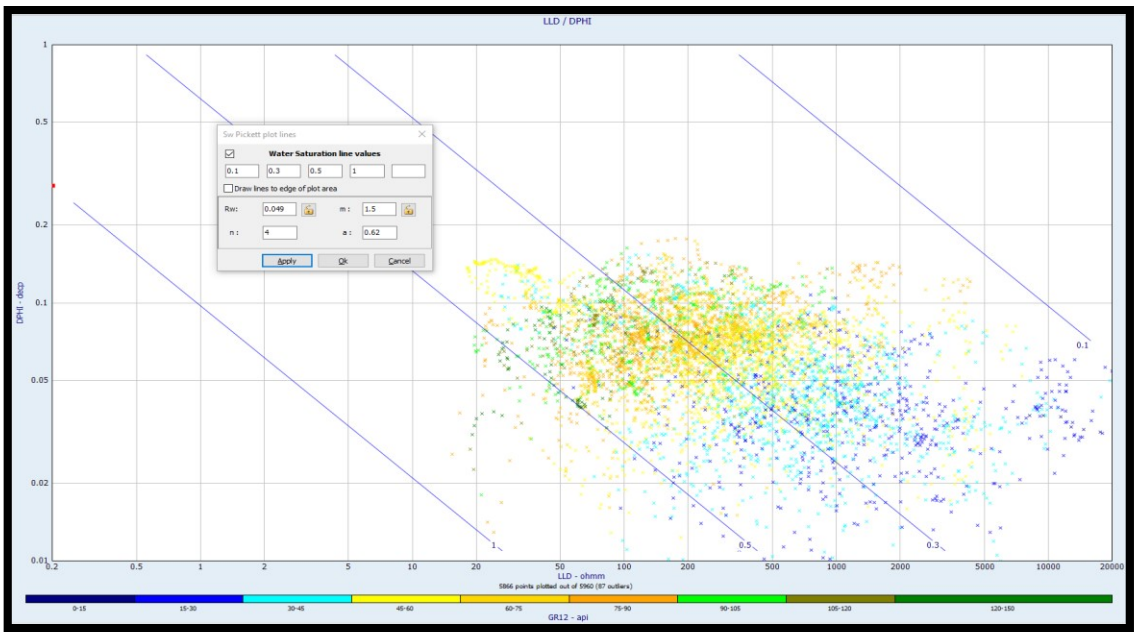

Figure 20. Pickett plot of organic rich mudstone in Bone Spring formation of UL 21 Freedom-1 well, cementation factor ‘m’ is 1.5 and saturation factor is 4.

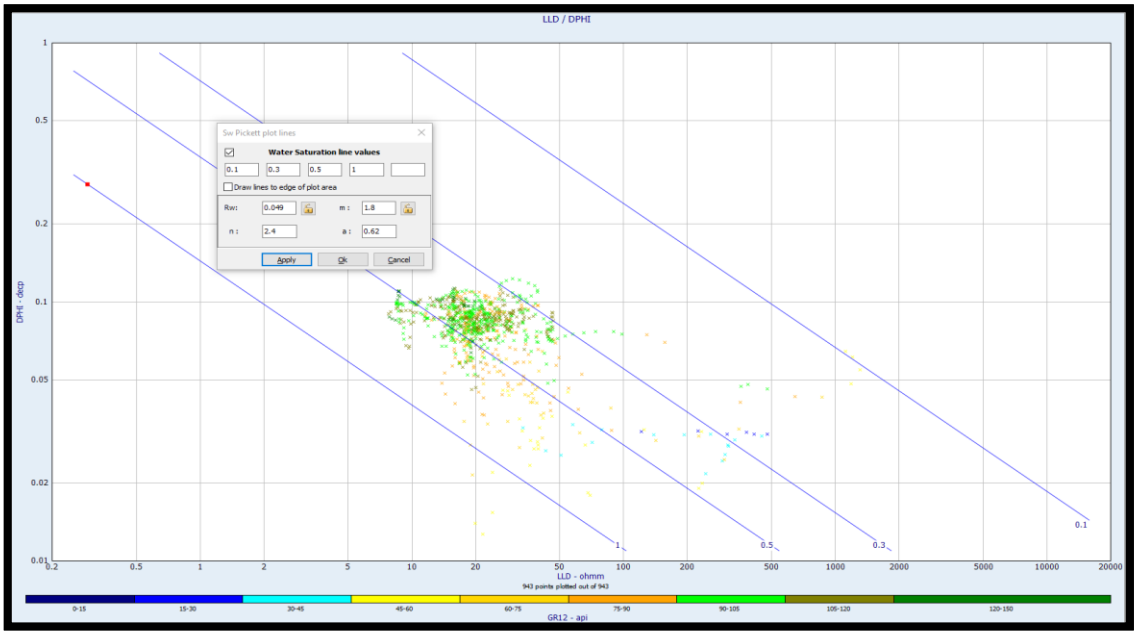

Figure 21. Pickett plot of shale in Bone Spring formation of UL 21 Freedom-1 well, cementation factor ‘m’ is 1.8 and saturation factor is 2.4.

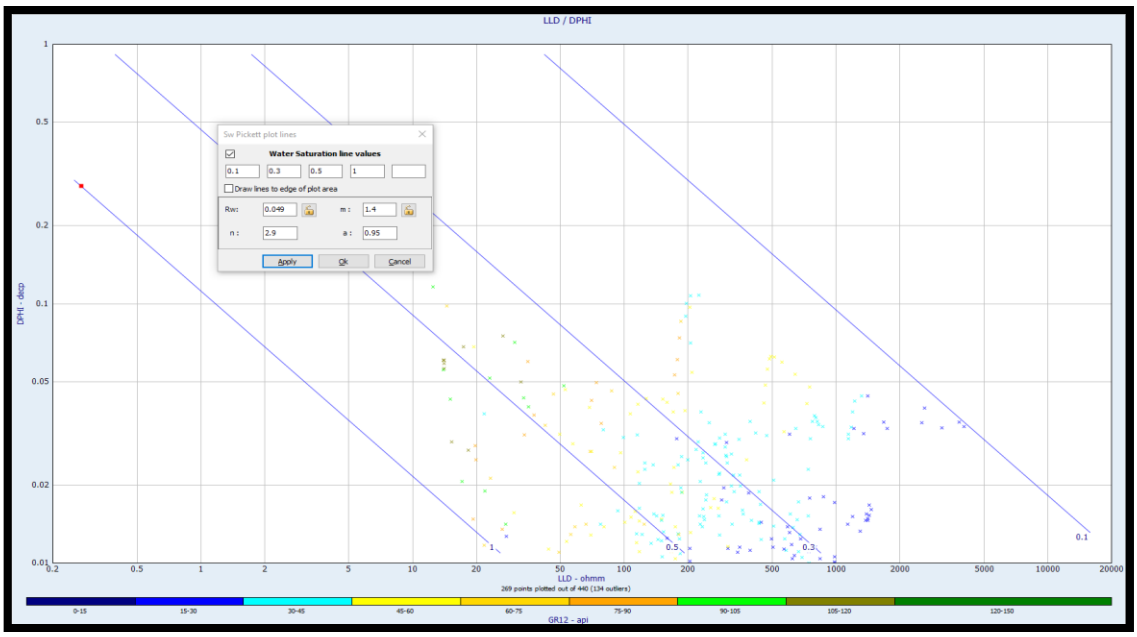

Figure 22. Pickett plot of cherty limestone in Wolfcamp formation of UL 21 Freedom-1 well, cementation factor 'm' is 1.4 and saturation factor is 2.9.

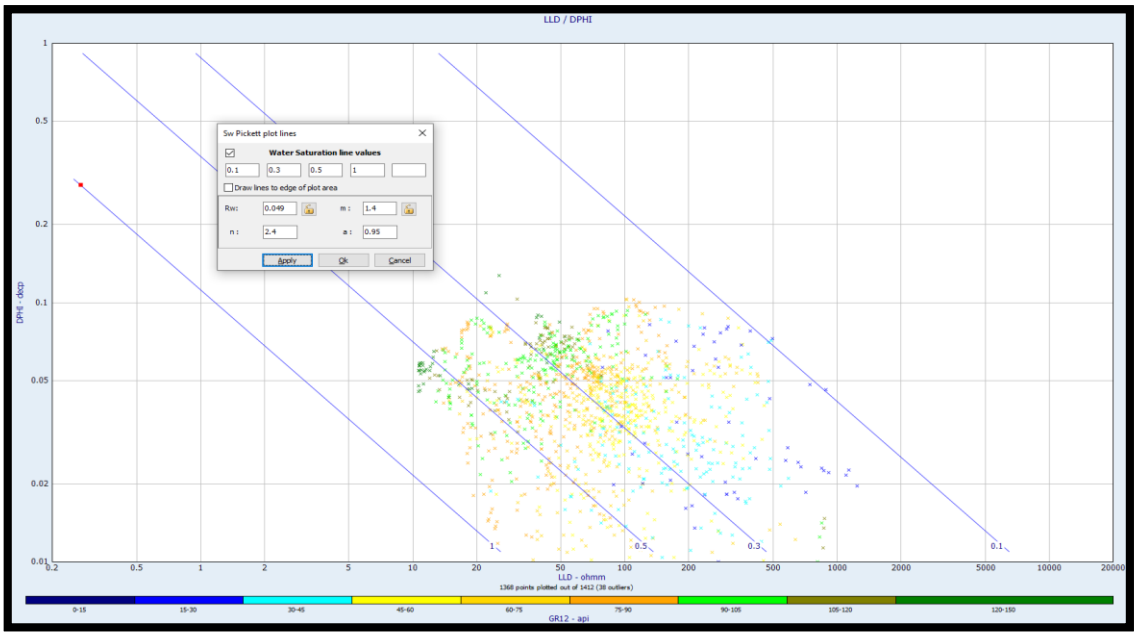

Figure 23. Pickett plot of Organic rich mudstone interbedded with shale in Wolfcamp formation of UL 21 Freedom-1 well, cementation factor 'm' is 1.4 and saturation factor is 2.4.

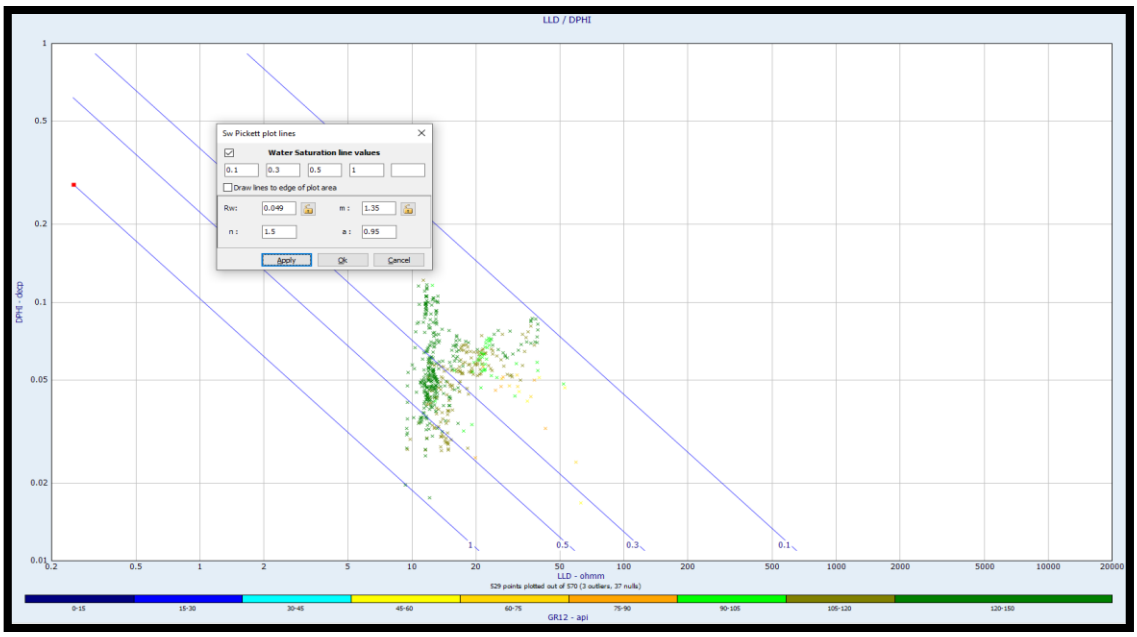

Figure 24. Pickett plot of shale in Wolfcamp formation of UL 21 Freedom-1 well, cementation factor ‘m’ is 1.35 and saturation factor is 1.5.

In Pickett plot analysis of UL 21 Freedom-1 well, saturation factor ‘n’ found to be higher than 2 in the cherty limestone and organic rich mudstone zones of both formations which indicates that the rock matrix has resistive fluid ‘oil wet’ matured organic matter in the matrix, as seen in figures 19, 20, 22 & 23, while shale in Wolfcamp formation has saturation factor ‘n’ around 2 which means the rock matrix has conductive fluid ‘water wet’ due to the presence of clay bound water, figures 21 & 24. Having all the variable in Archie’s equation, water saturation can be calculated separately in each facies of both formations using density porosity because Density-Neutron porosity and average porosity do not fit the data interpretation in the picket plot, they are out of the water saturation lines range.

The estimation of hydrocarbon saturation from water saturation is not a proper method to be used in unconventional reservoirs but due to data limitations the method was used, water saturation estimation is shown figure 25. In order to determine the hydrocarbon saturation in the unconventional resources, the nature of storage and transportation of hydrocarbon within the mudrock system must be investigated. A better grasp and knowledge of the kerogen system, facies and their storage must be demonstrated to state their capacity whether to keep or release the hydrocarbon (Ahmed & Meehan, 2016).

Furthermore, water saturation was calculated based on the estimation of cementation and saturation exponents from Pickett plot and on the prediction of formation water resistivity in the invaded zones. As a result, the estimated water saturation in Bone Spring and Wolfcamp formations is around 30% to 40% in Wolfbone field which agrees with the high-water production that was recorded from the nearby field along the same intervals.

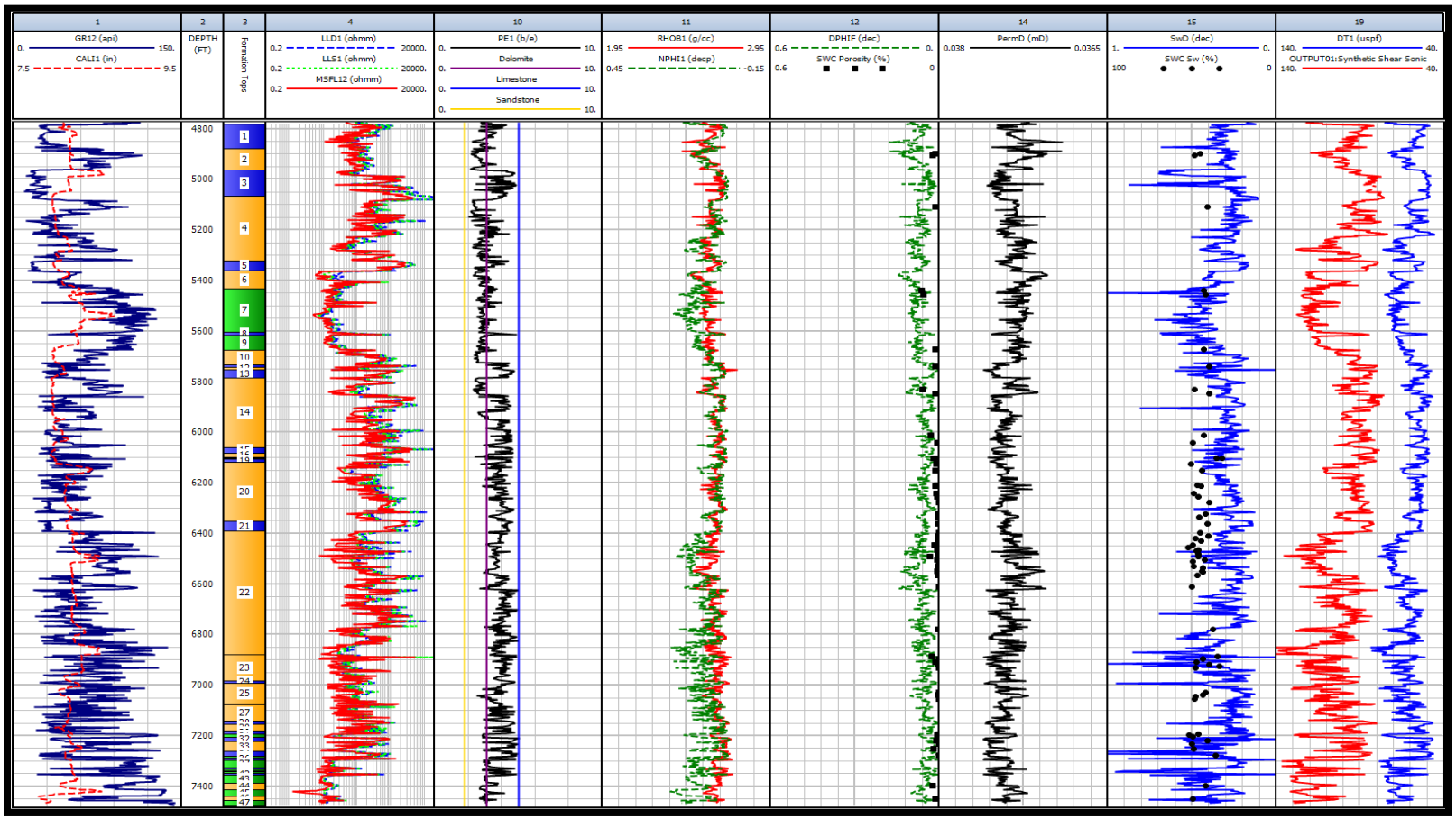

Figure 25. Calculated water saturation of each facies in both formation of UL 21 Freedom-1 well in track 15.

Geomechanical Analysis

Brittleness Index Determinations

Brittle rocks break without significant plastic deformation when they are under stress and can absorb small energy prior to fractures. Generally, brittleness is predicted from laboratory measurements of stress-strain, properties of rocks and analysis of mineral contents using well logs. This brittleness index can support Geoscientists and Engineers to define their best horizontal zones in terms of developing hydraulic fractures to maximize the flow of fluid 'permeability' and to enhance hydrocarbon production. Accordingly (Rickman, et al., 2008) utilized elastic parameters of Poisson's Ratio 'PR' and Young's Modulus 'YM' to provide the concept of rock brittleness index. Poisson's Ratio defines the ability of rocks to fail under stress while Young's Modulus describes the ability to maintain the fracture open once the material is fractured. In their work (Rickman, et al., 2008), it is assumed that high Young's Modulus and low Poisson Ratio indicate more brittle rock. Rickman's equations are as follow:

$$YM_{BRIT} = \frac{YM-1}{8-1} * 100 \quad (26)$$

Where 1 and 8 are Rickman et al lowest and highest values of Young's Modulus in their data range.

$$PR_{BRIT} = \frac{PR-0.4}{0.15-0.4} * 100 \quad (27)$$

Where 0.4 and 0.15 are Rickman et al highest and lowest values of Poisson's Ratio in their data range.

$$Brittleness\ Index = \frac{YM\_BRIT + PR\_BRIT}{2} \quad (28)$$

The above equations were used to compute the Poisson's Ratio and Young's Modulus in Bone Spring and Wolfcamp formations of UL 21 Freedom-1 well but with different minimum and maximum values of PR and YM that represent Bone Spring and Wolfcamp data set. The minimum value used for YM in Bone Spring is 3.07 and the maximum value used is 11.9 while the minimum value used for PR in the same formation is 0.039 and the maximum value is 0.29, figure 26. However, in Wolfcamp formation the minimum value used for YM is 3.59 and the maximum value is 10.6 while the minimum and maximum values for PR are 0.136 and 0.329 respectevely as shown in figure 27.

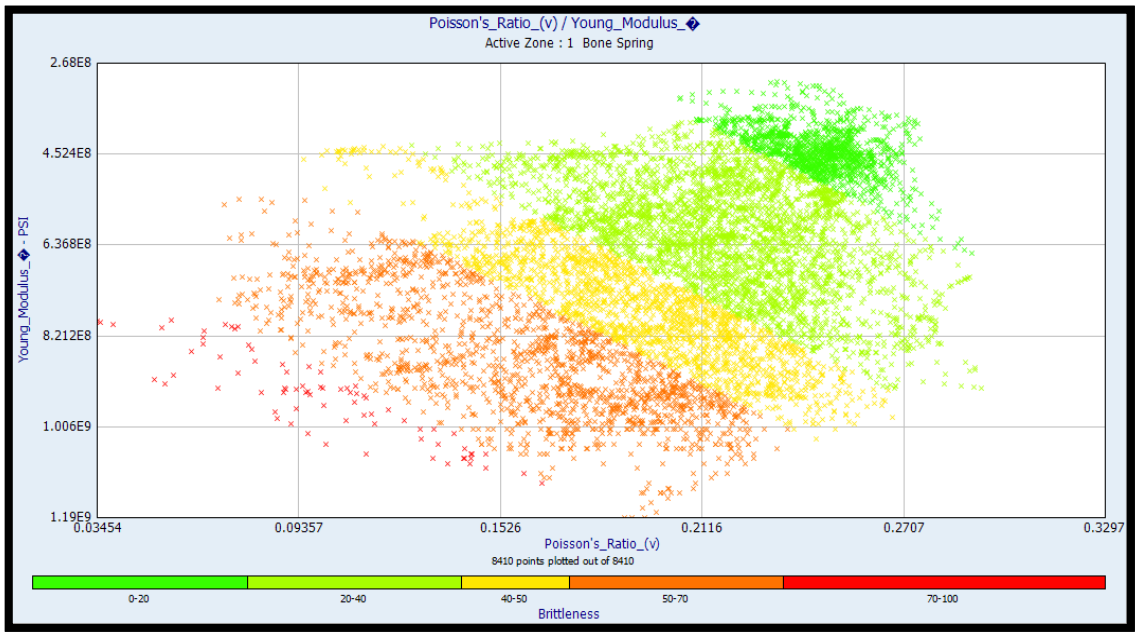

Figure 26. Cross plot of Bone Spring Formation Young's Modulus and Poisson's Ratio in UL 21 Freedom-1 well.

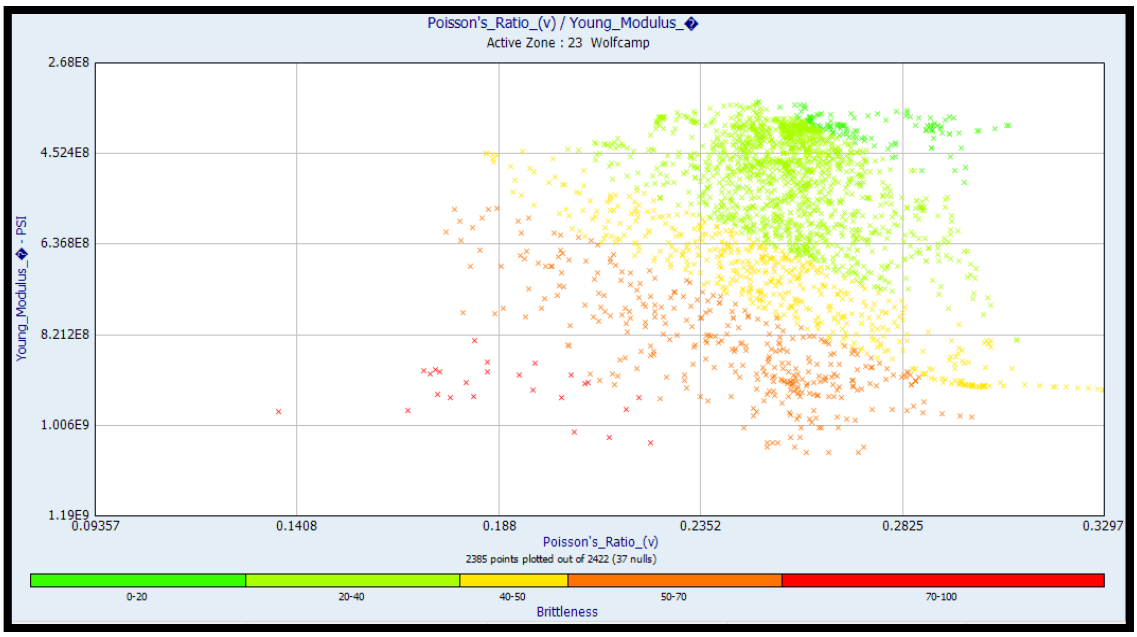

Figure 27. Cross plot of Wolfcamp Formation Young's Modulus and Poisson's Ratio in UL 21 Freedom-1 well.

Brittleness index can be calculated differently using (Goodway, et al., 2010). He proposed that the best fracable intervals can reside in a low Lambda 'λ' "Incompressibility" and high Shear Modulus 'μ' "rigidity" and their equation is as follow:

$$Brittleness\ Index = \frac{\lambda+2*\mu}{\lambda} \quad (29)$$

In order to use equations 26, 27 and 29, the next equations are required to solve (White, 1983):

$$Velocity\ of\ Compressional\ Wave\ (Vc) = \frac{10^6}{DTc} \quad \text{(ft/s)} \quad (30)$$

$$Velocity\ of\ Shear\ Wave\ (Vs) = \frac{10^6}{DTs} \quad \text{(ft/s)} \quad (31)$$

$$Poisson's\ Ratio\ (\nu) = \frac{(0.5*(\frac{Vc}{Vs})^2)-1}{(\frac{Vc}{Vs})^2-1} \quad (32)$$

$$Shear\ Modulus\ (\mu) = RHOB * Vs^2 \quad \text{(Psi)} \quad (33)$$

$$Young's\ Modulus\ (E) = 2 * \mu * (1+\nu) \quad \text{(Psi)} \quad (34)$$

$$Bulk\ Modulud\ (K) = RHOB * (Vc^2 - (\frac{4*Vs^2}{3}) \quad \text{(Psi)} \quad (35)$$

$$Compressibility\ (cb) = \frac{1}{K} \quad \text{(1/Psi)} \quad (36)$$

$$Lambda\ (\lambda) = RHOB * (Vc^2 - 2 * Vs^2) \quad (37)$$

Both models of Rickman's and Goodway's are used for estimating a brittleness index to have a confident geomechanical interpretation. In UL 21 Freedom-1 well, they seem to be compatible with high brittleness index especially in the low GR zones and low brittleness index in the high GR zones, figure 28 shows Rickman's brittleness in blue and Goodway's brittleness index in black in the last track.

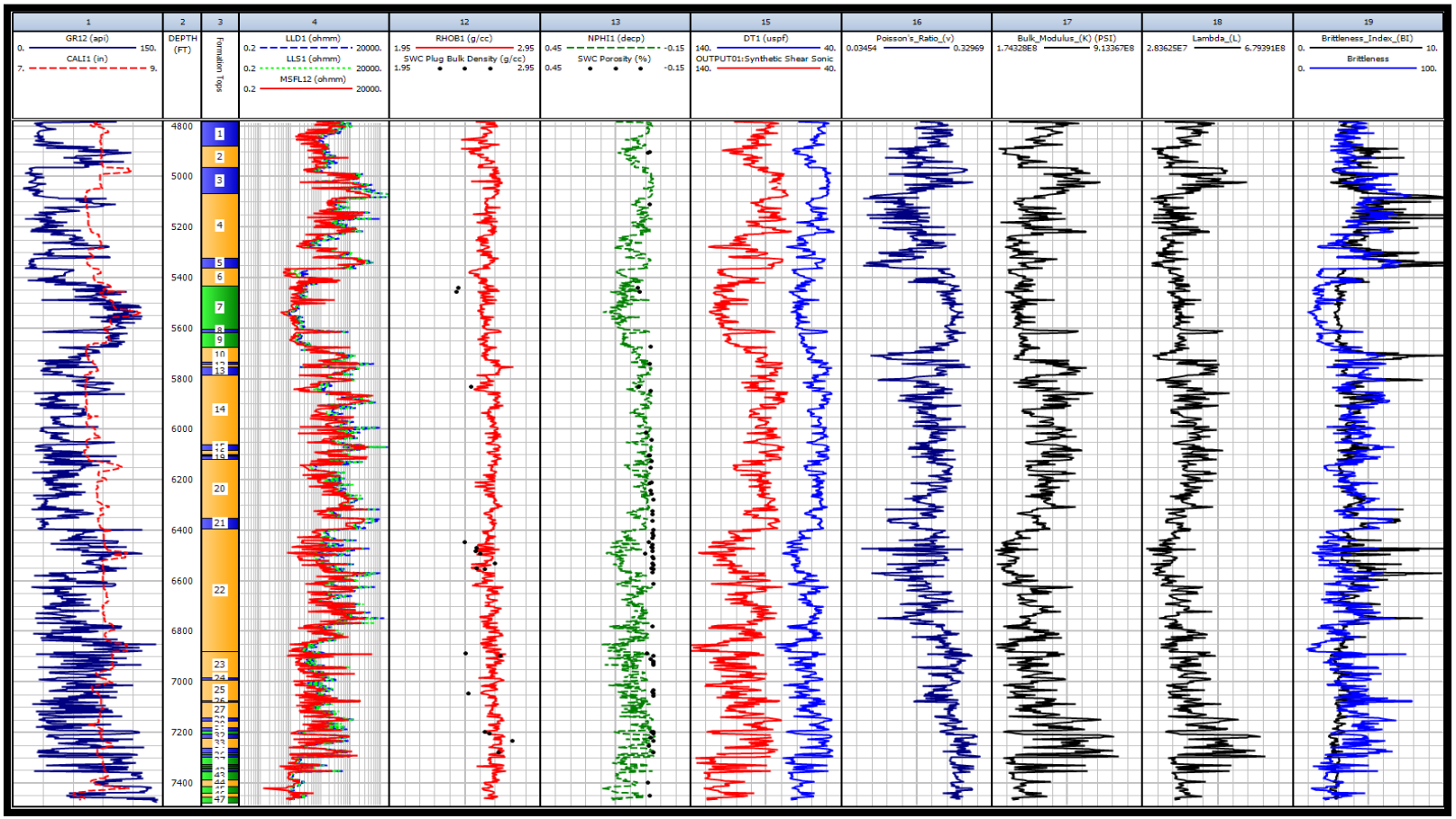

Figure 28. Brittleness (Rickman) and Brittleness Index (Goodway) of UL 21 Freedom-1 well in track 19.

Formation Evaluation Per Well

UL 21 Freedom-1

The thickness of Bone Spring formation is around 2,100 ft with a range of porosity from 0 to 18 %. The high porosity values correspond to the organic rich mudstone facies while the low porosity values represent part of the cherty limestone interval as well as shale interval. Bone Spring formation has a range of water saturation from 0 to 100 % with an average value of 40 %. Shale usually tends to have high water saturation due to the presence of clay bound water while cherty limestone and organic rich mudstone illustrate low water saturation reading. Although permeability curve was generated from a weak correlation from porosity, it shows low permeability 'tight' on the shale intervals while the cherty limestone and organic rich mudstone display relatively high permeability. This could be from microfracture systems that perhaps generated during hydrocarbon generation. Furthermore, brittleness index increases in cherty limestone and organic rich mudstone due to carbonate and silica mineral compositions which calibrated with the drilling cutting description from the mud log.

The penetrated interval of Wolfcamp is approximately 600 ft, it has a range of porosity from 0 to 15 % with an average value of 7 %. Based on the porosity prediction of both formations, Wolfcamp has lower porosity than Bone Spring does. The high clay content in Wolfcamp formation is a good reason of having this low average porosity value. Water saturation has a range of 0 to 100 % with an average value of almost 30%. Brittleness index fluctuates between 10 % to 68 % with tiny intervals of brittle rocks 'limestone and mudstone' interbedded with ductile rock 'shale', figure 30.

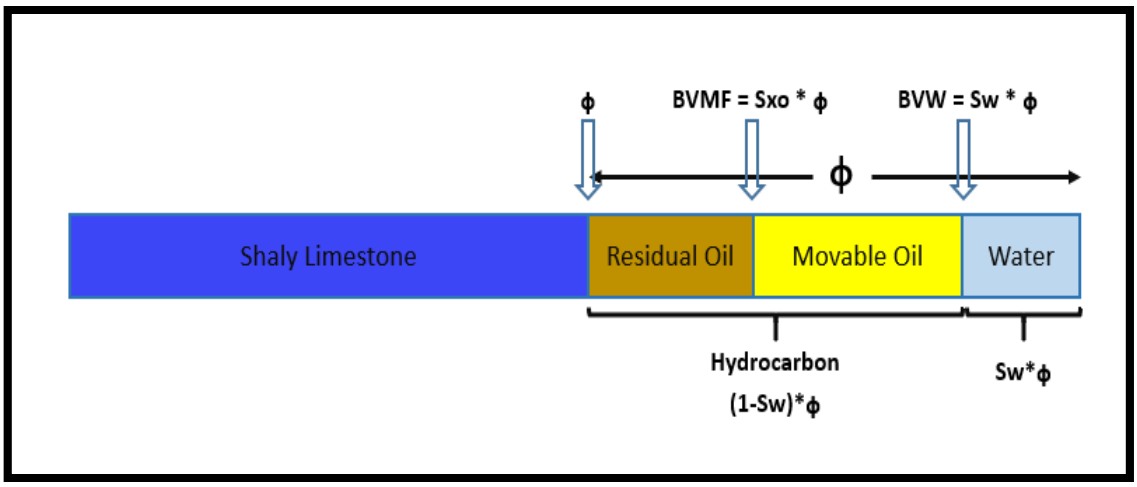

Figure 29. Volumetric estimation of bulk volume of mud filtrate 'BVMF', bulk volume of water 'BVW', and water with hydrocarbon 'Movable and Residual' in the pore system reprinted from (Kennedy, 2019).

Using the equations and illustration from figure 29, movable oil can be found only in few intervals of organic rich mudstone at almost 600 to 800 feet from the top of Bone Spring formation 'highlighted in green' while residual oil 'highlighted in orange' covers most of the intervals, figure 30. Residual oil and irreducible at wellbore left behind when mud filtrate flushed all the movable fluid in the invaded zones. In Wolfcamp, movable oil can be found in also organic rich mudstone at almost 400 feet from the top of the formation while residual oil covers most of the interval with less water in the pores comparing to Bone Spring formation.

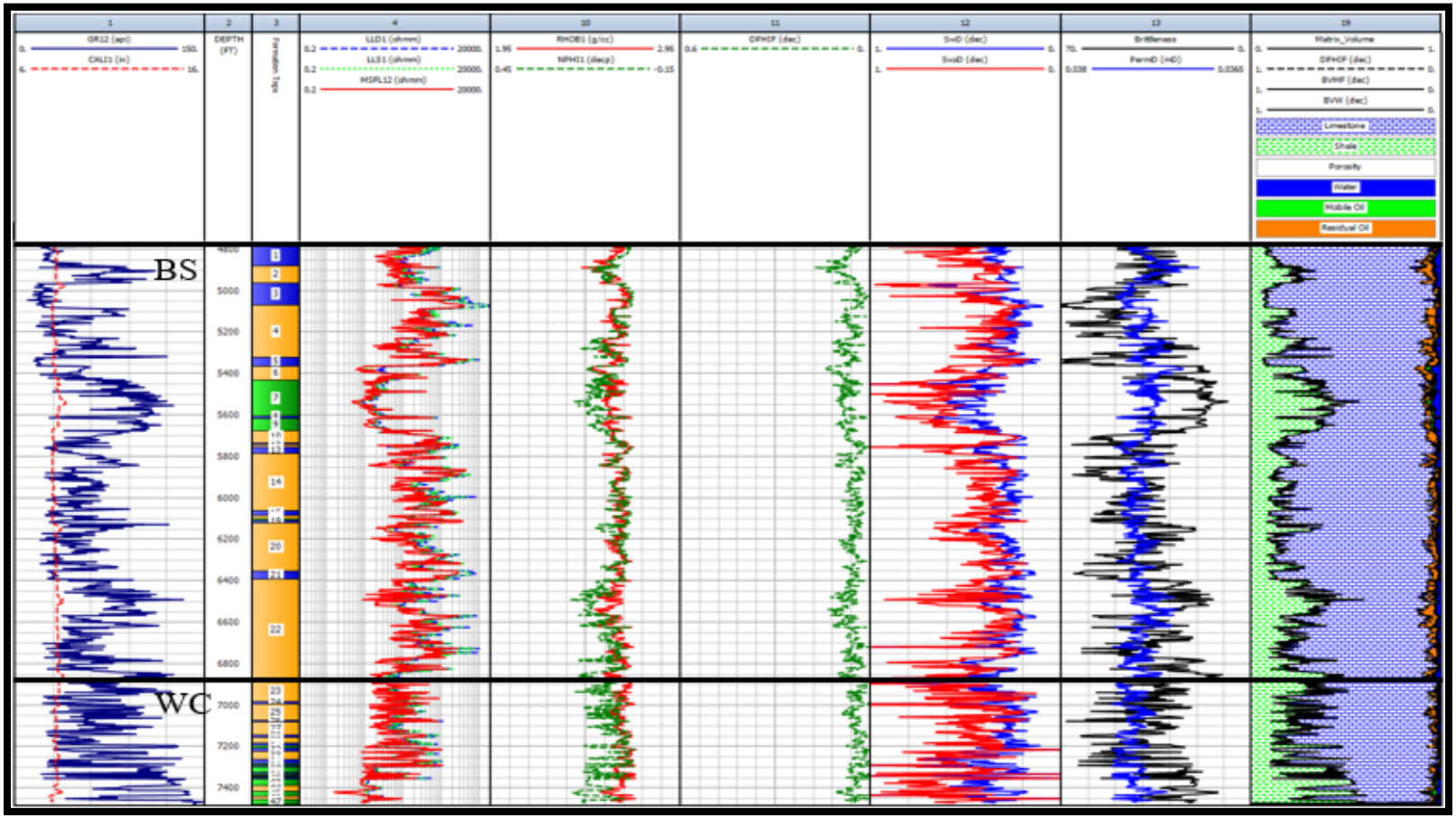

Figure 30. Petrophysical and Geomechanical outcomes of UL 21 Freedom-1 well.

Cunning Wolf UL 601

The thickness of Bone Spring formation is around 2,250 ft with a range of porosity from 0 to 19 %. The high porosity values correspond to the organic rich mudstone facies while the low porosity values represent part of the cherty limestone interval as well as shale interval. Bone Spring formation has a range of water saturation from 0 to 100 % with an average value of 40 %. Furthermore, brittleness index increases in cherty limestone and organic rich mudstone due to carbonate and silica mineral compositions which calibrated with the drilling cutting description from the mud log.

The penetrated interval of Wolfcamp is approximately 1,900 ft, it has a range of porosity from 0 to 18 % with an average value of 9 %. Based on the porosity prediction of both formations, Wolfcamp has lower porosity than Bone Spring does. The high clay content in Wolfcamp formation is a good reason of having this low average porosity value. Water saturation has a range of 0 to 100 % with an average value of almost 30%. Brittleness index fluctuates between 14 % to 63 % with tiny intervals of brittle rocks 'limestone and mudstone' interbedded with ductile rock 'shale'.

Movable oil can be found in cherty limestone interval of the Bone Spring formation at almost 200 feet from the top of the formation with a pay interval of 600 feet. Few intervals of organic rich mudstone at the base of the formation with a pay zone of 400 ft displays also movable oil 'highlighted in green' while residual oil 'highlighted in orange' covers most of the intervals of Bone Spring Formation, figure 31. In Wolfcamp, movable oil can be found in also organic rich mudstone at three different intervals from the top of the formation to almost 600 feet.

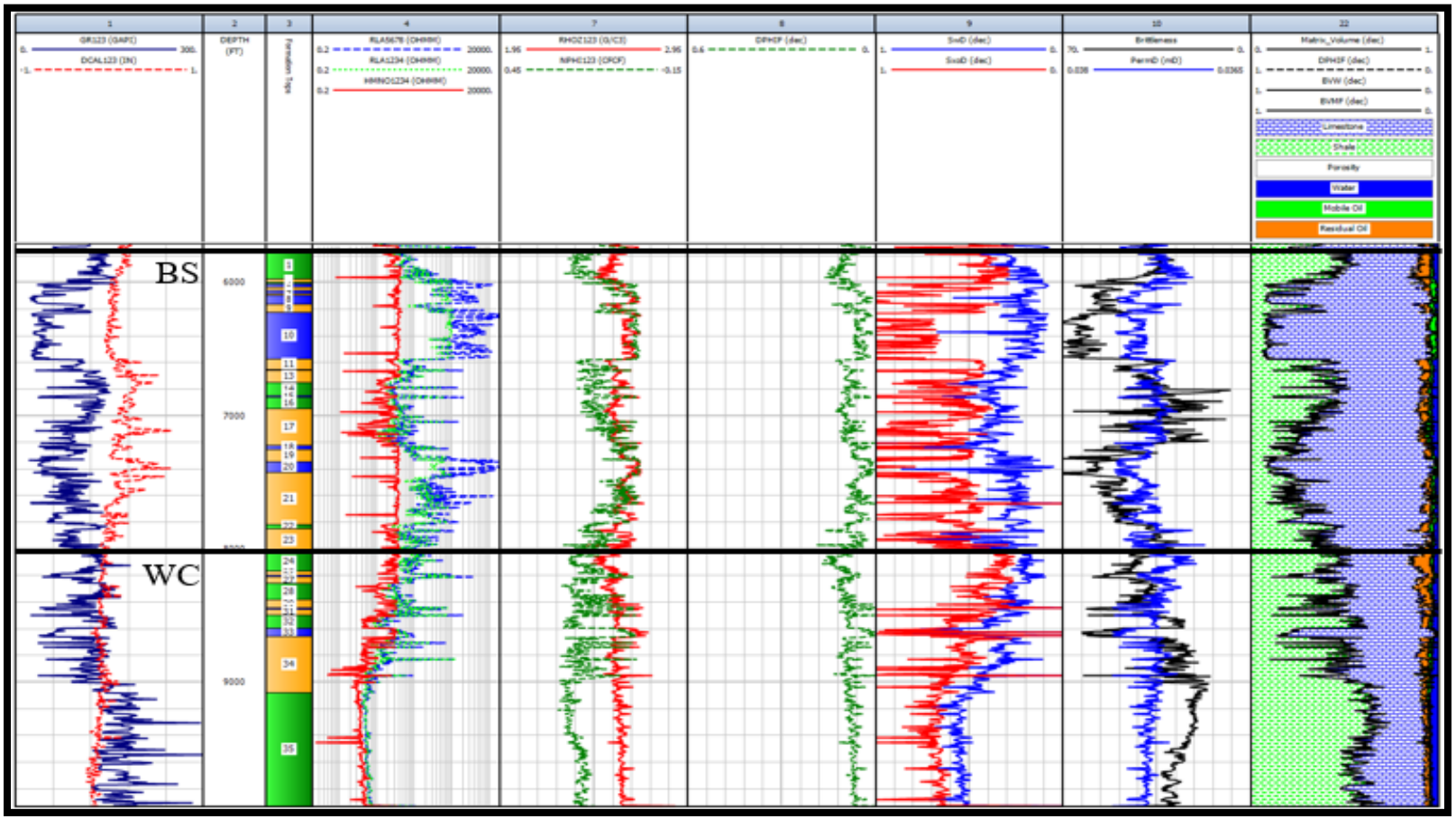

Figure 31. Petrophysical and Geomechanical outcomes of Cunning Wolf UL 601 well.

UL 23 Curiosity-1

The thickness of Bone Spring formation is around 2,186 ft with a range of porosity from 0 to 21 %. The high porosity values correspond to the organic rich mudstone facies while the low porosity values represent part of the cherty limestone interval as well as shale interval. Bone Spring formation has a range of water saturation from 0 to 100 % with an average value of 30 %. Furthermore, brittleness index increases in cherty limestone and organic rich mudstone due to carbonate and silica mineral compositions which calibrated with the drilling cutting description from the mud log.

The penetrated interval of Wolfcamp is approximately 750 ft, it has a range of porosity from 0 to 14 % with an average value of 8 %. Based on the porosity prediction of both formations, Wolfcamp has lower porosity than Bone Spring does. The high clay content in Wolfcamp formation is a good reason of having this low average porosity value. Water saturation has a range of 0 to 100 % with an average value of almost 30%. Brittleness index fluctuates between 20 % to 70 % with tiny intervals of brittle rocks 'limestone and mudstone' interbedded with ductile rock 'shale'.

Movable oil can be found in few cherty limestone intervals of the Bone Spring and most of the organic rich mudstone intervals. Residual oil can be seen in only 50 % of the Bone Spring Interval. In Wolfcamp, movable oil can be found in also organic rich mudstone at the top and the base of the formation while residual oil covers 50 % of the formation with less water in the pores comparing to Bone Spring formation, figure 32.

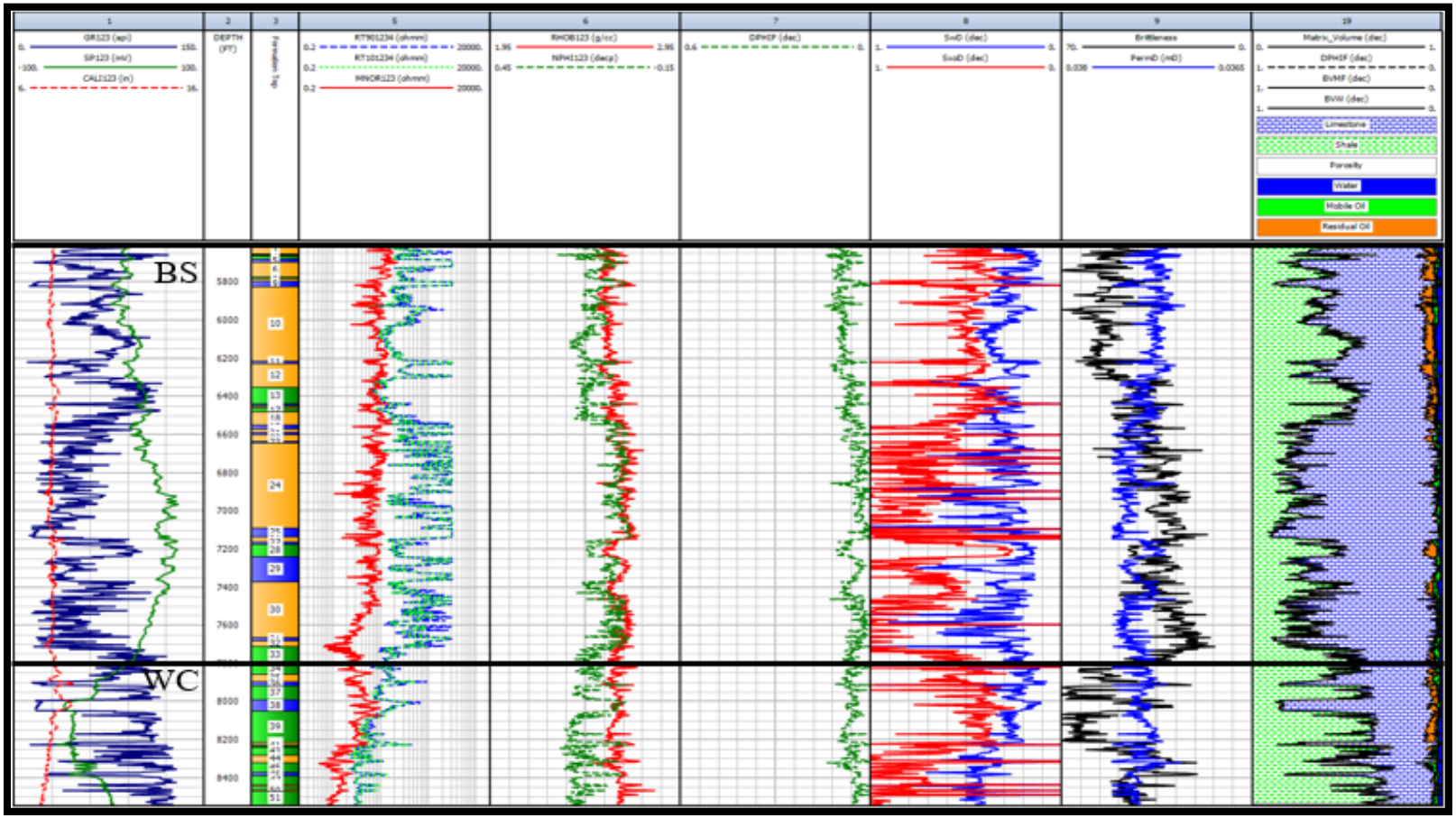

Figure 32. Petrophysical and Geomechanical outcomes of UL 23 Curiosity-1 well.

UL 24 Voyager-1

The thickness of Bone Spring formation is around 2,186 ft with a range of porosity from 0 to 19 %. The high porosity values correspond to the organic rich mudstone facies while the low porosity values represent part of the cherty limestone interval as well as shale interval. Bone Spring formation has a range of water saturation from 0 to 100 % with an average value of 35 %. Furthermore, brittleness index increases in cherty limestone and organic rich mudstone due to carbonate and silica mineral compositions which calibrated with the drilling cutting description from the mud log.

The penetrated interval of Wolfcamp is approximately 400 ft, it has a range of porosity from 0 to 20 % with an average value of 5 %. Based on the porosity prediction of both formations, Wolfcamp has lower porosity than Bone Spring does. The high clay content in Wolfcamp formation is a good reason of having this low average porosity value. Water saturation has a range of 0 to 100 % with an average value of almost 30%. Brittleness index fluctuates between 20 % to 70 % with tiny intervals of brittle rocks 'limestone and mudstone' interbedded with ductile rock 'shale'.

Movable oil can be found in organic rich mudstone facies at around 400 ft from the base of the Bone Spring while residual oil covers 30 % of the Bone Spring. In Wolfcamp, movable oil can be found in organic rich mudstone facies at the top of the formation while residual oil covers most of the formation with less water in the pores comparing to Bone Spring formation, figure 33.

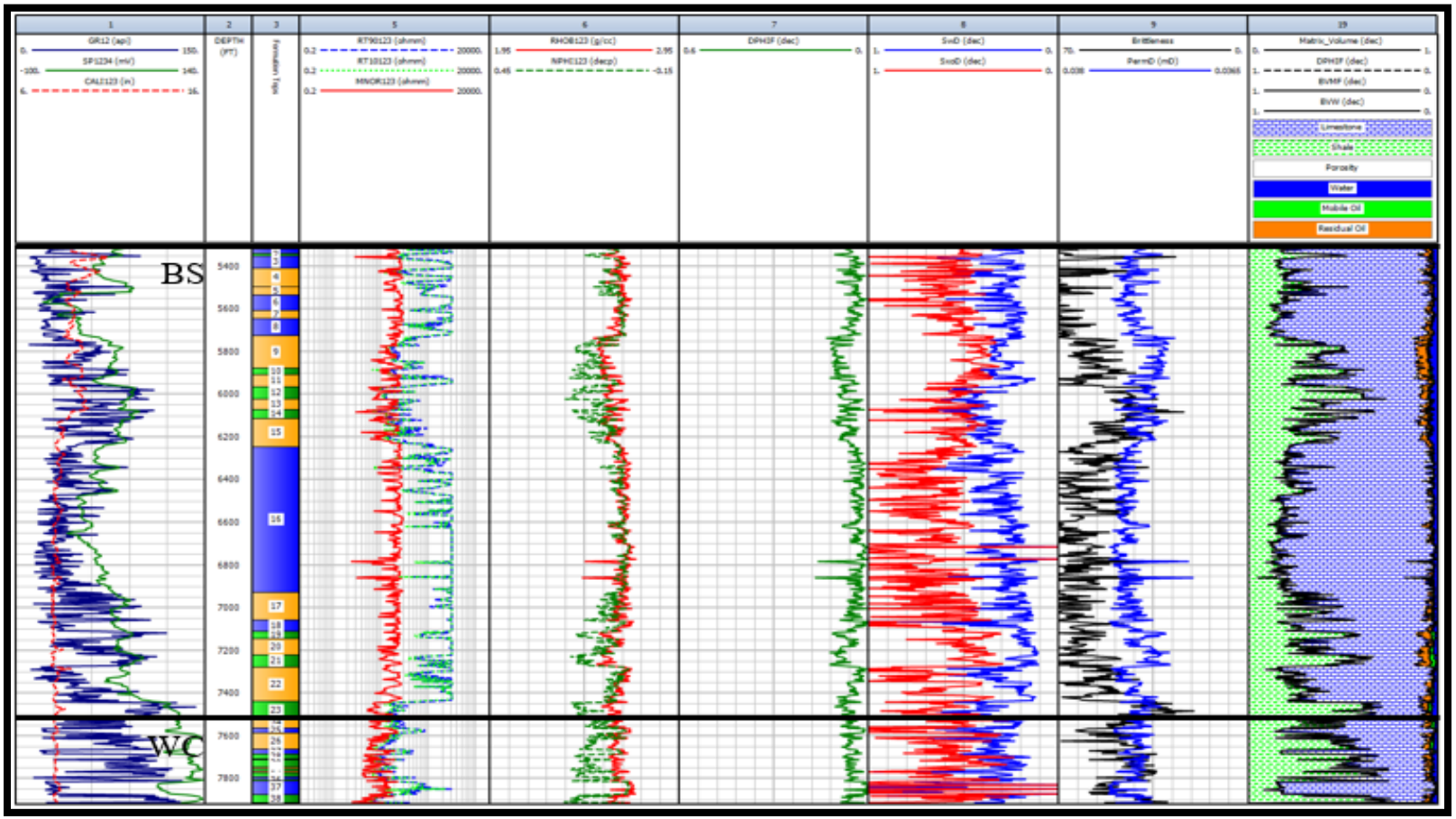

Figure 33. Petrophysical and Geomechanical outcomes of UL 24 Voyager-1 well.

Cunning Wolf UL 702

In this well, synthetic logs were used for petrophysical and geomechanical analysis and those logs do not represent the actual rock signature at the location but just an imaginary data. The thickness of Bone Spring formation is around 1,870 ft with a range of porosity from 0 to 19 %. Bone Spring formation has a range of water saturation from 0 to 100 % with an average value of 30 %. The high porosity and low water saturation values are due to the synthetic logs that were generated to fill the missing raw data of the subjected well. Furthermore, brittleness index increases in cherty limestone and organic rich mudstone due to carbonate and silica mineral compositions which calibrated with the drilling cutting description from the mud log.

The penetrated interval of Wolfcamp is approximately 1,200 ft, it has a range of porosity from 0 to 21 % with an average value of 8 %. Based on the porosity prediction of both formations, Wolfcamp has lower porosity than Bone Spring does. The high clay content in Wolfcamp formation is a good reason of having this low average porosity value. Water saturation has a range of 0 to 100 % with an average value of almost 30%. Brittleness index fluctuates between 7 % to 58 % with tiny intervals of brittle rocks ‘limestone and mudstone’ interbedded with ductile rock ‘shale’.

Movable oil can be found in the cherty limestone facies at the top of the Bone Spring while residual oil covers most of the Bone Spring. In Wolfcamp, residual oil can be found in most of the organic rich mudstone facies of the formation while movable oil is missed with more water in the pores comparing to Bone Spring formation, figure 34.

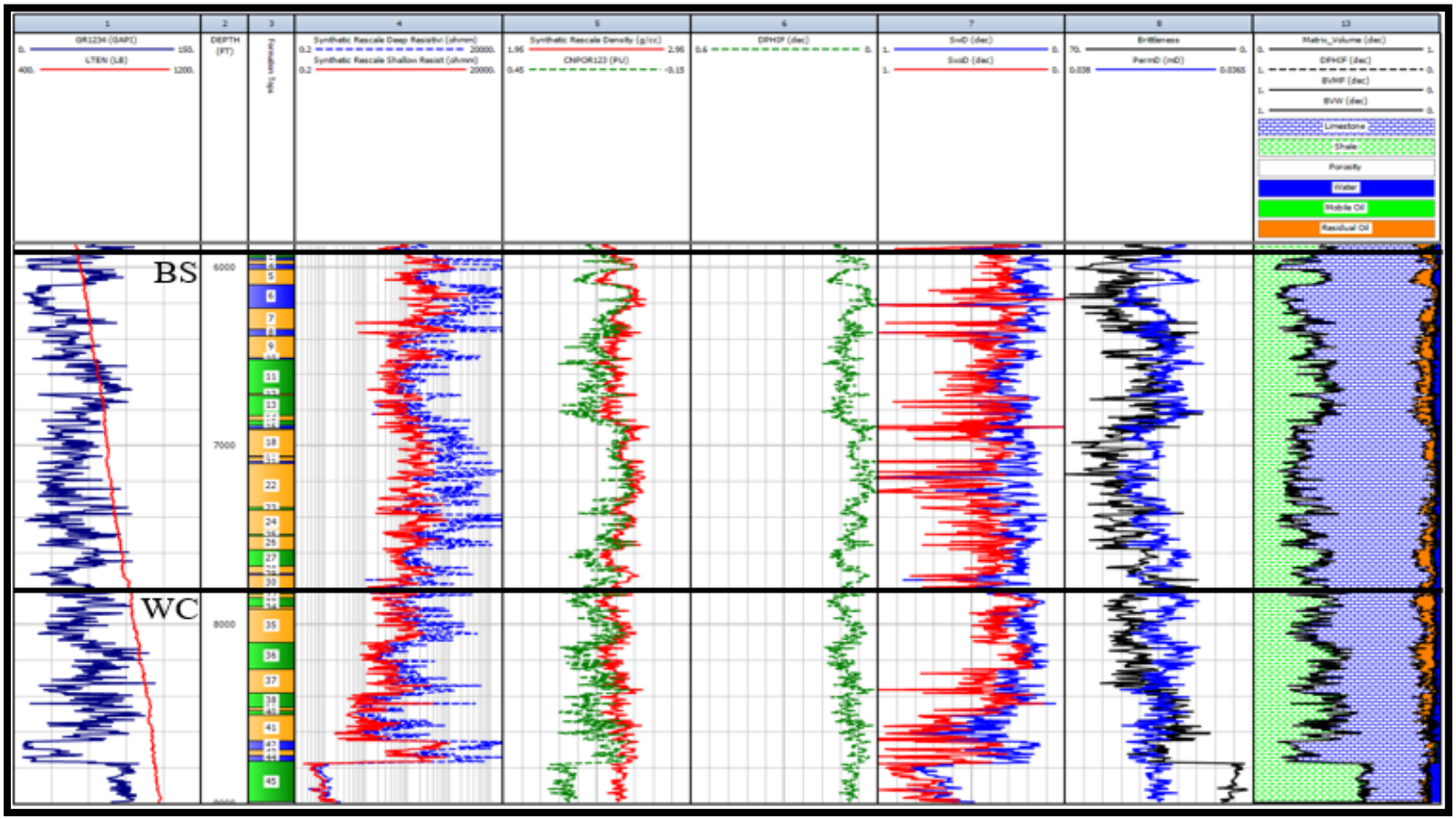

Figure 34. Petrophysical and Geomechanical outcomes of Cunning Wolf UL 702 well.

Cunning Wolf UL 1801

In this well, synthetic logs were used for petrophysical and geomechanical analysis and those logs do not represent the actual rock signature at the location but just an imaginary data. The thickness of Bone Spring formation is around 1,680 ft with a range of porosity from 0 to 22 %. Bone Spring formation has a range of water saturation from 0 to 22 % with an average value of 11 %. The high porosity and low water saturation values are due to the synthetic logs that were generated to fill the missing raw data of the subjected well. Furthermore, brittleness index increases in cherty limestone and organic rich mudstone due to carbonate and silica mineral compositions which calibrated with the drilling cutting description from the mud log.

The penetrated interval of Wolfcamp is approximately 1,180 ft, it has a range of porosity from 0 to 35 % with an average value of 14 %. Based on the porosity prediction of both formations, Wolfcamp has lower porosity than Bone Spring does. The high clay content in Wolfcamp formation is a good reason of having this low average porosity value. Water saturation has a range of 0 to 20 % with an average value of almost 12%. Brittleness index fluctuates between 6 % to 70 % with tiny intervals of brittle rocks 'limestone and mudstone' interbedded with ductile rock 'shale'.

Movable oil can be found in organic rich mudstone facies at around 300 ft from the top of the Bone Spring while residual oil covers all the intervals of the Bone Spring. In Wolfcamp, movable oil can be found in organic rich mudstone facies at the base of the formation while residual oil covers all the intervals of the formation with more water in the pores comparing to Bone Spring formation, figure 35.

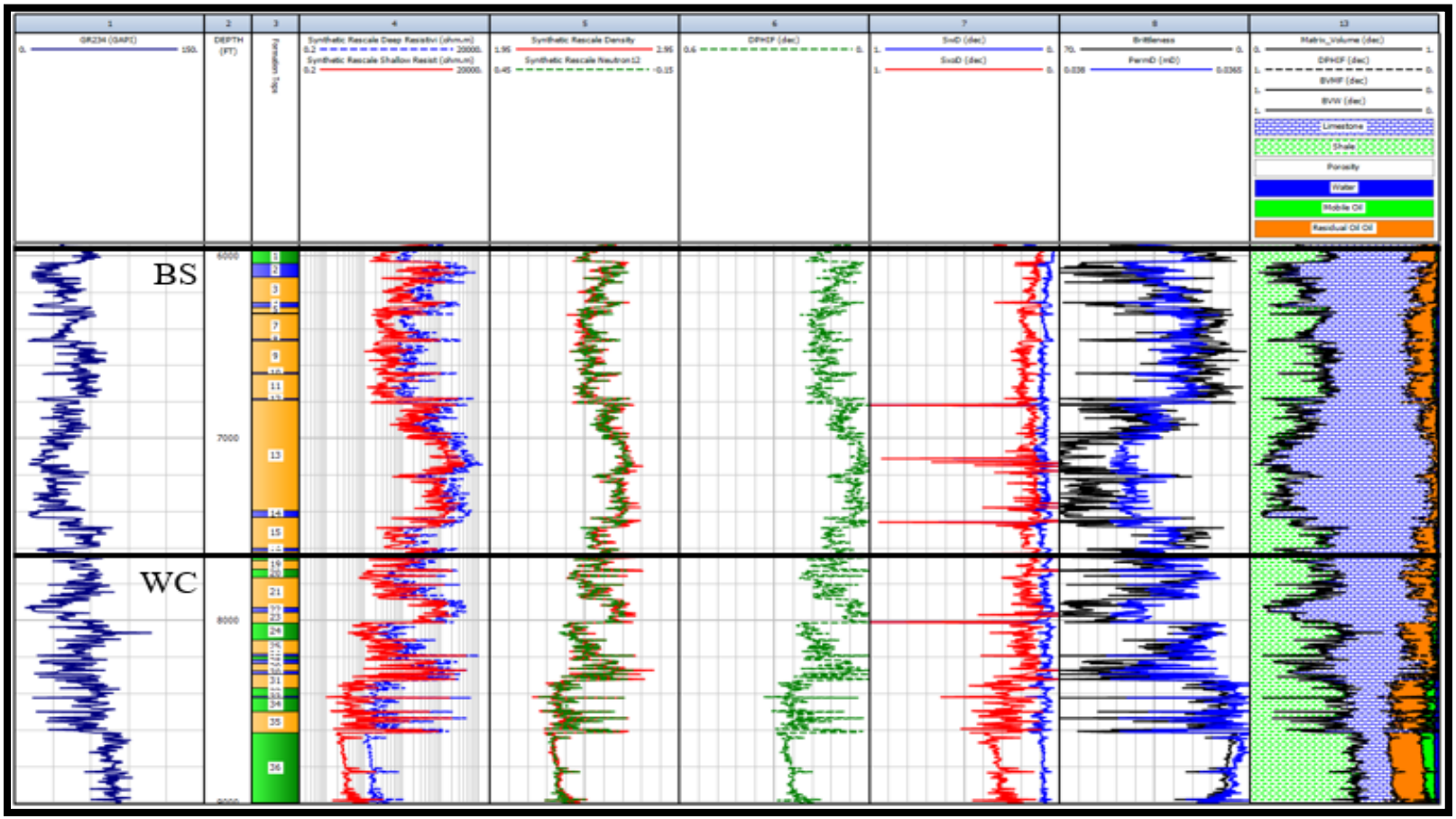

Figure 35. Petrophysical and Geomechanical outcomes of Cunning Wolf UL 1801 well.

Peacemaker UL 3023

In this well, synthetic logs were used for petrophysical and geomechanical analysis and those logs do not represent the actual rock signature at the location but just an imaginary data. The thickness of Bone Spring formation is around 1,930 ft with a range of porosity from 0 to 31 %. Bone Spring formation has a range of water saturation from 0 to 100 % with an average value of 25 %. The high porosity and low water saturation values are due to the synthetic logs that were generated to fill the missing raw data of the subjected well. Furthermore, brittleness index increases in cherty limestone and organic rich mudstone due to carbonate and silica mineral compositions which calibrated with the drilling cutting description from the mud log.

The penetrated interval of Wolfcamp is approximately 850 ft, it has a range of porosity from 0 to 22 % with an average value of 7 %. Based on the porosity prediction of both formations, Wolfcamp has lower porosity than Bone Spring does. The high clay content in Wolfcamp formation is a good reason of having this low average porosity value. Water saturation has a range of 0 to 100 % with an average value of almost 25%. Brittleness index fluctuates between 18 % to 70 % with tiny intervals of brittle rocks 'limestone and mudstone' interbedded with ductile rock 'shale'.

Movable oil can be found in organic rich mudstone and few cherty limestone facies with almost 1000 ft pay of the Bone Spring while residual oil covers most of the Bone Spring. In Wolfcamp, movable oil can be found in organic rich mudstone facies at the base of the formation while residual oil covers most of the formation with less water in the pores comparing to Bone Spring formation, figure 36.

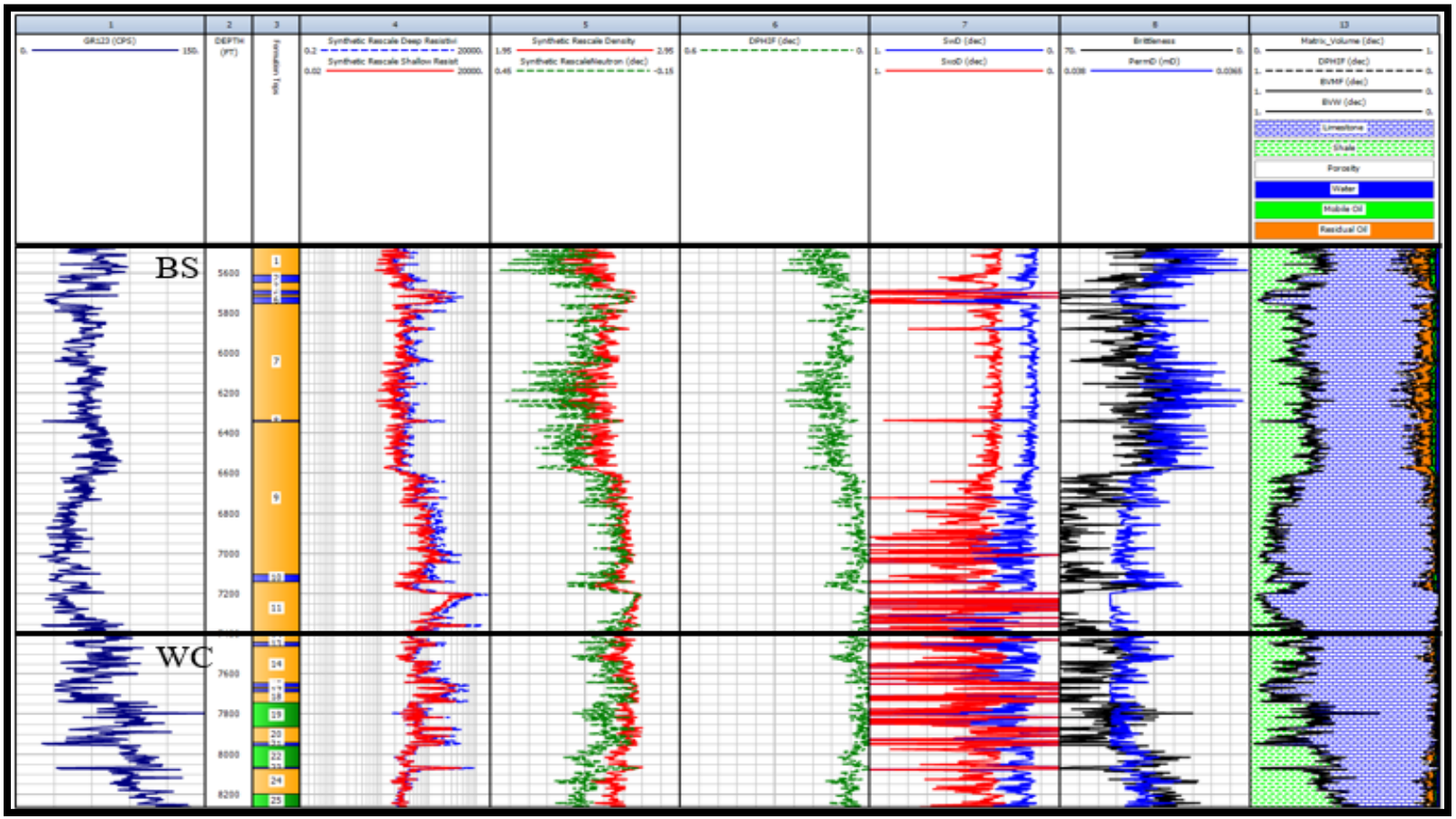

Figure 36. Petrophysical and Geomechanical outcomes of Cunning Peacemaker UL 3023 well.

CHAPTER IV

3D GEOLOGICAL MODELING

Geological modeling in form of structure, sedimentological and petrophysical properties is extremely important to better understand the subsurface geology and to provide more reasonable volumetric estimations when compared with 2D methods. The aim is to improve the reliability of natural resources evaluation and for better decision-making. However, data preparation and quality controls are crucial in the process of 3D geological modeling since they provide a robust foundation for building a meaningful model. Data utilized in our PETREL project is the wireline logs of 7 wells as stated and analyzed in the previous sections.

Structural Modeling

The structural model represents the volume and spatial framework 'skeleton' of the reservoir and forms the foundation of reservoir property modeling. The area of interest 'Boundary' has a dimension of 7 x 9.5 miles with an average area of 66 square miles. The structural model of this project is relatively simple since seismic data and faults are not involved. Thus, two models were created to represent each formation separately. In both models, simple gridding was formed based on the well top surfaces with gridding increment of 250 x 250 feet, figures 38 & 39. The first model is the Bone Spring Model where the top limit is the top of Bone Spring formation and the base limit is the top of Wolfcamp formation. While the second model is the Wolfcamp Model where the top limit is the top of Wolfcamp formation, and the base limit is the base of the log interval in each well. The Gridding size and position for both models were

picked automatic from input data/boundary. The boundary is the area of interest and was picked to cover the area of the 7 wells.

Since sedimentological analysis was not included in this project due to data limitation of missing core descriptions, thin sections and mineralogical composition analysis, one zone was created in each model 'formation' using the same horizons utilized in generating 3D grids. A layering procedure was then applied to determine the vertical resolution of the model based on the average thickness of each formation to define the quantity of preferred cell layers. The vertical resolution 'layers' of the grids should be determined based on the properties that need to be modeled. Typically, the definition of layer thickness should account for the data resolution and the machine's computation/storage capacity. In this project, the layer thickness is around 3 ft in the grids of both models. In Bone Spring model, the average thickness of Bone Spring Formation was estimated to be around 2,087 ft leading to 696 layers while in Wolfcamp model the average thickness of Wolfcamp formation was approximately 656 ft resulting in 219 layers, figures 37, 40 & 41. The layering creation method used in both models was proportional between the top and the bottom horizons of the model, which means the number of layers will be constant in the entire zones.

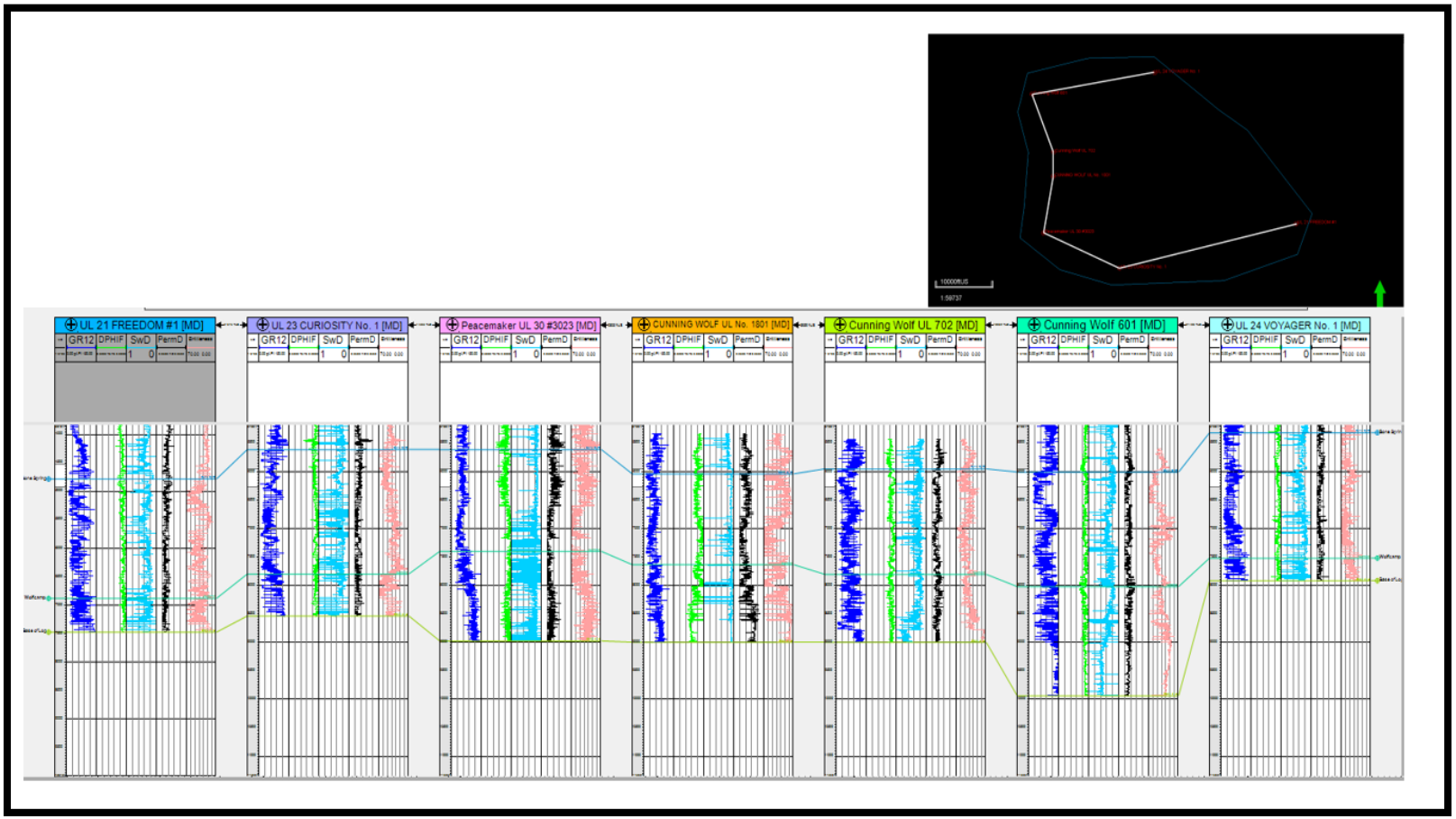

Figure 37. Structural cross-section shows thickness of Bone Spring and Wolfcamp formations, orientation starts from east-west-north and ends east.

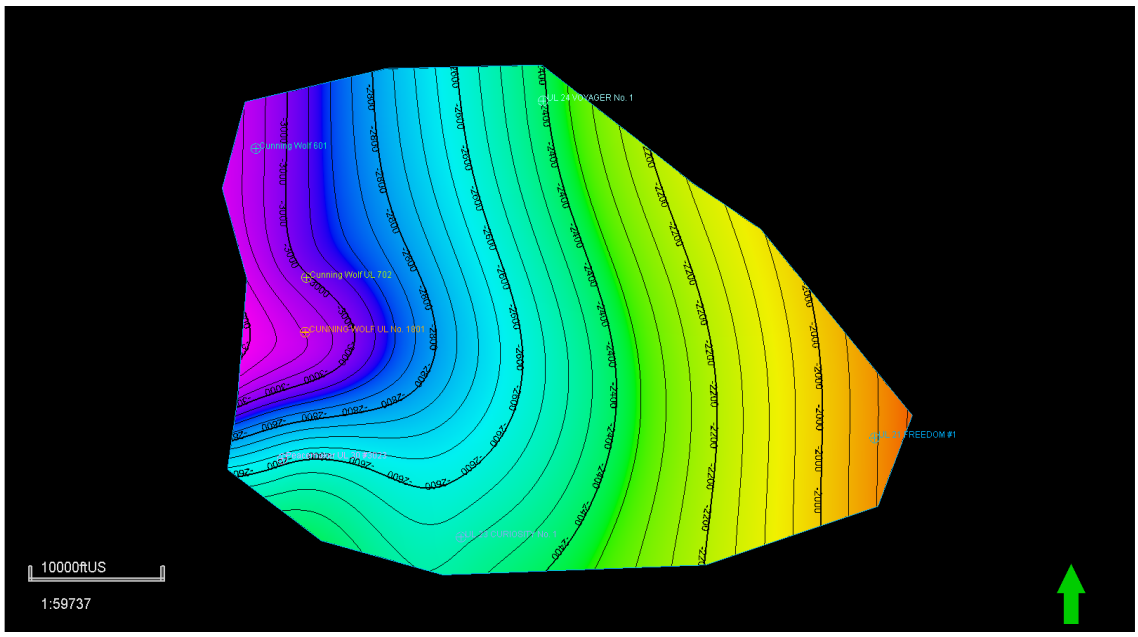

Figure 38. Bone Spring Structural map, up dip structure towards east ‘bold contour’ is at -2,000 ft and down dip structure towards west ‘bold contour’ is at -3,000 ft ‘CI: 50ft’.

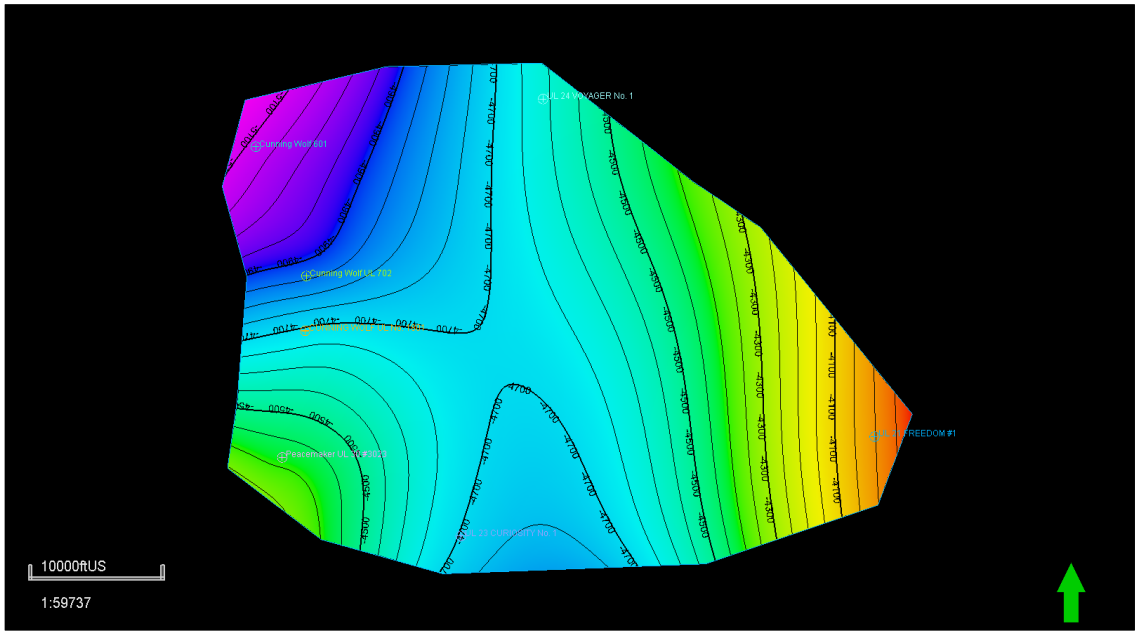

Figure 39. Wolfcamp Structural map, up dip structure towards east ‘bold contour’ is at -4,100 ft and down dip structure towards west ‘bold contour’ is at -5,100 ft ‘CI: 50ft’.

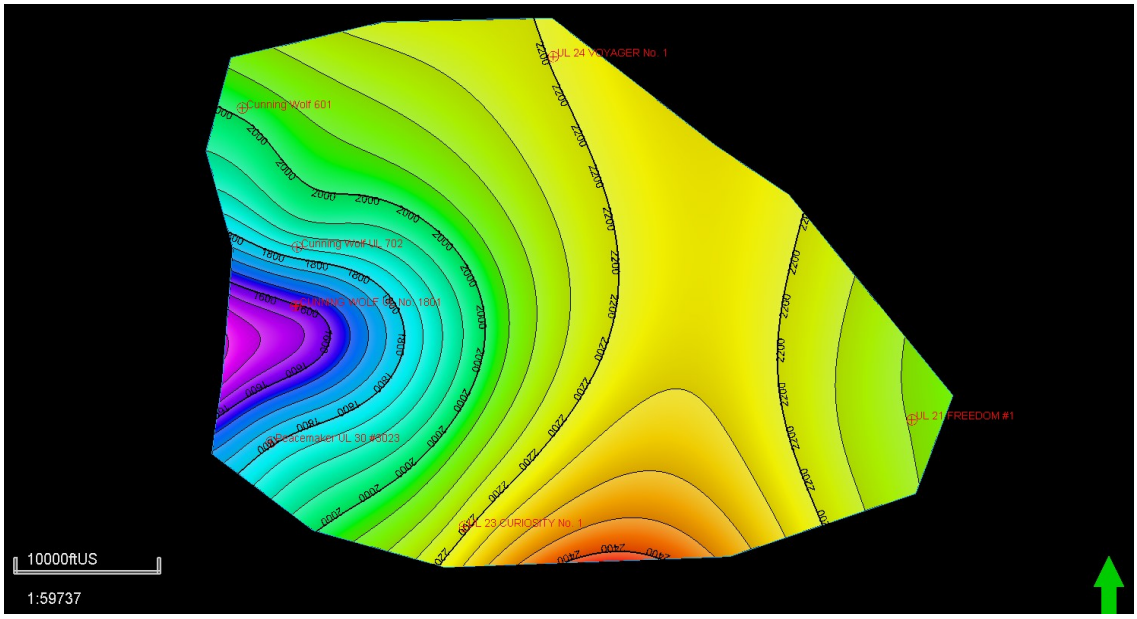

Figure 40. Thickness map of Bone Spring formation, thinning towards the west and thickening towards south and north.

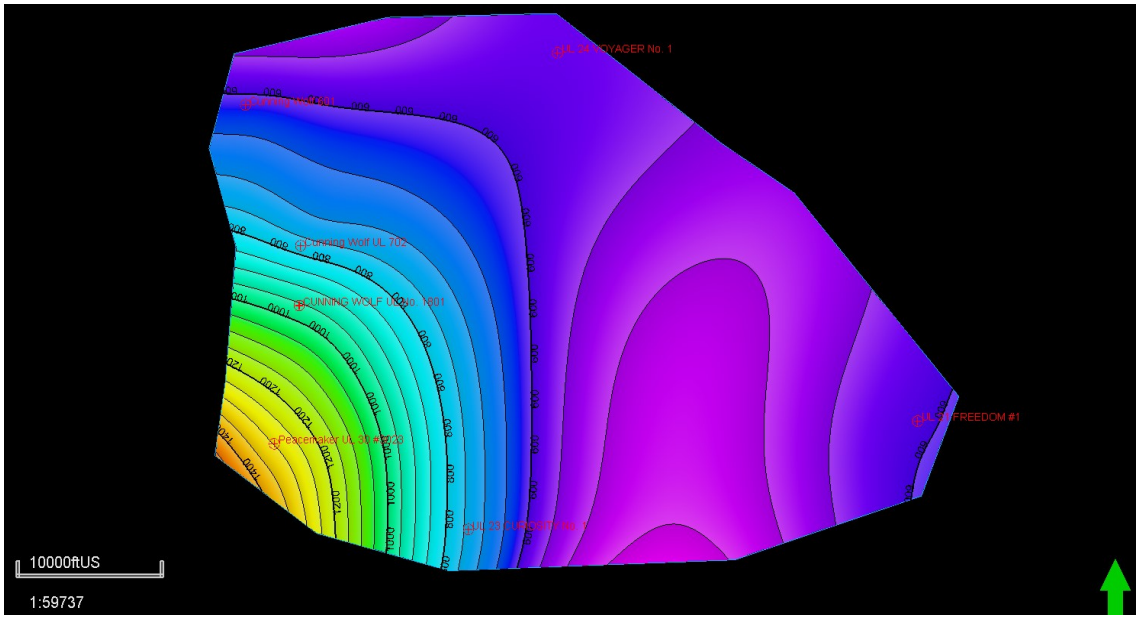

Figure 41. Thickness map of Wolfcamp formation, thinning towards the northeast and east and thickening towards south west. This map does not represent the actual thickness of Wolfcamp formation, but it shows the penetration interval.

Upscaling of Well Properties

This terminology basically means assigning effective properties in a course cell from the fine scale cells. In upscaling process, arithmetic averaging method was used to upscale porosity and brittleness index. As for water saturation, since porosity is the rock capacity to hold any fluids and saturation is the portion of that capacity which holds the same fluids, the averaging method used to upscale water saturation was arithmetic but weighted to the porosity values.

Property Modeling

In this section, histograms 'the frequency distribution' of porosity, water saturation and brittleness index of both Bone Spring and Wolfcamp models were generated to investigate the spread of the data. Then, data were transformed to follow standard normal distribution for further statistical analysis. At that point, spatial distributions of formation parameters were analyzed using geostatistical method called variogram analysis. Variograms are statistical correlation methods used to quantify the spatial variability or similarity between points of a certain distance and direction in a field (Baker, Al-Jawad & Abdulla, 2016). In general, the variogram increases with distance, and may reach a sill. The sill corresponds to the variance of the data and the distance of reaching the sill is called the range of the variogram. The variogram value at the distance between two points close to zero is called nugget (Yarus & Chambers, 2006).

In Petrel, the variogram is computed in three directions; vertical, major and minor. The major direction corresponds to the lateral maximum range while the minor direction is perpendicular to the major direction (Yarus & Chambers, 2006).

In both models of the field, variogram maps were generated from porosity, water saturation and brittleness index to identify the major direction 'orientation'. Unfortunately, the major direction could not be defined due to small number of wells, which are mostly aligned South-North. We compute the variograms in the vertical and lateral major directions using the parameters in table 1. We assume the variogram in the minor direction is the same as in the major direction because not enough data is provided and no clear evidence of anisotropy in terms of sedimentation and heterogeneity in the studied area.

Direction	Azimuth	Dip	Number of Lags	Lag Distance	Band Width	Tolerance Angle	Lag Tolerance
Vertical	NA	90	15	3	481.8	90	50
Lateral	0	0	6	4000	5238.4	45	50

Table 1. Experimental variogram computation parameters, feet is a unit used for scaling in Petrel software.

Bone Spring Model

The histogram in figure 42-a represents the porosity parameter of Bone Spring formation. The total number of upscaled points is 4,872 the porosity value range is between 0 and 0.25 with an average around 0.071. For simulating porosity in Bone Spring formation using Gaussian method, the normal score transformation was performed. The transformed data has a mean value of 0.011 and 0.89 standard deviation which differs to 1 due to significant percentage of zero porosity as shown in figure 42.

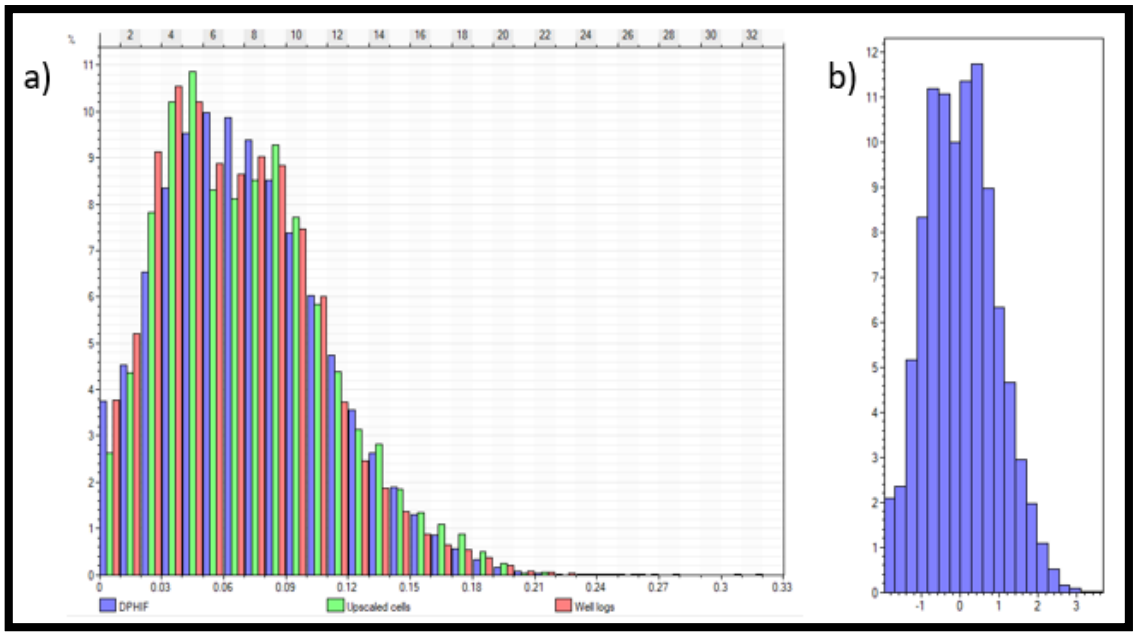

Figure 42. a) Histogram of porosity in Bone Spring Formation where well log data is displayed on a percentage of samples basis 'red' and upscaled cells are displayed on green, b) Porosity transformation of the same formation.

In variogram analysis, the vertical ranges were calculated, fitting the first 5 points, to 7.3 ft and 124 ft with a nugget of 0.0001 and a total sill of 0.88. Lateral ranges were also computed, fitting the first and third points, to 4400 ft and 6900 ft, as shown in figure 43.

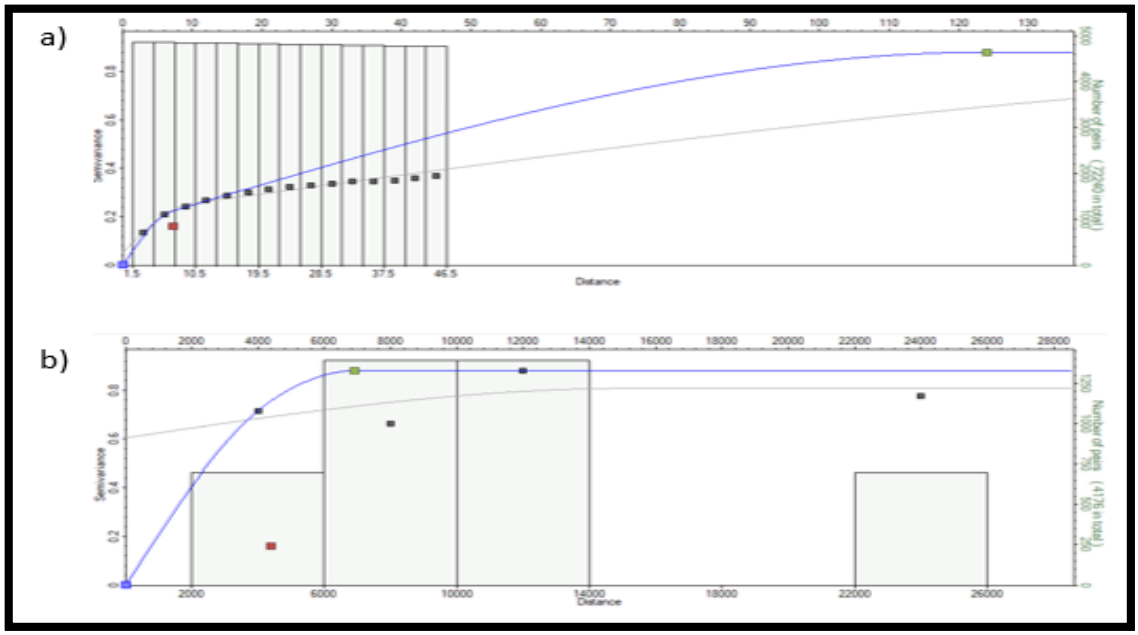

Figure 43. a) Vertical variogram of porosity in Bone Spring Formation, b) Major variogram of the same property.

For porosity in Bone Spring formation, the Gaussian Random Function Simulation method was applied to interpolate the data in the entire model where the petrophysical properties distribution were characterized without taking the rock type parameters in consideration. Therefore, modelled cells ‘blue’ are slightly underestimated comparing with upscaled cells ‘green’ providing a slightly more conservative propagation of cell values in the model except the interval between 5 and 7% where modelled cells are slightly overestimated, figure 42-a. The average map of Bone Spring’s porosity shows the highest values of 8% along the central region and along the strike of three wells ‘Peacemaker UL 3023, Cunning Wolf UL 702 and Cunning Wolf UL 1801’ as shown in figure 44.

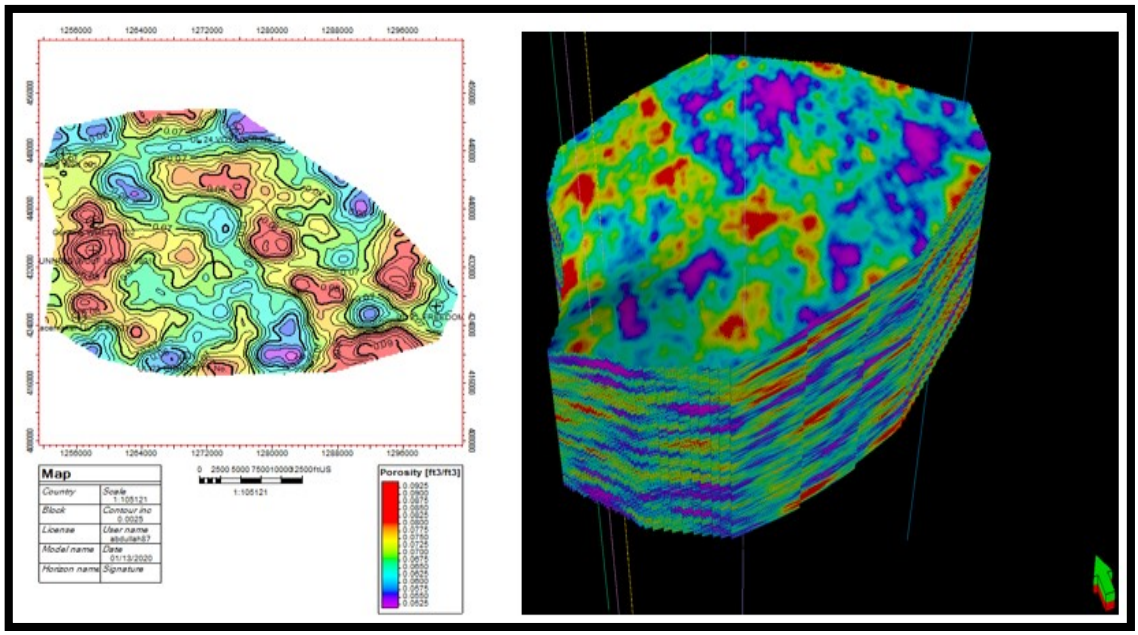

Figure 44. Average map of Bone Spring’s porosity and 3D model of porosity.

Well cross section of modelled porosity in Bone Spring formation displays highest value of porosity at western region 'center of the cross section' due to the high porosity that was calculated from the generated synthetic density logs from the three wells, figure 45. This synthetic density log created a noise or error while simulating porosity parameters in the Bone Spring model since it is an imaginary data and does not reflect the real geology of the subsurface. Thus, more logs are needed, not only from vertical wells, in the field to substitute the synthetic curves and create more efficient model to visualize the horizontal continuity and spatial variability of the reservoir properties.

However, no trend of porosity can be observed vertically and horizontally due to heterogeneity and facies distribution of the formation, but the organic rich facies tend to have more porosity than the clean carbonate. This is affected by the existence of kerogen that gets converted to bitumen and hosts micro organic porosity as stated in chapter II.

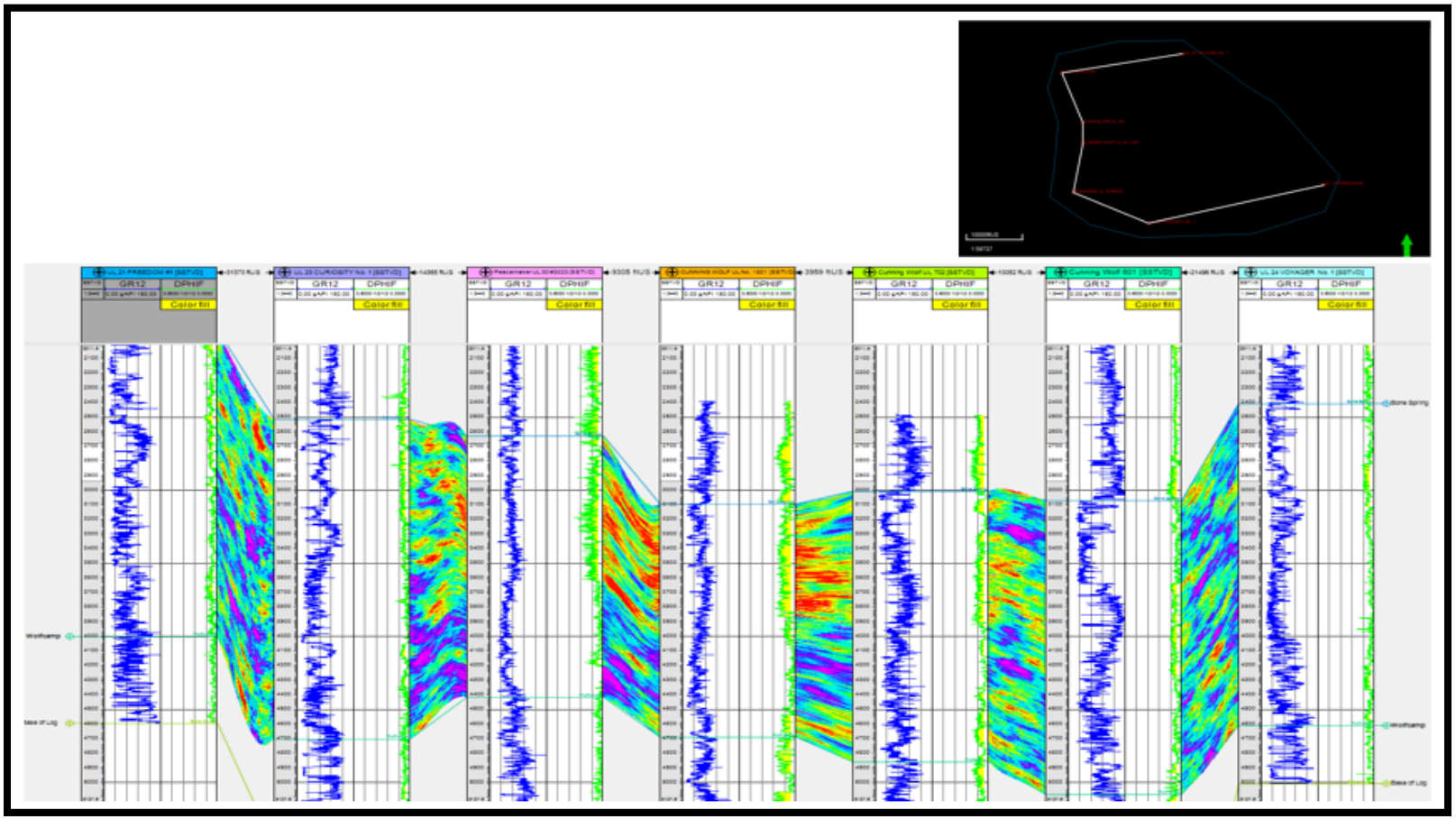

Figure 45. Well cross section of porosity model of Bone Spring formation showing highest porosity at the western region.

However, Permeability of Bone Spring formation was calculated from the above porosity model using equation number 20 in the petrophysical analysis section as shown in figure 46. The average map of permeability displays the highest value of 0.03736 mD around UL 21 Freedom-1 well and Cunning Wolf UL 601 well.

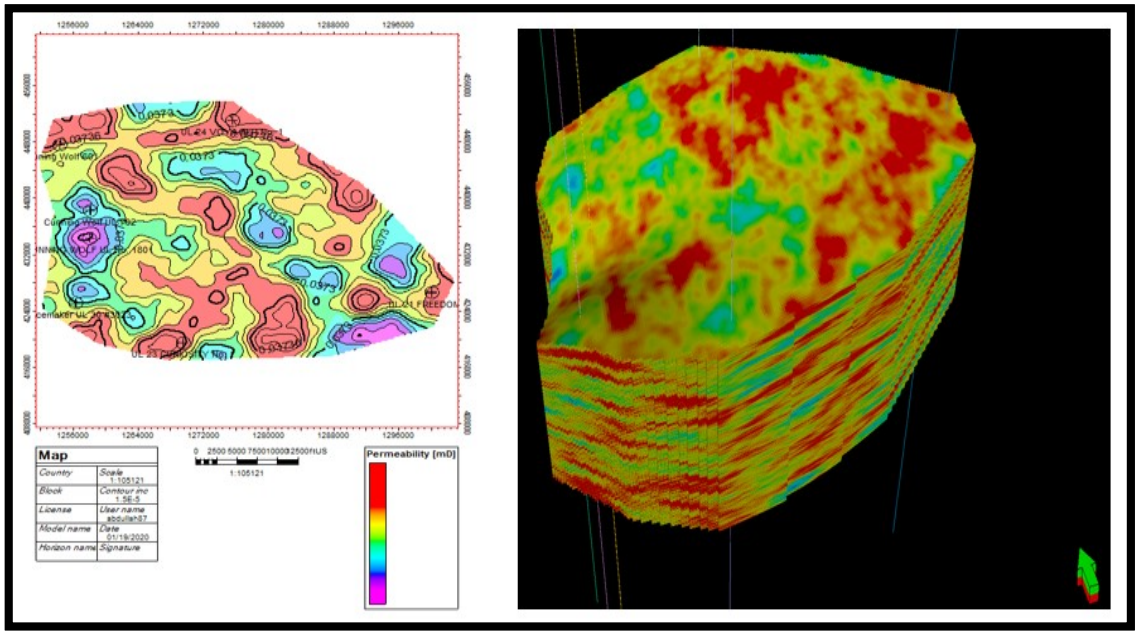

Figure 46. Average map of Bone Spring's permeability and 3D model of porosity.

The histogram in figure 47-a characterizes the water saturation parameter of Bone Spring formation. The total number of upscaled points is 4,872; the value range is between 0 and 1 with an average water saturation around 0.25. For simulating water saturation in Bone Spring formation using the Gaussian method, normal score transformation was performed. The transformed data has a mean value of 0.011 and 0.93 standard deviation which differs to 1 due to significant percentage of 1 water saturation as shown in figure 47.

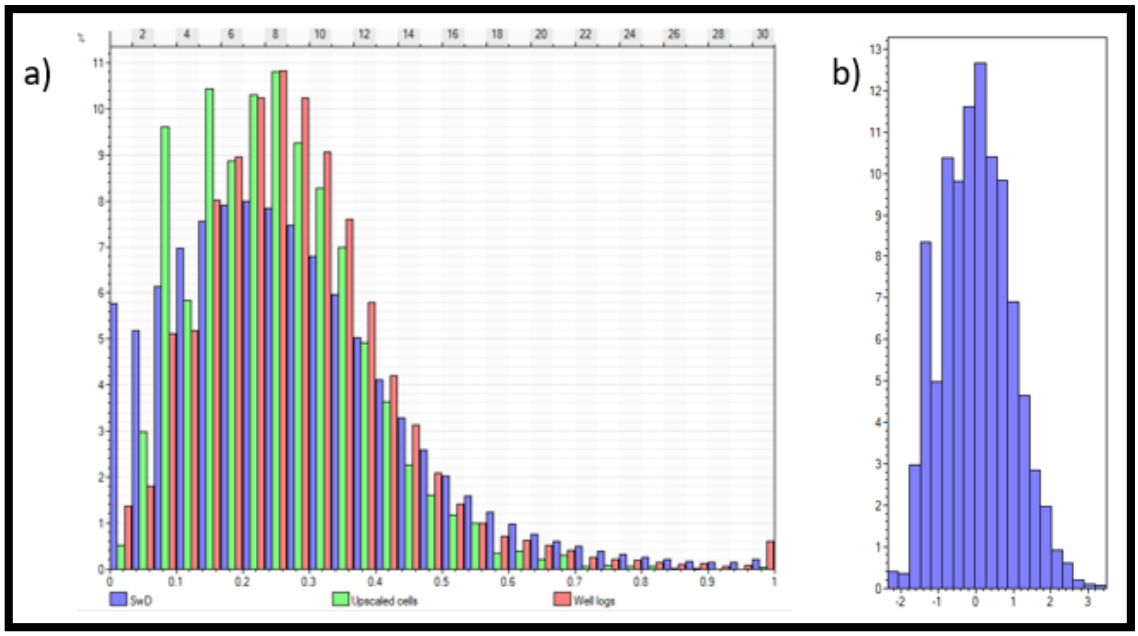

Figure 47. a) Histogram of water saturation in Bone Spring Formation where well log data is displayed on a percentage of samples basis 'red' and upscaled cells are displayed on green, b) Water saturation transformation of the same formation.

In variogram analysis, the vertical ranges were calculated, fitting the first 4 points, to 6 ft and 100 ft with a nugget of 0.0001 and a total sill of 0.86. Based on the experimental points, it is not possible to predict the lateral ranged but 500 ft and 5000 ft of ranges were picked to model water saturation property, as shown in figure 48.

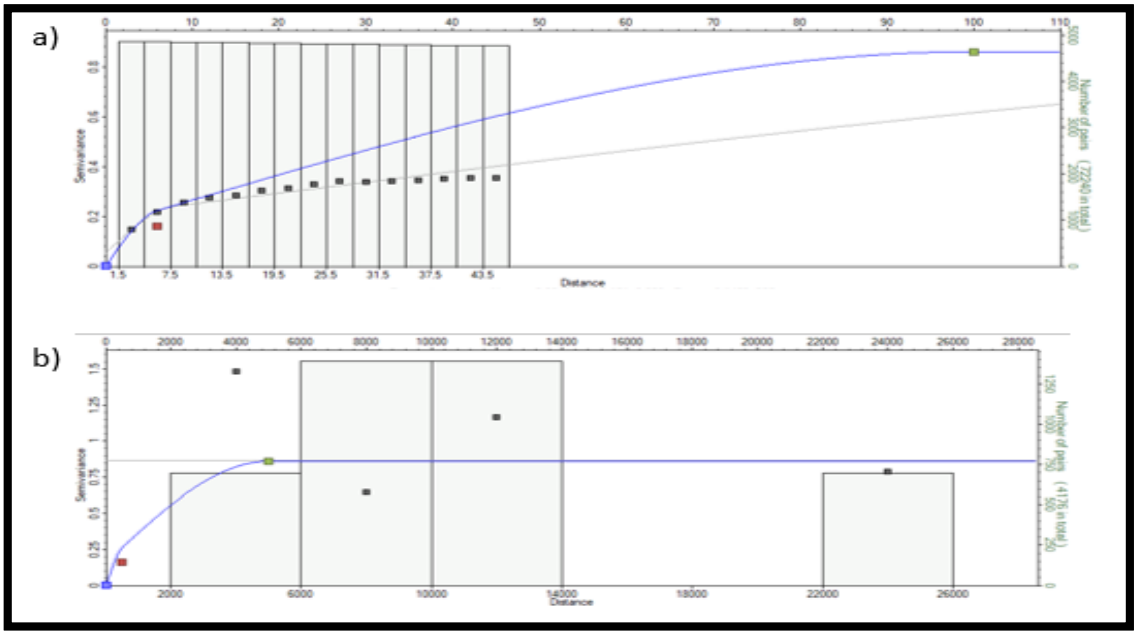

Figure 48. a) Vertical variogram of water saturation in Bone Spring Formation, b) Major variogram of the same property.

For water saturation in Bone Spring formation, the Gaussian Random Function Simulation method using the porosity volume as a secondary constraint through co-kriging to interpolate the data in the entire model where the petrophysical properties distribution were characterized without taking the rock type parameters in consideration. Therefore, modelled cells ‘blue’ in the interval between 7.5 and 35% are underestimated comparing with upscaled cells ‘green’ providing more conservative propagation of cell values in the model while other intervals show a slightly overestimation of modelled cells, figure 47-a. The average map of Bone Spring’s water saturation shows the highest values of 34% along the central region starting from UL 21 Freedom-1 towards UL 24 Voyager-1 well as shown in figure 49.

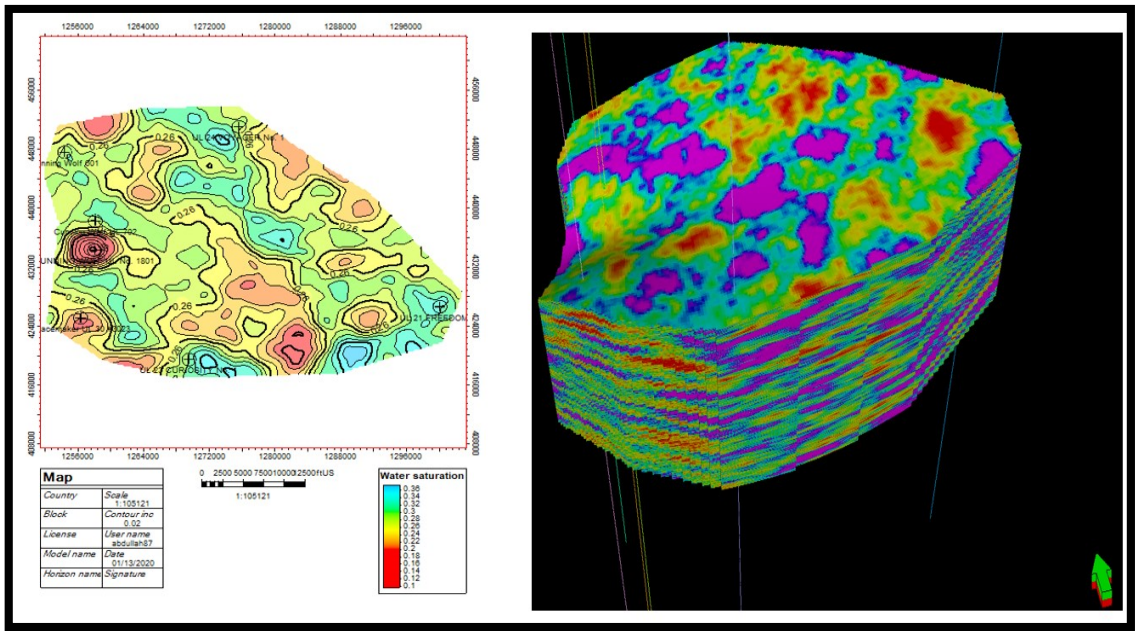

Figure 49. Average map of Bone Spring’s water saturation and 3D model of water saturation.

Well cross section of modelled water saturation in Bone Spring formation displays lowest value of water saturation at western region ‘center of the cross section’ due to the water saturation that was calculated from the generated synthetic resistivity logs from the three wells, figure 50. These synthetic resistivity logs created a noise or error while simulating water saturation parameters in the Bone Spring model since they are imaginary data and do not represent the actual conductivity of the subsurface formations. Thus, more logs are needed in the area of interest to substitute the synthetic curves in order to generate more efficient model to visualize the spatial variability of the reservoir properties.

However, no trend of water saturation can be observed vertically and horizontally but shale facies tend to have more water saturation than the clean carbonate due to the presence of the clay bound water. Yet, formation water interpretation and its chemistry could be impacted by the long history and widely use of CO_2 and water injection which result in weaknesses of formation water investigation (Melzer, 2013).

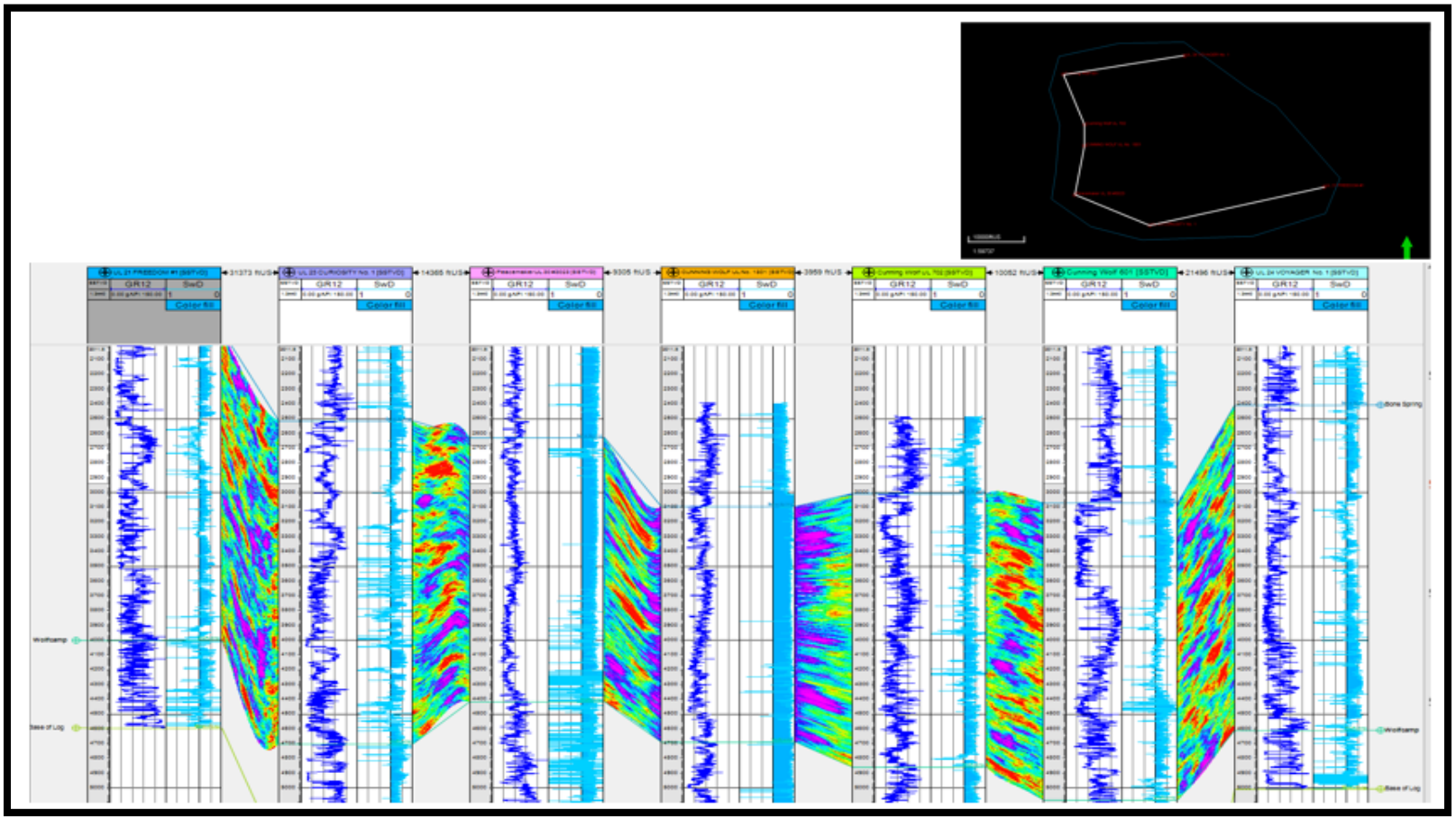

Figure 50. Well cross section of water saturation model of Bone Spring formation showing lowest water saturation at the western region.

The histogram in figure 51-a characterizes the brittleness index parameter of Bone Spring formation. The total number of upscaled points is also 4,872, the value range is between 1.5 and 70 with an average brittleness index around 45.6. For simulating brittleness index using the Gaussian method, the normal score transformation was performed. The transformed data has a mean value of - 0.01 and 0.89 standard deviation which differs to 1 due to significant percentage of 70 the maximum percentage of brittleness index, as shown in figure 51.

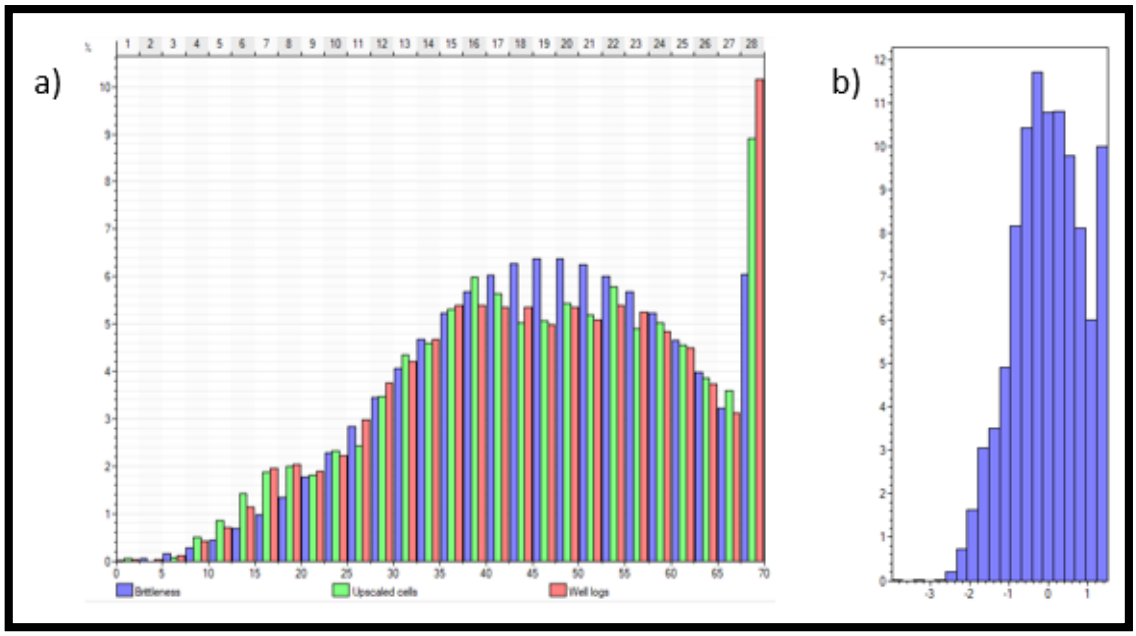

Figure 51. a) Histogram of brittleness index in Bone Spring Formation where well log data is displayed on a percentage of samples basis ‘red’ and upscaled cells are displayed on green, b) Brittleness index transformation of the same formation.

In variogram analysis, the vertical ranges were calculated, fitting the first 7 points, to 8.5 ft, 19 ft and 300 ft with a nugget of 0 and a total sill of 0.87. Lateral ranges were also computed, fitting the first experimental point, to 3370 ft and 6400 ft, as shown in figure 52.

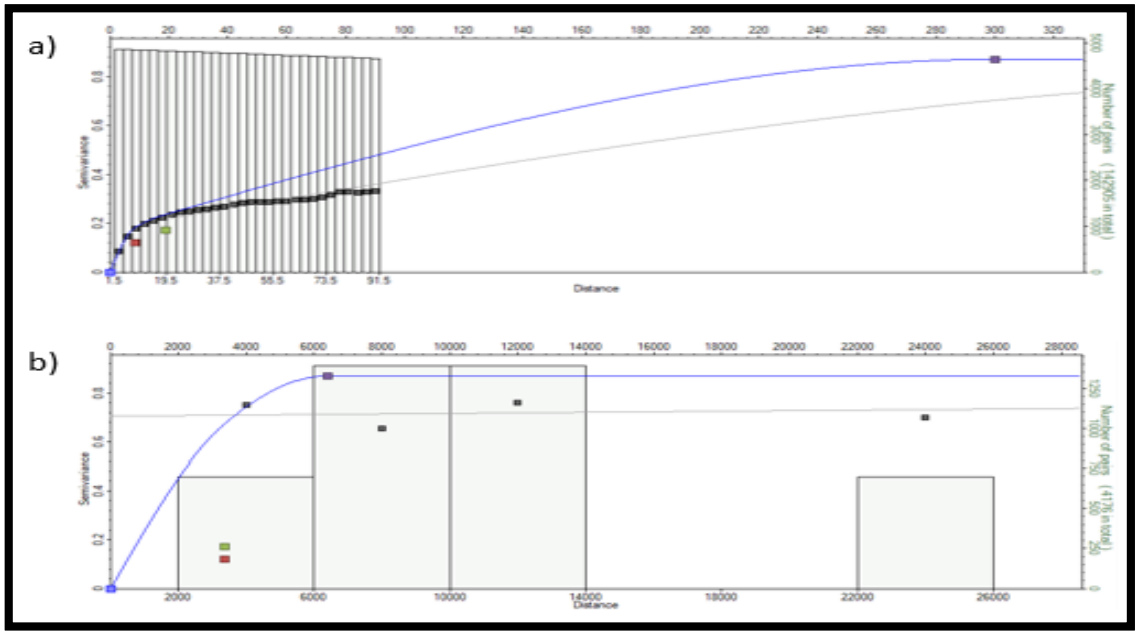

Figure 52. a) Vertical variogram of brittleness index in Bone Spring Formation, b) Major variogram of the same property.

For Brittleness index in Bone Spring formation, the Gaussian Random Function Simulation method was applied to interpolate the data in the entire model where the geomechanical properties distribution were characterized without taking the rock type parameters in consideration. Therefore, modelled cells ‘blue’ are slightly underestimated comparing with upscaled cells ‘green’ providing a slightly more conservative propagation of cell values in the model except the interval between 40 and 57% where modelled cells are slightly overestimated, figure 51-b. The average map of Bone Spring’s brittleness index shows the highest values of 55% around Peacemaker UL 3023 and UL 24 Voyager-1 well as shown in figure 53.

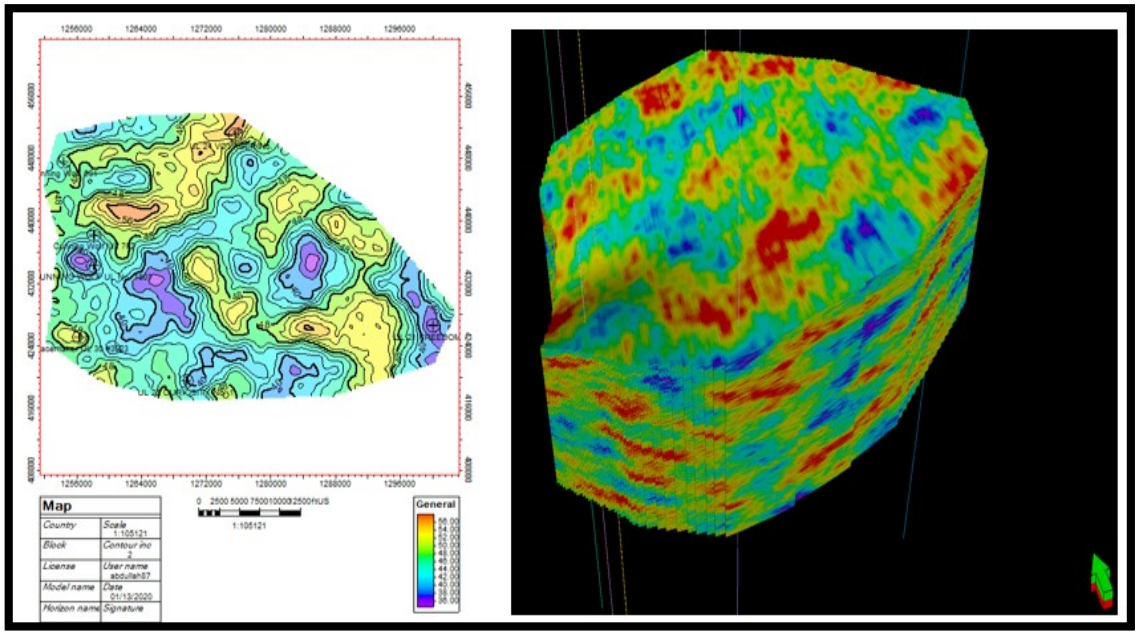

Figure 53. Average map of Bone Spring’s brittleness index and 3D model of the same property.

Well cross section of the modelled brittleness index in Bone Spring formation displays highest value of brittleness index at northern and eastern regions due to probable mineral composition of the high gamma ray facies of the third Bone Spring member which tend to be composed of more carbonate and silica instead of clay, figure 54. Moreover, the petrophysical analysis confirms the presence of organic rich mudstone facies in the third Bone Spring member.

Formation	**Bone Spring**						
Property	**Porosity**		**Water Saturation**		**Brittleness Index**		
Type	Spherical		Spherical		Spherical		
Sill	0.16	0.72	0.16	0.7	0.12	0.05	0.7
Lateral	4400	6900	500	5000	3370	3370	6400
Vertical	7.3	124	6	100	8.5	19	300

Table 2. Variogram analysis of porosity, water saturation and brittleness index in Bone Spring formation.

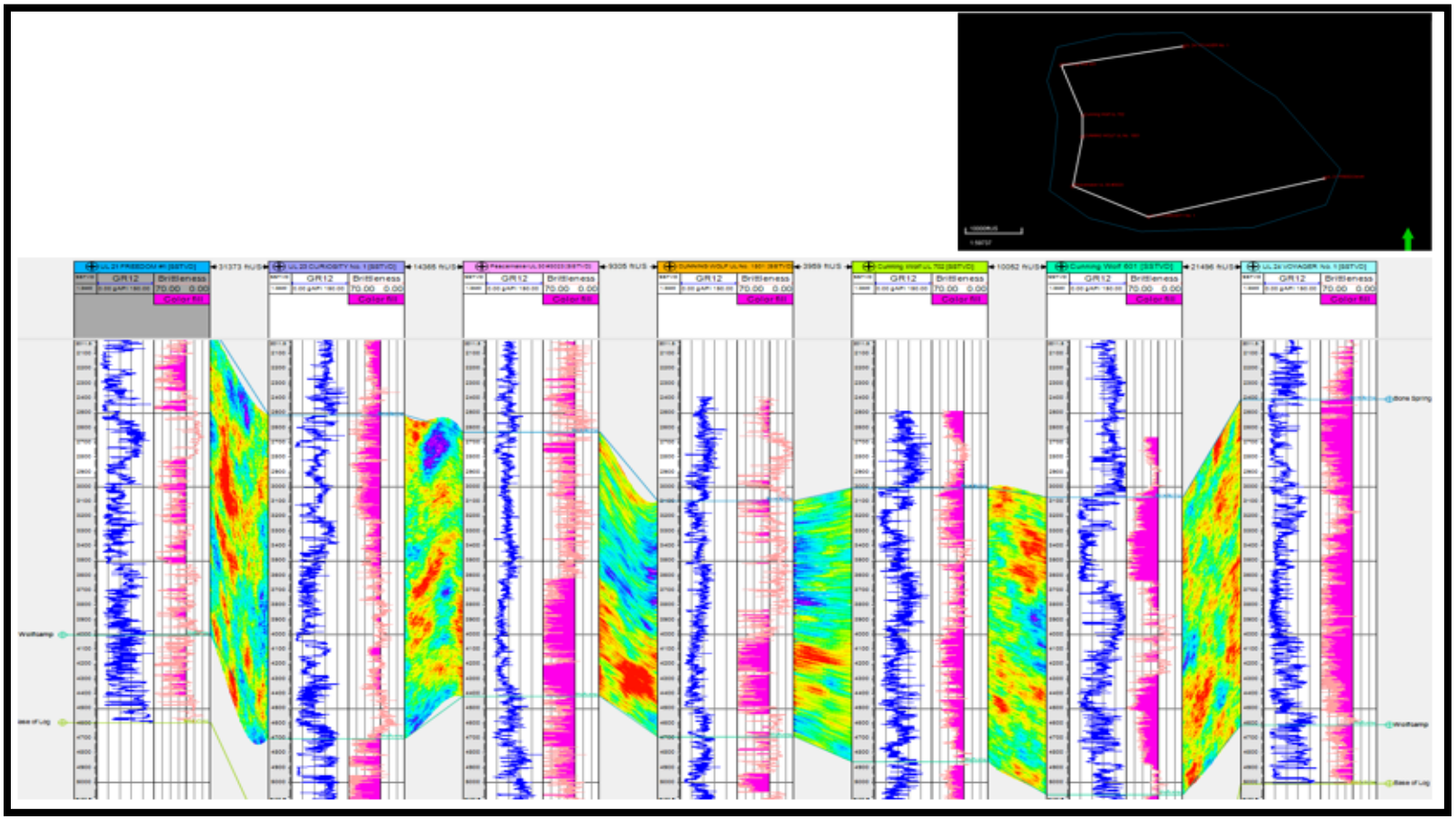

Figure 54. Well cross section of brittleness index model of Bone Spring formation showing lowest water saturation at the western region.

Wolfcamp Model

The histogram in figure 55-a represents the porosity parameter of Wolfcamp formation. The total number of upscaled points is 1,462; the value range is between 0 and 0.29 with an average porosity around 0.078. For simulating porosity in Wolfcamp formation using the Gaussian method, the normal score transformation was performed. The transformed data has a mean value of 0.011 and 0.92 standard deviation which differs to 1 due to significant percentage of 0 porosity as shown in figure 55.

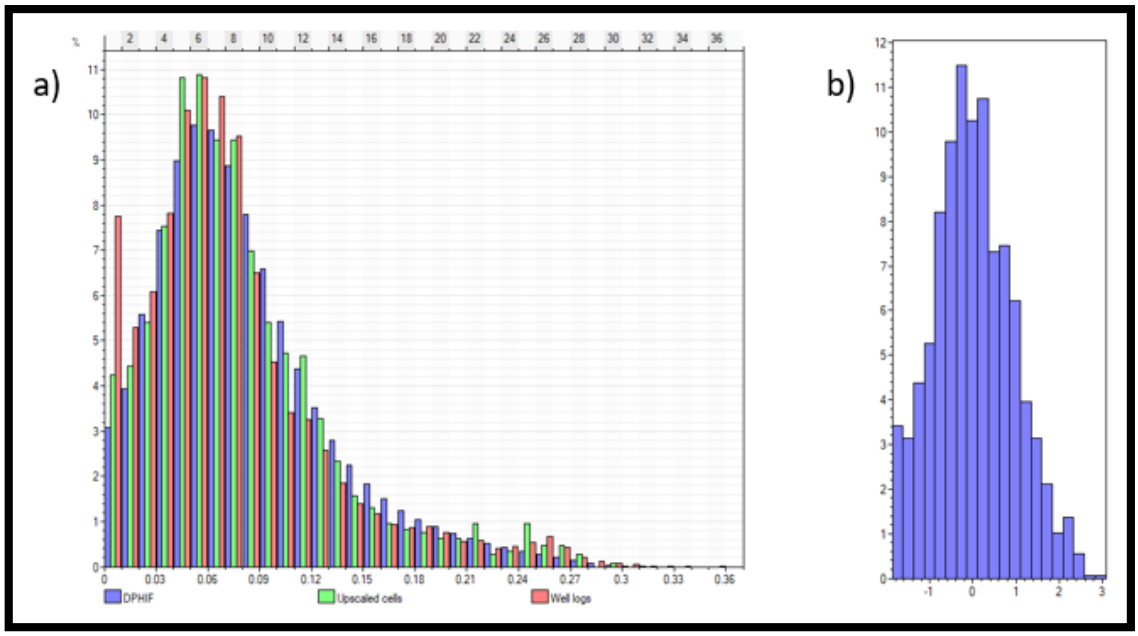

Figure 55. a) Histogram of porosity in Wolfcamp formation where well log data is displayed on a percentage of samples basis 'red' and upscaled cells are displayed on green, b) Porosity transformation of the same formation.

In variogram analysis, the vertical range were calculated, fitting the first 3 points, to 5.1 ft and 89 ft with a nugget of 0.0001 and a total sill of 0.99. Lateral ranges were also computed, fitting the first 3 points, to 500 ft and 7906 ft, as shown in figure 56.

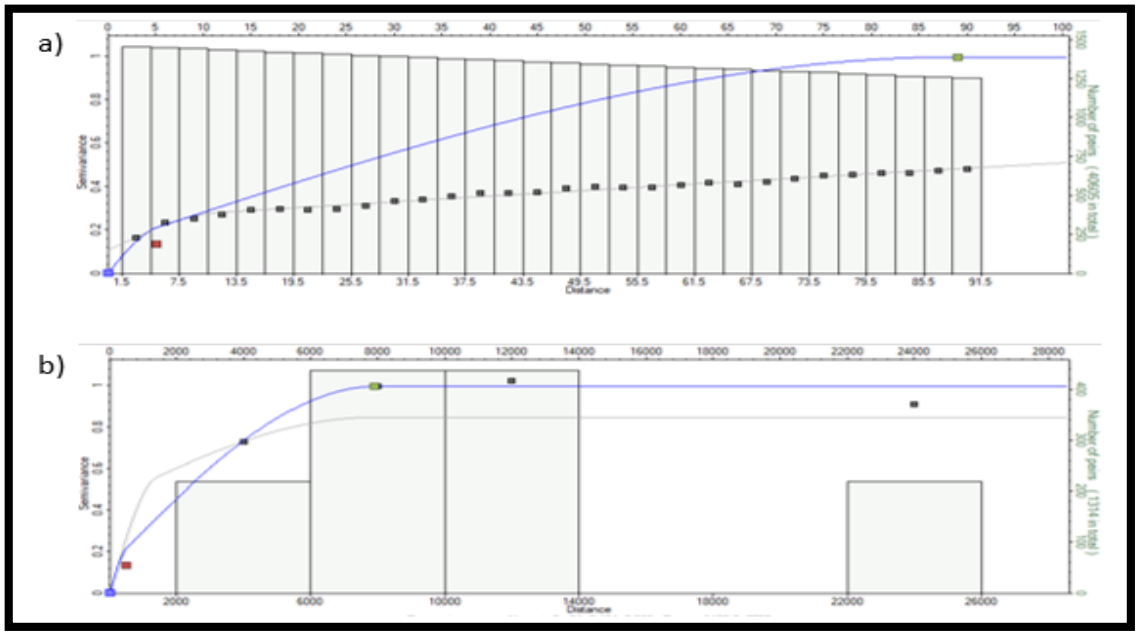

Figure 56. a) Vertical variogram of porosity in Wolfcamp Formation, b) Major Variogram of the same property.

For porosity in Wolfcamp formation, the Gaussian Random Function Simulation method was applied to interpolate the data in the entire model where the petrophysical properties distribution were characterized without taking the rock type parameters in consideration. Therefore, modelled cells ‘blue’ are slightly underestimated comparing with upscaled cells ‘green’ providing a slightly more conservative propagation of cell values in the model except the interval between 9 and 18% where modelled cells are slightly overestimated, figure 55-a. The average map of Wolfcamp’s porosity shows the highest values of 10% along the central region starting from Cunning Wolf UL 601 well towards the south to Cunning Wolf UL 702 and Cunning Wolf UL 1801 wells as shown in figure 57.

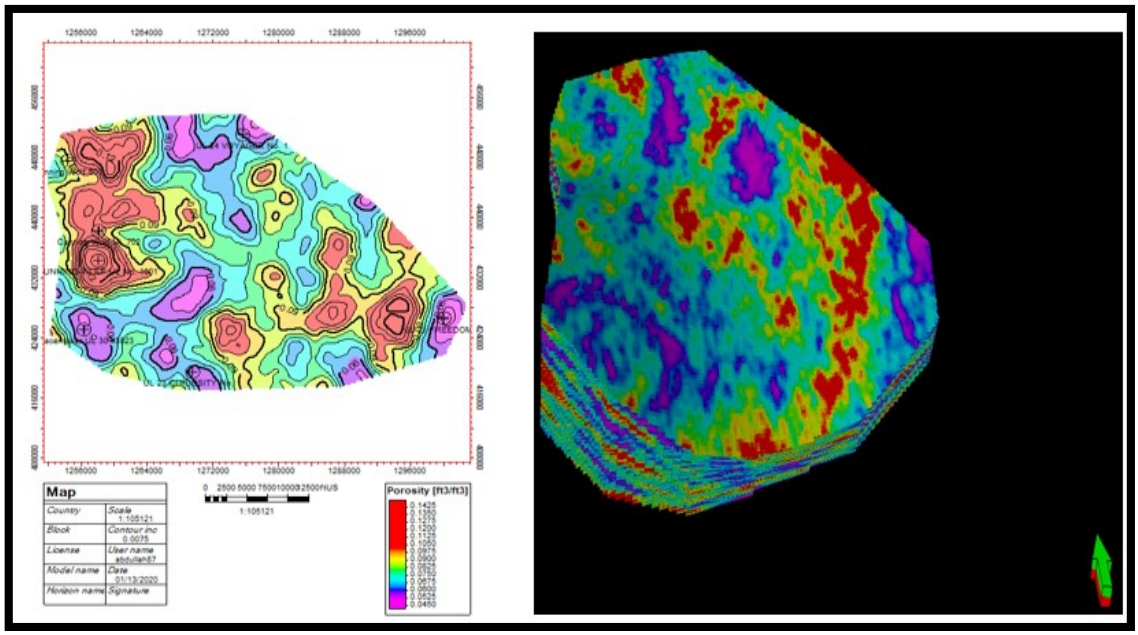

Figure 57. Average map of Wolfcamp’s porosity and 3D model of porosity.

Well cross section of modelled porosity in Wolfcamp formation displays highest value of porosity at western region 'center of the cross section' due to the high porosity that was calculated from the generated synthetic density logs from the three wells, figure 58. These synthetic density logs created a noise or error while simulating porosity parameters in the Wolfcamp model since they are imaginary data and do not reflect the real geology of the subsurface. Thus, more logs are needed in the field, not only from vertical wells, to substitute the synthetic curves and create more efficient model to visualize the horizontal continuity and spatial variability of the reservoir properties.

However, no trend of porosity can be observed vertically and horizontally due to heterogeneity and facies distribution of the formation, but the organic rich facies tend to have more porosity than the clean carbonate as stated in chapter II. This is affected by the existence of kerogen that gets converted to bitumen and hosts micro organic porosity.

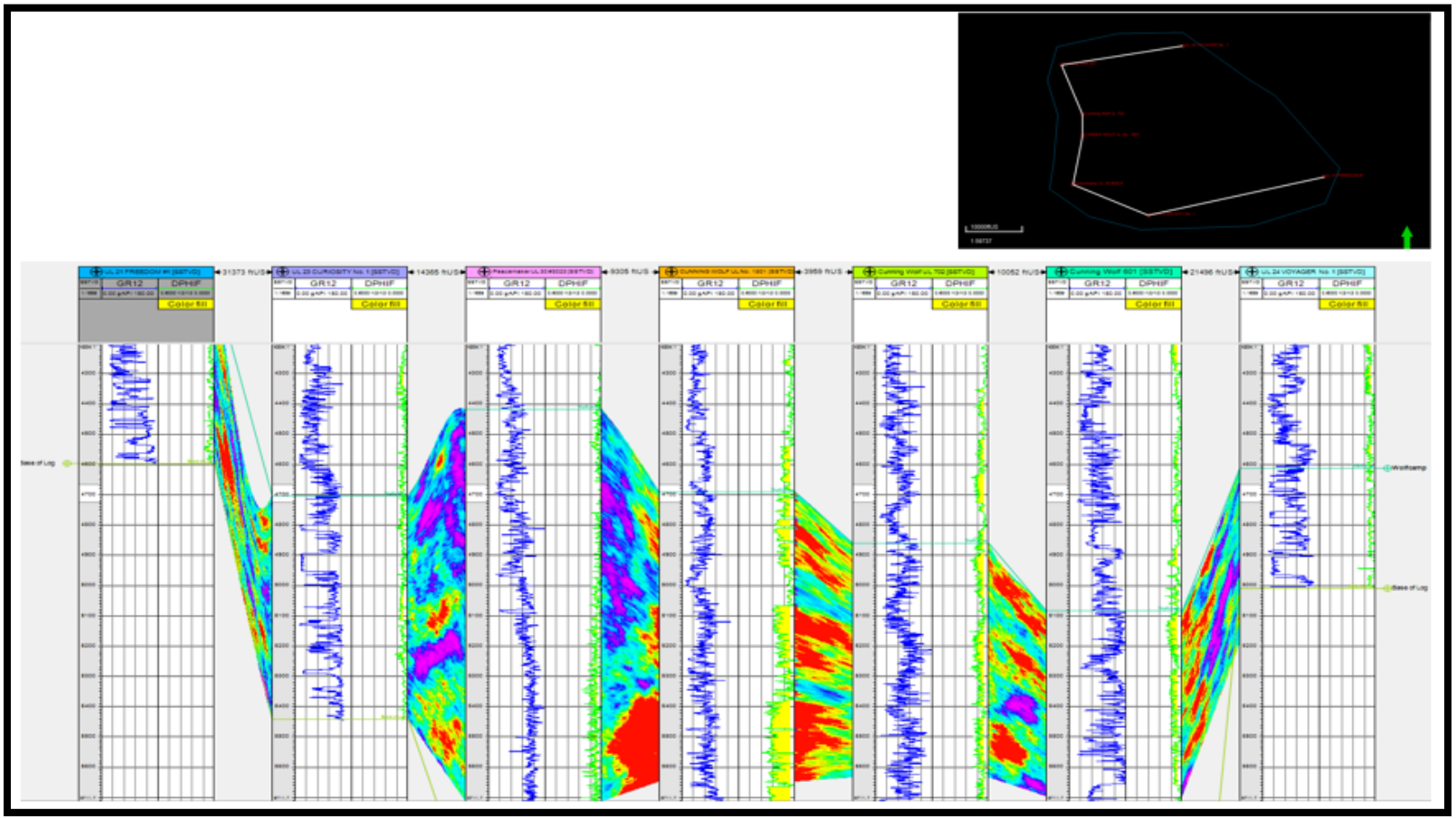

Figure 58. Well cross section of porosity model of Wolfcamp formation showing highest porosity at the western region.

The permeability of Wolfcamp formation was calculated from the above porosity model using equation number 20 in the petrophysical analysis section as shown in figure 59. The average map of permeability displays the highest value of 0.0373 mD around UL 21 Freedom-1 well, Peacemaker UL 3023 and UL 23 Curiosity-1 well.

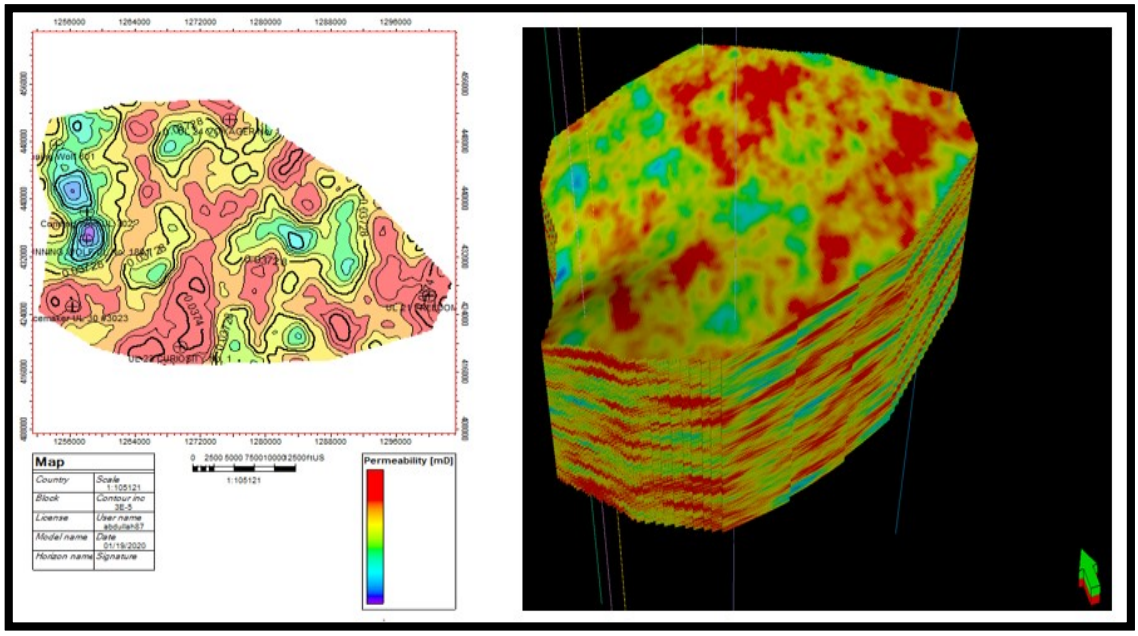

Figure 59. Average map of Wolfcamp's permeability and 3D model of porosity.

The histogram in figure 60-a characterizes the water saturation parameter of Wolfcamp formation. The total number of upscaled points is 1,462; the value range is between 0 and 1 with an average water saturation of around 0.25. For simulating water saturation in Wolfcamp formation using the Gaussian method, the normal score transformation was also performed. The transformed data has a mean value of 0.02 and 0.93 standard deviation which differs to 1 due to significant percentage of 1 water saturation as shown in figure 60.

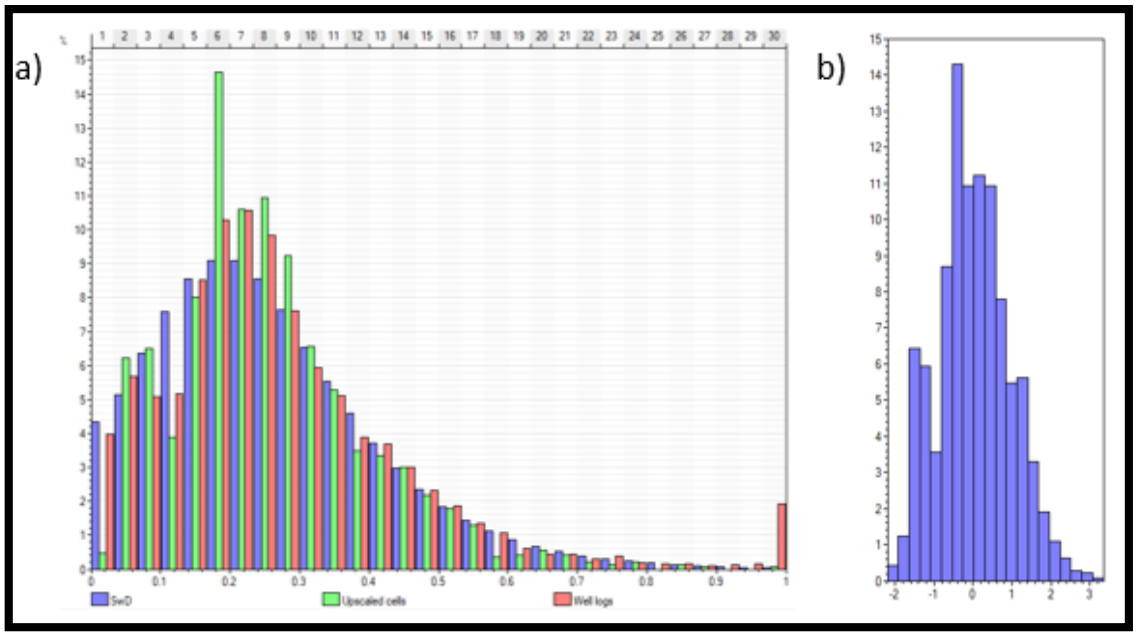

Figure 60. a) Histogram of water saturation in Wolfcamp formation where well log data is displayed on a percentage of samples basis 'red' and upscaled cells are displayed on green, b) Water saturation transformation of the same formation.

In variogram analysis, the vertical ranges were calculated, fitting the first 2 points, to 3.5 ft and 52 ft with a nugget of 0.0001 and a total sill of 0.85. This could be due the inconsistency of penetrated intervals of Wolfcamp formation. Based on the experimental points, it is not possible to predict the lateral ranges but 470 ft and 4940 ft were picked to model water saturation property, as shown in figure 61.

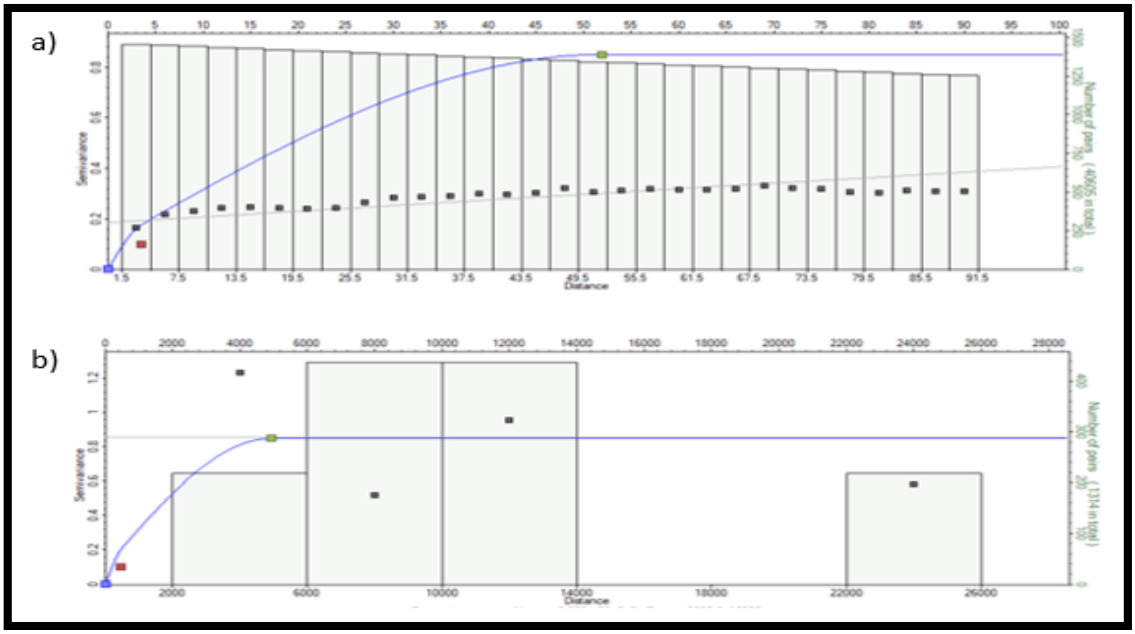

Figure 61. a) Vertical variogram of water saturation in Wolfcamp Formation, b) Major variogram of the same property.

For water saturation in Wolfcamp formation, the Gaussian Random Function Simulation method using porosity volume as a secondary constraint through co-kriging to interpolate the data in the entire model where the petrophysical properties distribution were characterized without taking the rock type parameters in consideration. Therefore, modelled cells 'blue' in the interval between 17.5 and 37.5% are underestimated comparing with upscaled cells 'green' providing more conservative propagation of cell values in the model while other intervals show a slightly overestimation of modelled cells, figure 60-a. The average map of Wolfcamp's water saturation shows the highest values of 33 % around UL 21 Freedom-1 and Cunning Wolf UL 601 well as shown in figure 62.

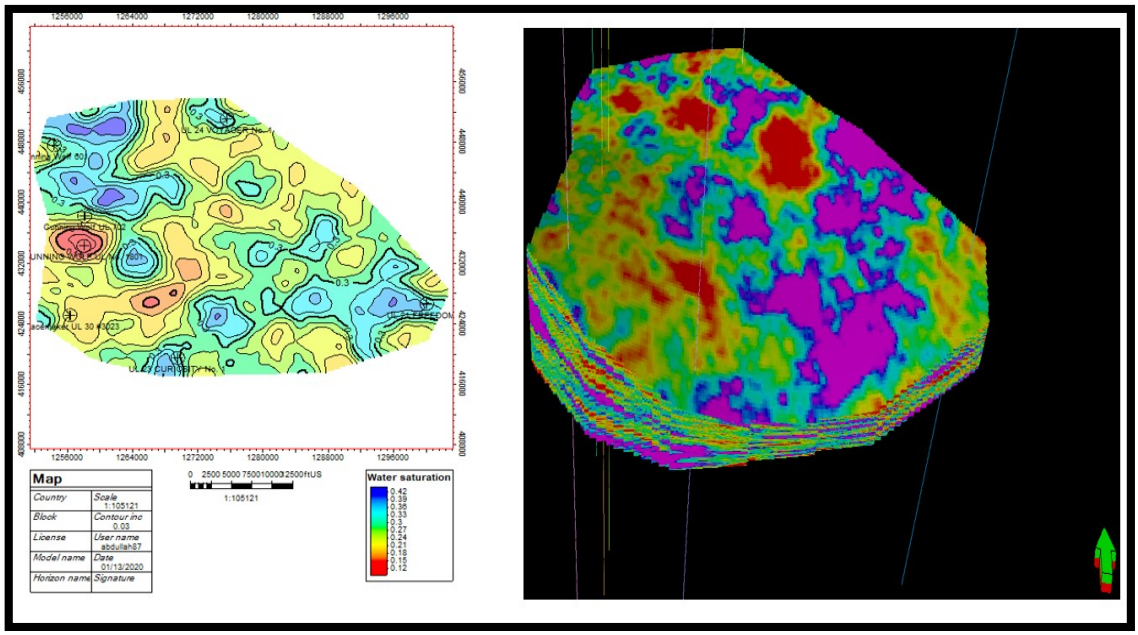

Figure 62. Average map of Wolfcamp's water saturation and 3D model of water saturation.

Well cross section of modelled water saturation in Wolfbone formation displays lowest value of water saturation at western region ‘center of the cross section’ due to the water saturation that was calculated from the generated synthetic resistivity logs from the three wells, figure 63. These synthetic resistivity logs created a noise or error while simulating the water saturation parameters in the Wolfcamp model since they are imaginary data and do not represent the actual conductivity of the subsurface formations. Thus, more logs are needed in the area of interest to substitute the synthetic curves in order to generate more efficient model to visualize the spatial variability of the reservoir properties.

However, no trend of water saturation can be observed vertically and horizontally but shale facies tend to have more water saturation than the clean carbonate due to the presence of the clay bound water. Yet, formation water interpretation and its chemistry could be impacted by the long history and widely use of Co_2 and water injection which result in weaknesses of formation water investigation (Melzer, 2013).

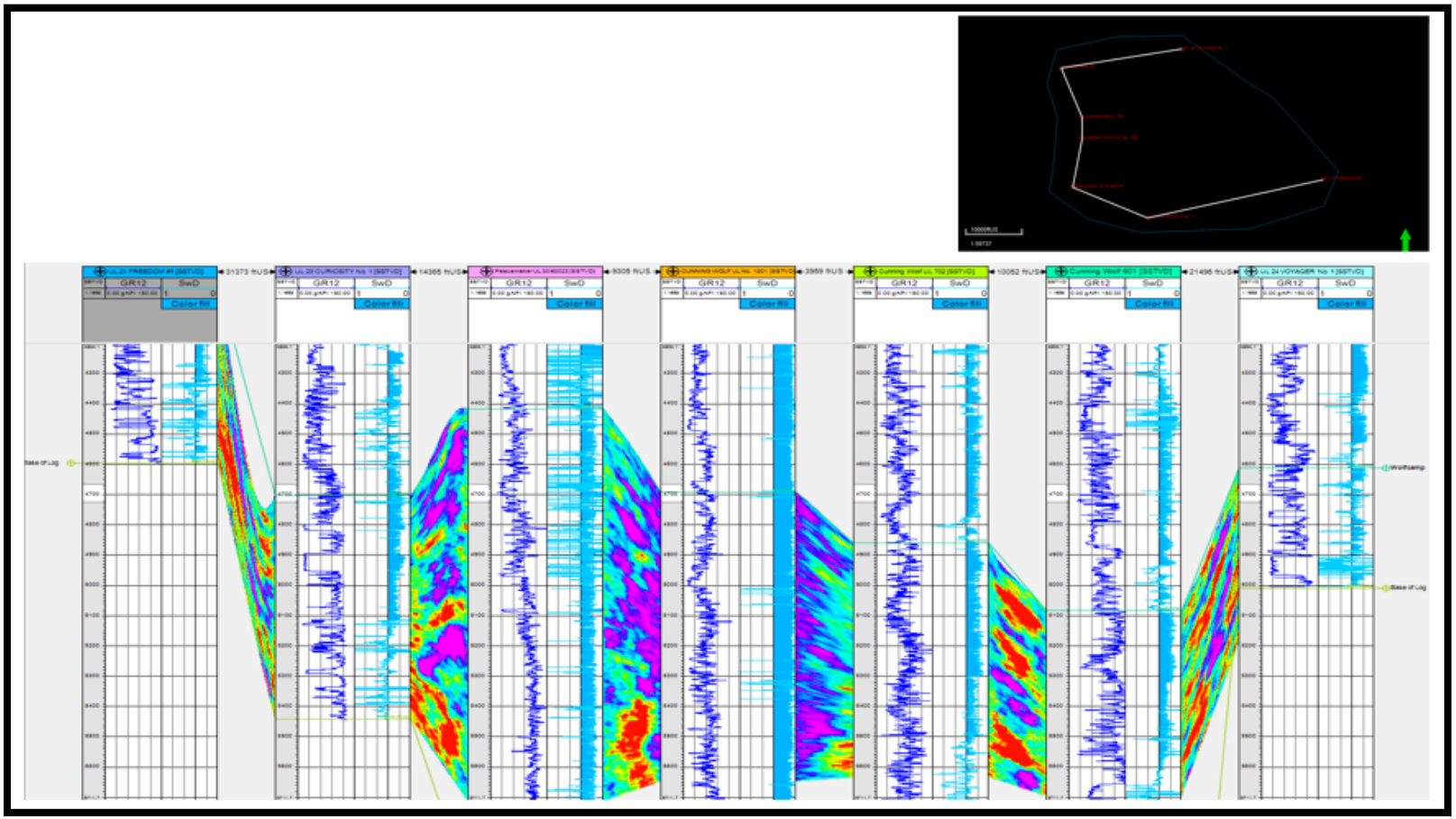

Figure 63. Well cross section of water saturation model of Wolfcamp formation showing lowest water saturation at the western region.

The histogram in figure 64-a characterizes the brittleness index parameter of Wolfcamp formation. The total number of upscaled points is also 1,462; the value range is between 1.5 and 70 with an average brittleness index around 45.6. For simulating brittleness index in Wolfcamp formation using the Gaussian method, the normal score transformation was performed. The transformed data a mean value of 0.03 and 0.92 standard deviation which differs to 1 due to significant percentage of 70 as a maximum value of brittleness index, figure 64.

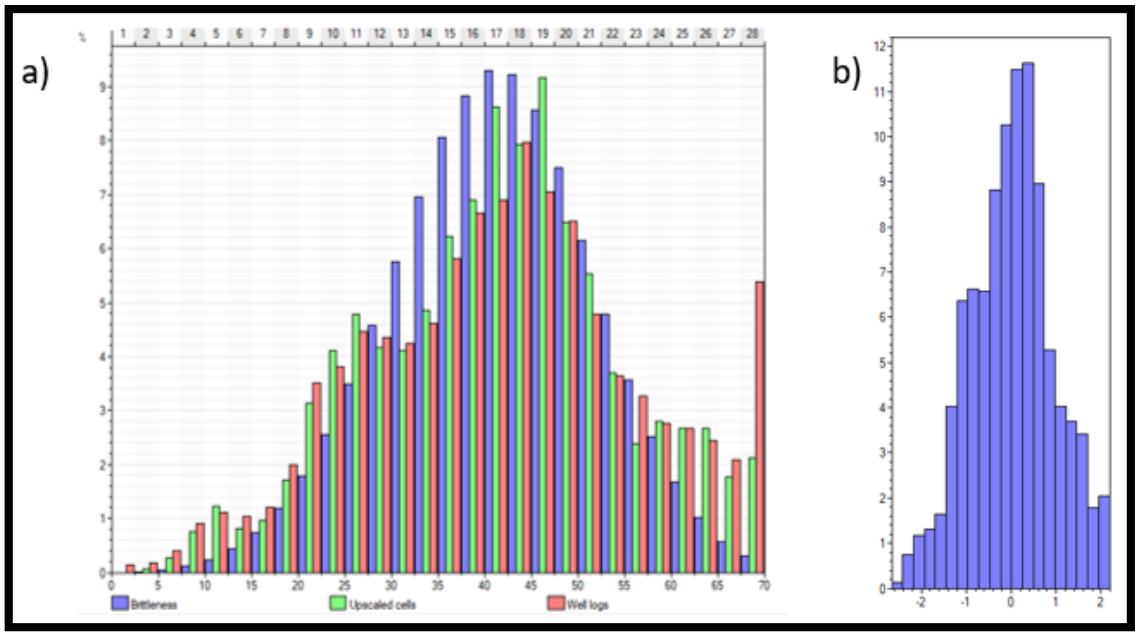

Figure 64. a) Histogram of brittleness index in Wolfcamp Formation where well log data is displayed on a percentage of samples basis 'red' and upscaled cells are displayed on green, b) Brittleness index transformation of the same formation.

In variogram analysis, the vertical ranges were calculated, fitting the first 6 points, to 7 ft and 100 ft with a nugget of 0.0001 and a total sill of 0.72. Lateral ranges were also computed, fitting the second experimental point, to 500 ft and 8350 ft, as shown in figure 65.

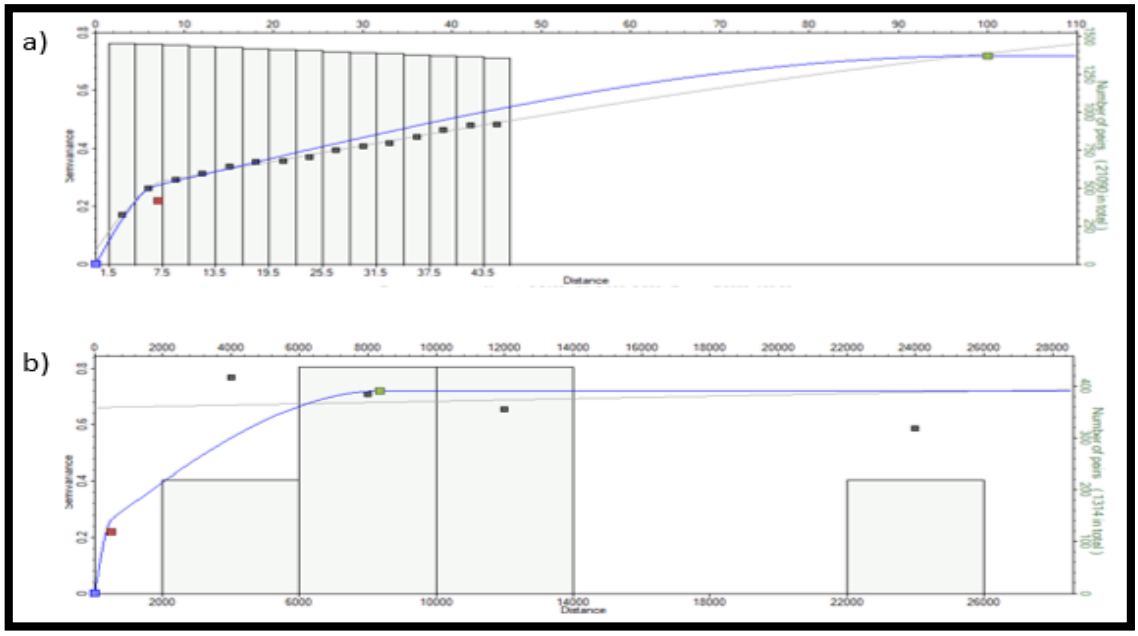

Figure 65. a) Vertical variogram of brittleness index in Wolfcamp Formation, b) Major variogram of the same property.

For Brittleness index in Wolfcamp formation, the Gaussian Random Function Simulation method was applied to interpolate the data in the entire model where the geomechanical properties distribution were characterized without taking the rock type parameters in consideration. Therefore, modelled cells 'blue' in the interval between 27.5 and 45% are overestimated comparing with upscaled cells 'green' while other intervals the modelled cells are underestimated providing more conservative propagation of cell values in the model, figure 64-a. The average map of Wolfcamp's brittleness index shows the highest values of 48% around UL 23 Curiosity-1 well and UL 24 Voyager-1 well as shown in figure 66.

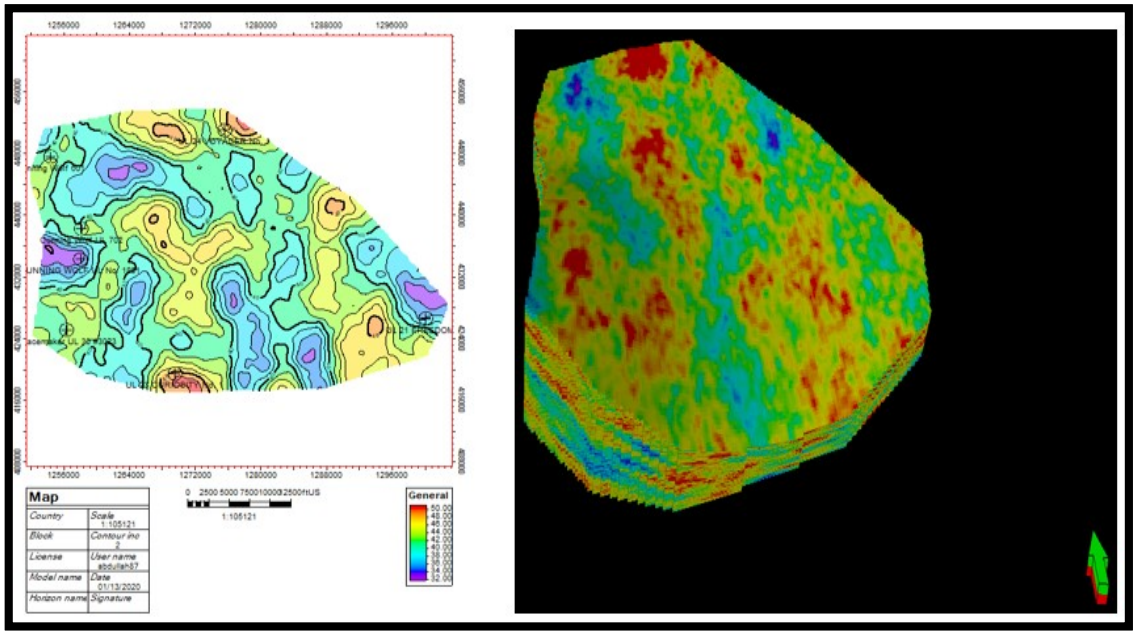

Figure 66. Average map of Wolfcamp's brittleness index and 3D model of the same property.

Well cross section of the modelled brittleness index in Wolfcamp formation displays highest value of brittleness index at the north and south regions due to probable mineral composition of the high gamma ray facies of the Wolfcamp formation which tend to be composed of more carbonate and silica instead of clay, figure 67. Moreover, the petrophysical analysis confirms the presence of organic rich mudstone facies in the Wolfcamp formation.

Formation	**Wolfcamp**					
Property	**Porosity**		**Water Saturation**		**Brittleness Index**	
Type	Spherical		Spherical		Spherical	
Sill	0.135	0.86	0.1	0.75	0.22	0.05
Lateral	500	7906	470	4940	500	8350
Vertical	5.1	89	3.5	52	7	100

Table 3. Variogram analysis of porosity, water saturation and brittleness index in Wolfcamp formation.

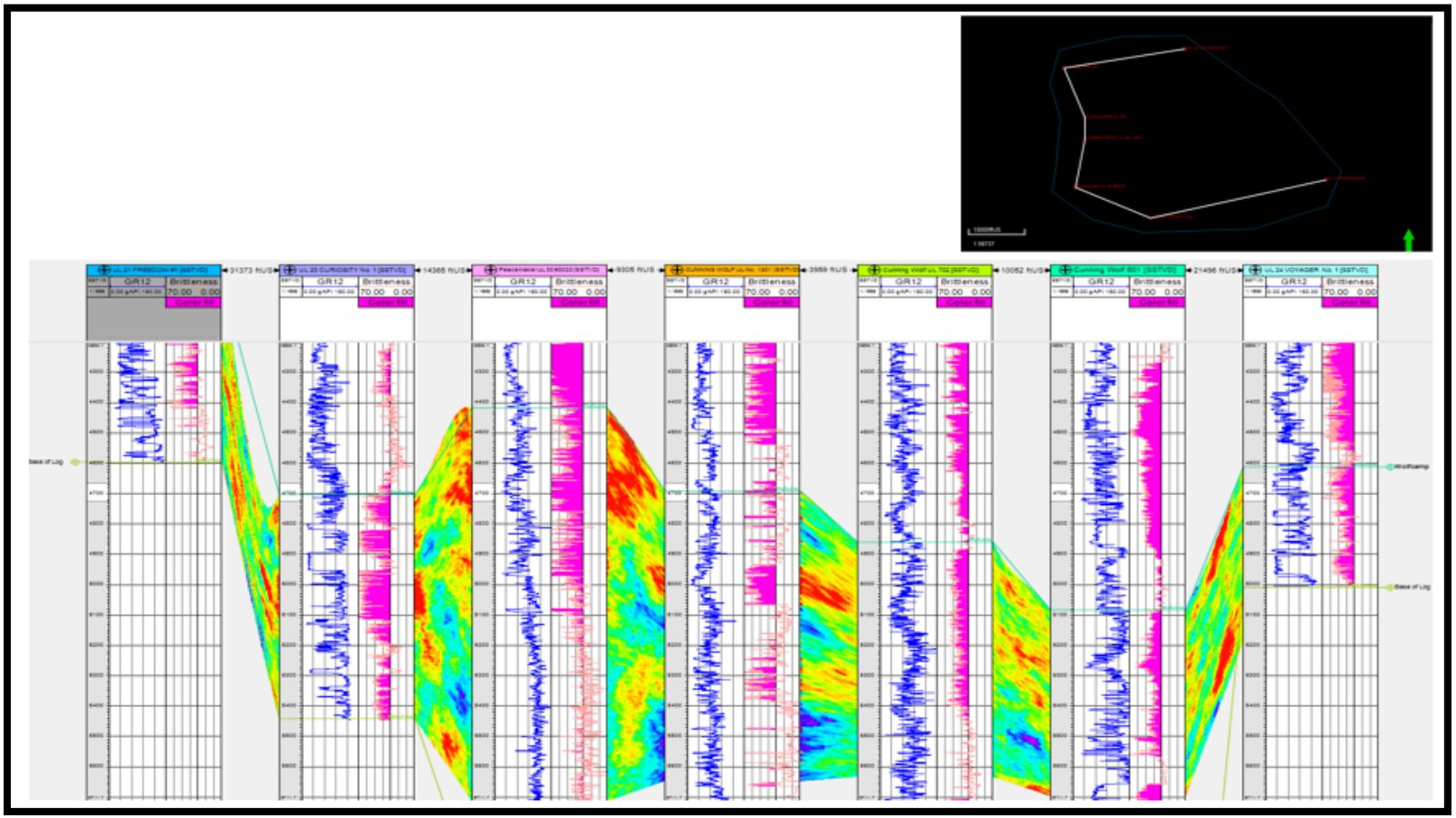

Figure 67. Well cross section of brittleness index model of Wolfcamp formation showing lowest brittleness index at the western region and high values at the north and south regions of the field.

CHAPTER V

MODEL APPLICATIONS

Volumetric

The studied area of interest in the Wolfbone field has an estimated ultimate recovery 'EUR' of almost 2 billion barrel of oil 'BBO' in the Bone Spring and Wolfcamp formations. The above EUR was calculated based on the 8% oil recovery factor and 1.3 of initial oil formation volume factor 'B_o' using the geological models (Gaswirth et al., 2018).

The Bone Spring formation has an OOIP of 18.6 BBO and EUR of 1.5 BBO as a total resource assessment using no cut off values. However, cut off values have been assigned to find the best tiers in the field for original oil in place 'OOIP' calculation. The net/gross is determined by applying suitable reservoir parameters cut offs so that uneconomic or unproductive zones are not included. Thus, tier 1 has cut offs that are applied to porosity above or equal to 5%, water saturation equal or less than 40 % and greater or equal to 30% brittleness index. Accordingly, the OOIP and EUR of the best area in the field for Bone Spring formation are calculated to be around 9.8 BBO and 786 million barrel of oil 'MMBO' respectively, which is not reasonable if comparing with an EUR of 14 BBO of the entire Delaware Basin (Gaswirth et al., 2018). The average maps of Net/Gross 'N/G' and OOIP of Bone Spring formation show the highest N/G of 0.6 and highest OOIP of 1.1 BBO in the western side of the Area of interest towards the deepest intervals of the formation as shown in figure 68.

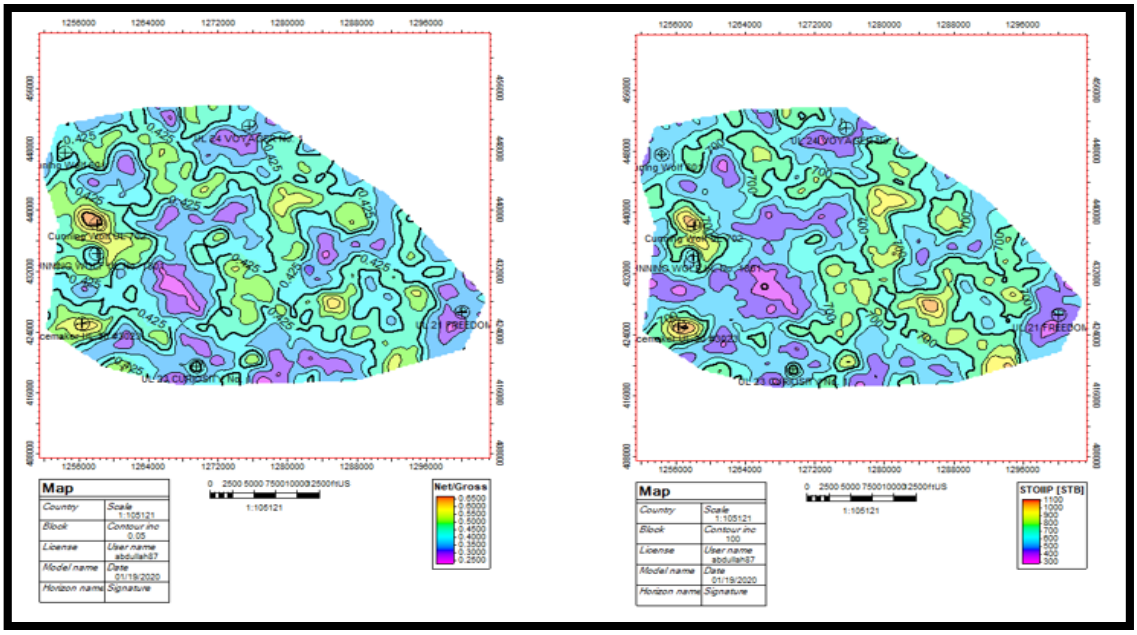

Figure 68. Average map of N/G and OOIP of Bone Spring formation using cutoffs.

Tier 2 has cut offs that are applied to porosity above or equal to 3%, water saturation equal or less than 60% and greater or equal to 30% brittleness index. These cutoffs were provided by University Lands ‘UL’ as a first pass and confirmed. Thus, the OOIP and EUR of the best area in the field for Bone Spring formation are calculated to be around 14.6 BBO and 1.1BBO respectively. The average maps of Net/Gross ‘N/G’ and OOIP of Bone Spring formation show the highest N/G of 0.9 and highest OOIP of 1.1 BBO in the western side of the Area of interest towards the deepest intervals of the formation as shown in figure 69.

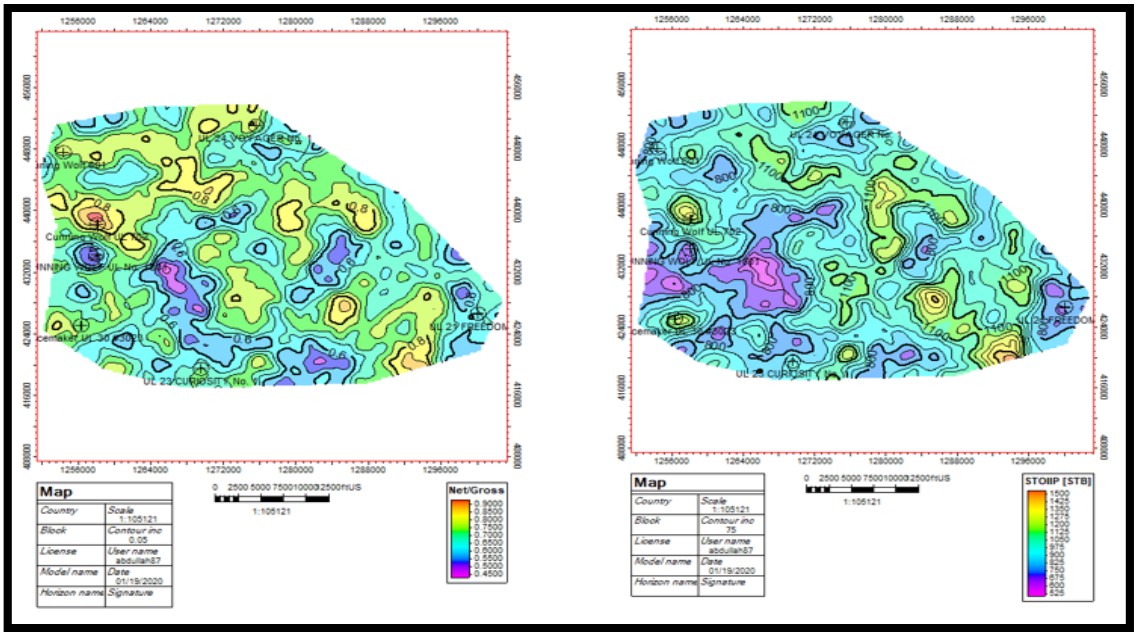

Figure 69. Average map of N/G and OOIP of Bone Spring formation using UL cutoffs.

The Wolfcamp formation has an OOIP of 6.5 BBO and EUR of 500 MMBO as a total resource assessment using no cut off values. However, tier 1 cutoff values have been also assigned to find the best tier in the field for original oil in place 'OOIP' calculation. The net/gross is determined by applying the same reservoir parameters cut offs as in Bone Spring formation tier 1. Thus, the OOIP and EUR of the best area in the field for Bone Wolfcamp are calculated to be around 3.4 BBO and 276 million barrel of oil 'MMBO' respectively, which is reasonable if comparing with 18 BBO of the entire Delaware Basin of Wolfcamp A and B (Gaswirth et al., 2018). In our case, we did not have full penetration of Wolfcamp A in some of the wells as well as Wolfcamp B. The average map of Net/Gross 'N/G' and OOIP of Wolfcamp formation display the highest

N/G of 0.7 and highest OOIP of 2.7 BBO in the western central western region around Cunning Wolf UL 601 and Cunning Wolf UL 702 wells towards the deepest intervals of the formation as shown in figure 70. Though, the Wolfcamp N/G and OOIP maps do not match as they do in the Bone Spring Formation where high values concentrated on the same regions of the field and this is due to the variation of thickness 'penetrated intervals' in Wolfcamp.

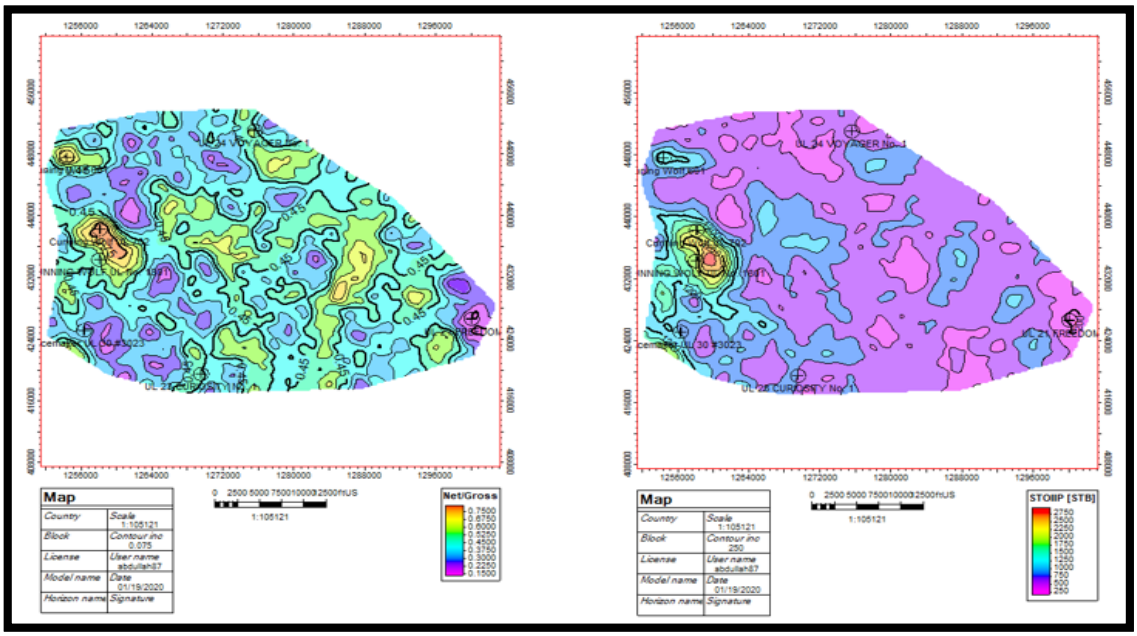

Figure 70. Average map of N/G and OOIP of Wolfcamp formation using cutoffs.

Tier 2 has cut offs that are applied to porosity above or equal to 3%, water saturation equal or less than 60% and greater or equal to 30% brittleness index. These cutoffs were provided by University Lands 'UL' as a first pass and confirmed. Thus, the OOIP and EUR of the best area in the field for Wolfcamp formation are calculated to be around 4.9 BBO and 400 MMBO respectively. The average maps of Net/Gross 'N/G'

and OOIP of Bone Spring formation show the highest N/G of 0.9 and highest OOIP of 1.1 BBO in the western side of the Area of interest towards the deepest intervals of the formation as shown in figure 71.

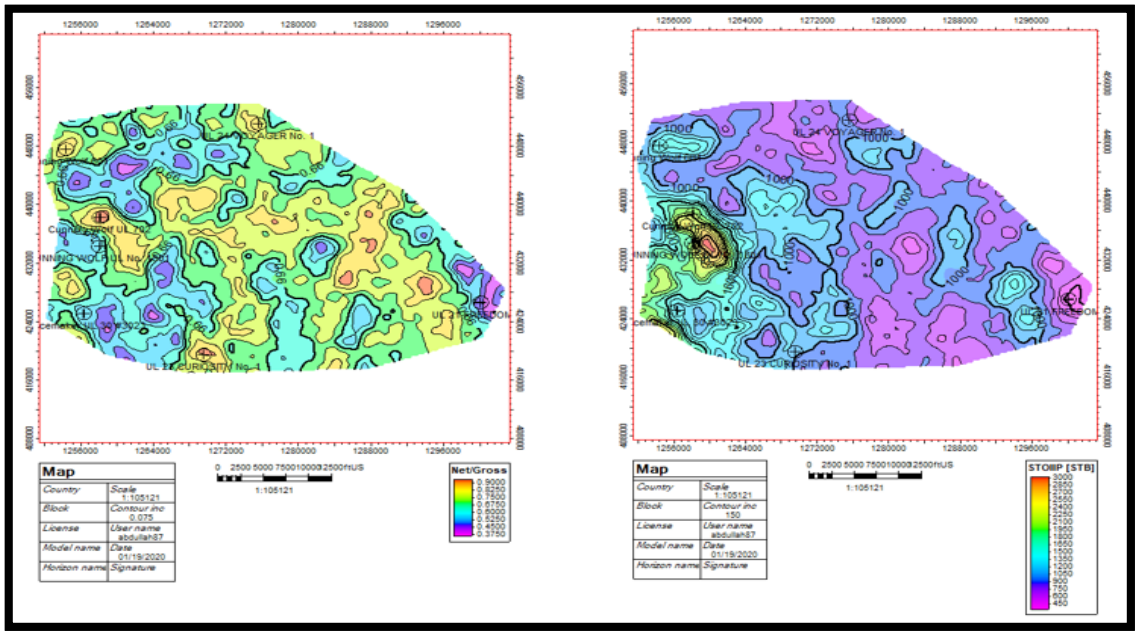

Figure 71. Average map of N/G and OOIP of Wolfcamp formation using UL cutoffs.

Table 4 displays the uncertainty in the original oil in place volume when using different cutoffs and this is common practice in the oil industry especially in the field development planning when dealing with few wells to express the need of more data 'wells' to reduce this uncertainty. However, there are two uncertain parameters in our project as stated in the structural model section. The Wolfcamp structural model, first uncertain parameter, was created based on the top of the Wolfcamp formation and the base of each well log interval 'Total Depth' rather than the actual formation base. The variation in the total depth of each log in Wolfcamp formation results in uncertain

thickness map hence uncertain 3D geological model. Likewise, the small number of wells that is the second uncertain parameter, are mostly aligned North-South, did not allow us to determine the possible anisotropy of properties distribution in both models. In order to mitigate these uncertainties, seismic data and horizontal wells are needed to have a better understanding of the reservoir architecture and quality as well as to visualize the horizontal continuity and spatial variability.

Tier	Porosity (%)	Water Saturation (%)	Brittleness Index (%)	OOIP (BBO)	EUR (BBO)
1	>5	<40	>30	13.2	1.06
2	>3	<60	>30	19.5	1.5
3	No Cutoffs	No Cutoffs	No Cutoffs	25.1	2

Table 4. Summary of the three tiers volumetric of both Bone Spring and Wolfcamp formations.

Placing Horizontal Targets

In unconventional reservoirs, heterogeneity varies vertically and horizontally from basin to another, and in order to maximize a horizontal well production; challenges to be made are as follows:

- Identify ideal reservoir intervals that fit best for well placement and fracture stimulation.
- Determine optimum lateral length, well orientation and spacing with petroleum engineers.

In formation evaluation section in chapter III, results were viewed and discussed in forms of log plots. Thus, the desired landing intervals in Bone Spring in the area of interest 'AOI' are:

- UL 21 Freedome-1, at 5,360 ft TVD where cherty limestone is overlying the organic rich mudstone that is triggered with mobile and residual oil in the zone. This locality has a porosity of greater than 13% and water saturation less than 15%.
- Cunning Wolf UL 601, at 6,100 ft TVD where rich organic mudstone lies between the two cherty limestone zones. This point of interest triggered also mobile and residual oil while the two cherty limestone intervals display excellent mobile oil in the pores. It displays a porosity value of around 6% and water saturation value of less than 20%.
- UL 23 Curiosity-1, there are two recommended intervals for landing. These are at 6,000 ft where rich organic mudstone facies have been identified and at 7,400

ft where the same facies have good oil as the previous interval but with less water in the pores. The landing point of 6,000 ft shows a porosity of approximately 10% and water saturation less than 30% while the point of 7,400 ft illustrates porosity of 9% and water saturation of 40%.

- UL 24 Voyager-1, at 7,220 ft where rich organic mudstone shows excellent mobile and residual oil in the pore system. This zone has 8% porosity and less than 15% water saturation.

While the desired landing zones in Wolfcamp formation are:

- Cunning Wolf 601, at 8,100 ft where organic rich mudstone facies shows good mobile and residual oil in the pore systems. This zone displays a porosity value of more than 12% and water saturation less than 15%.
- UL 23 Curiosity-1, displays good to excellent mobile and residual oil in the pores at a depth of 7,900 ft. This landing point has around 8% porosity and 20% water saturation.
- UL 24 Voyager-1, at 7,550 ft where organic rich mudstone facies triggered some little mobile oil with some residual oil in the pores. This point of interest has a porosity of 7% with a range of water saturation between 20 and 40%.

All the above intervals display good to excellent brittleness index in terms of elastic properties as well as mineral compositions where the rock is mainly composed of mainly carbonate and silicate. Therefore, fractures are easy to initiate and propagate around the wellbore and away from it.

As stated earlier in Brittleness index in chapter III, in situ stress systems and stability of wellbore while drilling may dictate the well orientation needed to effectively propagate fractures hence to maximize production. A stress map is made in the Permian Basin to show measured orientations of the maximum horizontal stress 'SHmax'. This map may provide a generalized orientation of minimum horizontal stress to be utilized in orienting the horizontal wells, figure 72, (Snee & Zoback, 2018).

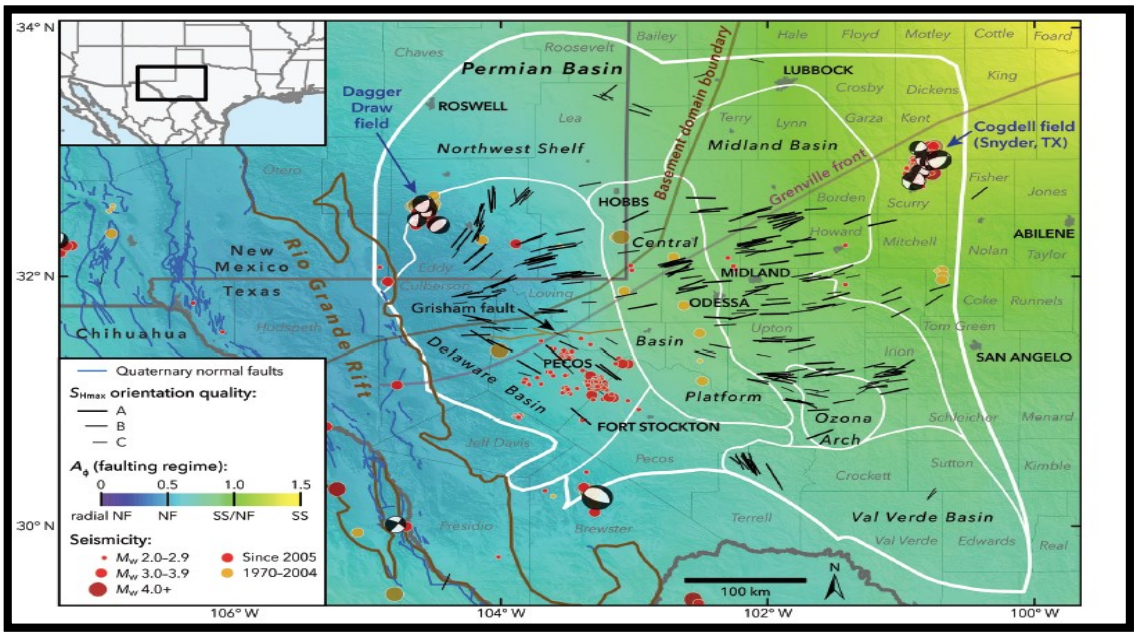

Figure 72. Permian basin state of stress that shows the orientation of the maximum horizontal stress 'Black Lines' reprinted from (Snee & Zoback, 2018).

CHAPTER VI

CONCLUSIONS

Discussion

Shale oil and gas as unconventional resources comprise of fine-grained sedimentary rock, organic rich and mud holding minerals like quartz and calcite. However, in the oil industry shale refers to formations that contain little shale lithology/mineralogy but are described as shale due to grain size only (Ahmed & Meehan, 2016). (King, 2010) mentioned that there are no two shale alike and they differ areally, vertically and along horizontal wellbores. Thus, shale resource plays have been defined as statistical plays where operators must drill huge number of wells and anticipate repeatable results with extracting different reservoir parameters for evaluating the economic viability and preparing effective well completion procedures for shale production (Aguilera, 2011). Theses parameters are total organic carbon content 'TOC', kerogen type, thermal maturity, oil and gas storage, porosity, mineralogy/lithology, thickness, depositional environment, brittleness, presence of natural fractures, stress regime and pressure (Ahmed & Meehan, 2016).

The most important parameter of a shale resource 'Source Rock' is the amount of total organic carbon 'TOC'. TOC and kerogen are often used mutually in the oil industry, but they are not similar (Ahmed & Meehan, 2016). TOC comprises of gas or oil present in the matrix, kerogen which expresses the accessible carbon that could be produced and the no potential residual carbon (Jarvie, 1991). Investigating the organic kerogen is a critical aspect in determining the upscaling of spatial characterization of

organic, inter-porosity and intra-porosity within a mud rock reservoir. Specific organic acids can be produced from specific organic kerogens that could be involved in improving or destroying mineral components and creating inter-particle or intra-particle porosity of a mudrock. Likewise, specific kerogen types by thermal transformation generate the fluids and gases leading to high hydrocarbon saturation in a nano-scale porosity along with irreducible water saturations. Thus, the advanced technologies such as the focused ion beam 'FIB' along with the advanced scanning electron microscopy 'SEM' are needed to visualize and image the nano-scale porosity systems (Ahmed & Meehan, 2016).

In 1979, Schmoker found a relationship between formation bulk density and TOC and determined TOC weight percentage from conventional wireline logs. Moreover, in 1990 Passy and his colleagues developed a method called delta R which is a graphical representation of porosity and resistivity using acoustic compressional slowness. This methodology can identify the organic rich intervals hence can be used to calculate the TOC weight percentage if the kerogen level of maturity 'LOM' is known. Therefore, it is important to have a full geochemistry analysis to calibrate and correct the TOC average weight percentage that could influence the porosity measurements (Bievenour, & Sonnenberg, 2019).

Minerology is another important characteristic in unconventional shale reservoirs. Mineral composition and fabric differences reflect huge differences in how effective the fracture stimulation affect the reservoir potential productivity. Therefore, technologies of conventional wireline logging and logging while drilling 'LWD',

wireline elemental spectroscopy logging and petrological with inorganic geochemistry core and cuttings analysis are required. Once mineral weight percent composition is derived, it can be combined with total porosity values to predict the volumetric percentage for implication into the petrophysical model (Ahmed & Meehan, 2016).

Hydrocarbons storage in conventional reservoirs are in the pores of matrix and calculated from wireline logs or laboratory analysis. Nevertheless, hydrocarbons in unconventional reservoirs 'Source Rocks' are stored as free gas or oil in inorganic and organic pores of the matrix and natural fractures, sorbed gas and oil that is adsorbed chemically to the organic matter or absorbed physically to the organic matter and dissolved gas in hydrocarbon liquid (Ahmed & Meehan, 2016). Thus, determining kerogen contained fluid saturation is very important rather than using Archie's equation to calculate the free gas or oil in the pores of matrix. Adsorption and desorption isotherm analysis for total and adsorbed gas/oil volumes calculation in unconventional resources is the primary method to determine hydrocarbon saturation and volumes (Bustin et al., 2009).

In this project, specifically in Wolfbone Field, the estimated calculation of water saturation is around 30 to 40% and this agrees with the high produced water that was recorded from the nearby field along the same intervals. The Permian basin conventional wells have produced water oil ratio 'PWOR' equals 13. This water is reused to enhance oil recovery by back injection into the depleted 'low Pressure' oil- producing zones (Scanlon et al., 2017). However, Unconventional wells have a much smaller PWOR around 3. This water cannot be reused for injection in the unconventional reservoirs due

to the low permeability. Thus, it can be disposed into nonproducing zones, such as Arbuckle formation near the basement. This leads to over pressuring and induced seismicity (Scanlon et al., 2017). (Melzer, 2013) mentioned that formation water interpretation and its chemistry could be impacted by the long history and widely use of CO_2 and water injection which result in weaknesses of formation water investigation.

Geomechanical analyses are crucial in unconventional resources development where the stress system in a basin must be examined during drilling wells, fracturing and production. Systems of in situ stress and stability of wellbores during drilling activities may dictate the well orientation. Indeed, stresses around the wellbore from both tectonic effects and the ones produced by the fracture growth will support initiating hydraulic fractures. Moreover, stress direction and magnitudes could be affected by changes in reservoir pressure in the subsurface (Addis & Yassir, 2010).

Conclusions

By using different cutoff values, the studied area of interest in the Wolfbone field in west Texas displays variation of the original oil in place ‘OOIP’ and estimated ultimate recovery ‘EUR’ in Bone Spring and Wolfcamp formations. However, the best tier of the two formations has a total resource assessment of EUR of 1 ‘BBO’. The OOIP was determined mainly by density porosity and water saturation of the three identified facies in both formations utilizing petrophysical ‘wireline’ logs. These are cherty limestone, organic rich mudstone interbedded with shale and shale facies.

The hydrocarbon storage adopted in this project is a function of only water saturation but not sorbed and adsorbed oil in total organic content ‘TOC’. Furthermore, water saturation was calculated based on the estimation of cementation and saturation exponents from Pickett plot and on the prediction of formation water resistivity in the invaded zones. As a result, the estimated water saturation of 30% to 40% in Wolfbone field agrees with the high produced water that was recorded from the nearby field along the same intervals.

The best landing zones of both formations were mainly associated with organic rich mudstone that show an average porosity of 10%, water saturation less than 20%, brittleness index less than 35% and permeability around 3.7 nD. Indeed, a facies model can be derived based on these properties criteria to predict the best horizontal targets for geosteering.

Because of the difficulties in classifying facies using only petrophysical logs without examining the actual rock and its mineralogy, permeability estimation is not

implemented in this project due to the weak correlation coefficient between the measured porosity and the measured permeability.

Reservoir characterization of porosity, water saturation and brittleness index were incorporated in a 3D geological model to achieve the aim of this project. Two 3D geological models were created to represent each formation separately. However, the Wolfcamp structural model was created based on the top of the Wolfcamp formation and the base of each well log interval 'Total Depth' rather than the actual formation base. The variation in the total depth of each log in Wolfcamp formation results in uncertain thickness map hence uncertain 3D geological model. Likewise, the small number of wells, which are mostly aligned North-South, did not allow us to determine the possible anisotropy of properties distribution in both models. In order to reduce the uncertainty in our petrophysical and geomechanical analysis along with 3D geological model, more data are required.

Future Work

- Gather seismic data to conduct a more robust sequence stratigraphy, facies discontinuity and regional mapping study for a better understanding of reservoir architecture.
- Collect cutting and plug samples to conduct thin section, x-ray diffraction ‘XRD’, x-ray fluorescence ‘XRF’, scanning electron microscopy ‘SEM’ and focused ion beam ‘FIB’ for a better understanding of organic matter mineral and elemental composition that may affect the porosity, permeability and TOC measurement.
- Acquire coring samples on the Area of Interest ‘AOI’ to interpret and describe facies to build a 3D facies model.
- Conduct adsorption and desorption isotherm analysis for total and adsorbed gas/oil volumes calculation to reduce the uncertainty in determining hydrocarbon saturation hence original oil in place ‘OOIP’.
- Collect petrophysical, geomechanical and cutting description of horizontal wells in AOI to visualize the horizontal continuity and spatial variability in the reservoir properties.
- Quantify type of fractures, natural fractures presence and intensity in relation to identified facies to evaluate the reservoir quality for landing and completing horizontal wells.

- Conduct a volumetric uncertainty analysis by defining the uncertain parameters, their ranges and distribution and analyzing the sensitivity of the model in order to find a good relationship between the variability of input and the output response.

REFERENCES

Addis, M., & Yassir, N. (2010). An Overview of Geomechanical Engineering Aspects of Tight Gas Sand Developments. *SPE/DGS Saudi Arabia Section Technical Symposium And Exhibition*. doi: 10.2118/136919-ms.

Ahmed, U., & Meehan, D. N. (2016). *Unconventional Oil and Gas Resources: Exploitation and Development*. United States: CRC Press.

Amirov, E. (2016). Formation Evaluation Manual. Retrieved 15 March 2019, from http://hdl.handle.net/20.500.12323/3270

Archie, G. (1942). The Electrical Resistivity Log as an Aid in Determining Some Reservoir Characteristics. *Transactions Of The AIME*, *146*(01), 54-62. doi: 10.2118/942054-g.

Aguilera, R. (2011). Guidelines for Application of the Petroleum Resources Management System. Unconventional Resources Estimation in Tight Gas Formations. Retrieved 22 June 2019, from http://rca.spe.org/files/3814/0834/5934/PRMS_Guidelines_Nov2011.pdf

Bievenour, A., & Sonnenberg, S. (2019). Reservoir Characterization of the Bone Spring and Wolfcamp Formations, Delaware Basin, Ward County, West Texas. *Proceedings Of The 7Th Unconventional Resources Technology Conference*. doi: 10.15530/urtec-2019-633.

Baker, H., Al-Jawad, S., & Abdulla, A. (2016). Applied Spatial Data Analysis Technique on Petrophysical Properties of MA unit of Mishrif Formation/Noor Field. *Iraqi Journal Of Chemical And Petroleum Engineering*, *17*(3), 75-81.

Bustin, R., Bustin, A., Ross, D., Chalmers, G., Murthy, V., Laxmi, C., & Cui, X. (2009). Shale Gas Opportunities and Challenges. *American Association Of Petroleum Geologists*, Article 40382. Retrieved from http://www.searchanddiscovery.com/documents/2009/40382bustin/ndx_bustin.pdf

Crosby, C. (2015). *Depositional History and High Resolution Sequence Stratigraphy of the Leonardian Bone Spring Formation, Northern Delaware Basin, Eddy and Lea Counties, New Mexico*. University of Oklahoma.

Cys, J., & Gibson, W. (1988). Pennsylvanian and Permian geology of the Permian basin region, in Sloss, L. L., ed., Sedimentary cover—North American craton: The Geology of North America. *Geological Society Of America*, *D-2*, 277-289.

EIA. (2014). Six Formations Are Responsible for Surge in Permian Basin Crude Oil Production - Today in Energy - U.S. Energy Information Administration. Retrieved 11 March 2019, from https://www.eia.gov/todayinenergy/detail.php?id=17031

EIA. (2018). Permian Basin Wolfcamp Shale Play, Geology Overview - U.S. Energy Information Administration. Retrieved 11 March 2019, from https://www.eia.gov/maps/pdf/PermianBasin_Wolfcamp_EIAReport_Oct2018.pdf.

Ellis, D., & Singer, J. (2007). *Well logging for earth scientists* (2nd ed.). Dordrecht, The Netherlands: Springer.

Engle, M., Reyes, F., Varonka, M., Orem, W., Ma, L., & Ianno, A. et al. (2016). Geochemistry of formation waters from the Wolfcamp and "Cline" shales: Insights into brine origin, reservoir connectivity, and fluid flow in the Permian Basin, USA. *Chemical Geology*, *425*, 76-92. doi: 10.1016/j.chemgeo.2016.01.025.

Fairhurst, B., & Hanson, M. (2012). Evolution and Development of the Wolfbone Play, Southern Delaware Basin, West Texas: An Emerging Frontier, An Oil-Rich Unconventional Resource. *American Association Of Petroleum Geologists*, Article 10411. Retrieved from http://www.searchanddiscovery.com/documents/2012/10411fairhurst/ndx_fairhurst.pdf

Galley, J. (1958). Oil and Geology in the Permian Basin of Texas and New Mexico, in Weeks, L. G., ed., Habitat of oil—a symposium: Tulsa, Oklahoma: *American Association Of Petroleum Geologists*, *Special Publicaion*, 394-446.

Gaswirth, S., French, K., Pitman, J., Marra, K., Mercier, T., & Leathers-Miller, H. et al. (2018). Assessment of undiscovered continuous oil and gas resources in the Wolfcamp Shale and Bone Spring Formation of the Delaware Basin, Permian Basin Province, New Mexico and Texas, 2018. *Fact Sheet*. doi: 10.3133/fs20183073.

Gawloski, T. (1986). Nature, Distribution, and Petroleum Potential of Bone Spring Carbonate Detrital Sediments Along North Shelf of Delaware Basin, Lea County, New Mexico: ABSTRACT. *AAPG Bulletin*, *70*(5). doi: 10.1306/94885caf-1704-11d7-8645000102c1865d.

Goodway, B., Perez, M., Varsek, J., & Abaco, C. (2010). Seismic petrophysics and isotropic-anisotropic AVO methods for unconventional gas exploration. *The Leading Edge*, *29*(12), 1500-1508. doi: 10.1190/1.3525367.

Harrick, D., & Kennedy, W. (2009). On the Quagmire of "Shaly Sand" Saturation Equations. *Society Of Petrophysicists And Well Log Analysis, 50Th Annual Logging Symposium*.

Hills, J. (1963). Late Paleozoic Tectonics and Mountain Ranges, Western Texas to Southern Colorado: ABSTRACT. *AAPG Bulletin*, *47*, 1709-1725. doi: 10.1306/bc7439e5-16be-11d7-8645000102c1865d.

Jackson, K., Palisch, T., & Lehman, L. (2014). Completion Optimization with Ceramics Provides Step Changes in Horizontal Performance for the 2nd Bone Spring Formation – A Southeastern New Mexico Case History. *SPE Annual Technical Conference And Exhibition*, *5*, 1928-1950. doi: 10.2118/170720-ms.

Jarvie, D. (1991). Total Organic Carbon (TOC) Analysis in Merrill, R., Source and migration processes and evaluation techniques. Tulsa, Okla. U.S.A.: *American Association of Petroleum Geologists*. 113-118.

Keller, G., Hills, J., & Djeddi, R. (1980). A Regional Geological and Geophysical Study of the Delaware Basin, New Mexico and West Texas: Guidebook. Retrieved 19 April 2019, from https://nmgs.nmt.edu/publications/guidebooks/downloads/31/31_p0105_p0111.pdf

Kelly, L., Bachmann, J., Amoss, D., Angelico, B., Corales, B., & Fernandez, B. et al. (2012). Permian Basin: Easy to Oversimplify, Hard to Overlook. Exploration & Production. Retrieved 19 April 2020, from https://www.pdffiller.com/jsfiller-desk18/?projectId=418087875#82db04c634ad1a30370177ac4d6be52e

Kennedy, W. (2019). *Density and Photoelectic Log II, Well Logging Method, PETE 608*. Lecture, Texas A&M University.

King, G. (2010). Thirty Years of Gas Shale Fracturing: What Have We Learned?. *SPE Annual Technical Conference And Exhibition*. doi: 10.2118/133456-ms.

Lohoefer, D., Keener, B., Snyder, D., & Ezeldin, S. (2014). Development of the Wolfbone Formation Using Open Hole Multistage Vertical Completion Technology. *SPE Hydraulic Fracturing Technology Conference*. doi: 10.2118/168643-ms.

Melzer. (2013). An Updated Assessment of the CO2 Enhanced Oil Recovery Potential in the Vicinity of the Waste Isolation Pilot Plant. Retrieved 19 April 2019, from https://wipp.energy.gov/library/CRA/CRA-2014/References/Others/Melzer_2013_An_Updated_Assessment_of_the_CO2_Enhanced_Recovery_Potential_in_the_Vicinity_of_the_WIPP.pdf

Montgomery, S. (1997). Permian Bone Spring Formation: Sandstone Play in the Delaware Basin Part I-Slope. *AAPG Bulletin*, *81 (1997)*, 1239-1258. doi: 10.1306/522b4dc5-1727-11d7-8645000102c1865d.

PASSEY, Q., Creaney, S., Kulla, B., Moretti, F., & Stroud, J. (1990). A Practical Model for Organic Richness from Porosity and Resistivity Logs. *AAPG Bulletin*, *74*(12), 1777-1794. doi: 10.1306/0c9b25c9-1710-11d7-8645000102c1865d.

Rickman, R., Mullen, M., Petre, J., Grieser, W., & Kundert, D. (2008). A Practical Use of Shale Petrophysics for Stimulation Design Optimization: All Shale Plays Are Not Clones of the Barnett Shale. *SPE Annual Technical Conference And Exhibition*. doi: 10.2118/115258-ms.

RRC. (2019). Permian Basin Information. Retrieved 13 August 2019, from https://www.rrc.state.tx.us/oil-gas/major-oil-and-gas-formations/permian-basin-information/

Scanlon, B., Reedy, R., Male, F., & Walsh, M. (2017). Water Issues Related to Transitioning from Conventional to Unconventional Oil Production in the Permian Basin. *Environmental Science & Technology*, *51*(18), 10903-10912. doi: 10.1021/acs.est.7b02185.

Schmoker, J. (1979). Determination of Organic Content of Appalachian Devonian Shales from Formation-Density Logs: GEOLOGIC NOTES. *AAPG Bulletin*, *63*(9), 1504-1537. doi: 10.1306/2f9185d1-16ce-11d7-8645000102c1865d.

Schwartz, K. (2018). Reservoir Characterization and Development Strategies of the Permian Wolfcamp and Bone Spring Formations of the Delaware Basin, West Texas and Southeast New Mexico. Retrieved 19 August 2019, from https://geoconvention.com/wp-content/uploads/abstracts/2018/299_GC2018_Reservoir_Characterization_and_Dev_Strategies_Permian_Wolfcamp_and_Bone_Spring.pdf

Sieler, J. (2018). What Makes the Delaware Tick?. Retrieved 11 March 2019, from https://spee.org/sites/spee.org/files/houston-2018-01-10-sieler.pdf

Snee, J., & Zoback, M. (2018). State of stress in the Permian Basin, Texas and New Mexico: Implications for induced seismicity. *The Leading Edge*, *37*(2), 127-134. doi: 10.1190/tle37020127.1

Soreghan, G., & Soreghan, M. (2013). Tracing Clastic Delivery To the Permian Delaware Basin, U.S.A.: Implications For Paleogeography and Circulation In Westernmost Equatorial Pangea. *Journal Of Sedimentary Research*, *83*(9), 786-802. doi: 10.2110/jsr.2013.63

University Lands. (2019). ArcGIS Web Application. Retrieved 5 April 2019, from https://gis.utlands.utsystem.edu/WellDataApp/

White, J. (1983). *Underground sound: Application of Seismic Waves.* Amsterdam a.o: Elsevier.

Yang, K., & Dorobek, S. (1995). The Permian Basin of West Texas and New Mexico: Tectonic History of A "Composite" Forland Basin and Its Effects of Stratigraphic Development. *Stratigraphic Evolution Of Foreland Basins*, *52*, 149-174. doi: 10.2110/pec.95.52.0149

Yarus, J., & Chambers, R. (2006). Practical Geostatistics - An Armchair Overview for Petroleum Reservoir Engineers. *Journal Of Petroleum Technology*, *58*(11), 78-86. doi: 10.2118/103357-ms